

**University of Alberta**

**MODELS FOR FOREST GROWTH AND MORTALITY:  
LINKING DEMOGRAPHY TO COMPETITION AND  
CLIMATE**

by

Andria Dawson

A thesis submitted to the Faculty of Graduate Studies and Research  
in partial fulfillment of the requirements for the degree of

**Doctor of Philosophy**

in

**Applied Mathematics**

Department of Mathematical and Statistical Sciences  
and  
Department of Renewable Resources

© Andria Dawson  
Fall, 2013  
Edmonton, Alberta

Permission is hereby granted to the University of Alberta Libraries to reproduce single copies of this thesis and to lend or sell such copies for private, scholarly, or scientific research purposes only. Where the thesis is converted to, or otherwise made available in digital form, the University of Alberta will advise potential users of the thesis of these terms.

The author reserves all other publication and other rights in association with the copyright in the thesis and, except as herein before provided, neither the thesis nor any substantial portion thereof may be printed or otherwise reproduced in any material form whatsoever without the author's prior written permission.

## Dedication

For my parents, Keith and Nancy Dawson, who offered me unconditional love and support throughout my years spent as a graduate student.

## Abstract

The Earth's forests are of great economic, ecological, and social importance, and sustaining them is paramount for mitigating climate change. To successfully sustain forests we must understand their internal demographic dynamics and their relationship to climate. In this thesis, I developed methods for investigating forest dynamics and understanding their relationship to climate. I applied these methods to data from the Alberta boreal forest and the oak forests of the Eastern United States. First, dendrochronological methods were used to develop a retrospective data set from the Alberta mixedwood boreal. This data was used to estimate white spruce mortality and construct mortality models based on either recent growth or competition. Both models classify dead or live spruce with 75% accuracy, indicating the potential of using more easily available competition data. Second, I developed a quantitative approach for predicting Alberta mixedwood demography as a function of tree size and competition predictors using a size-structured integral projection model (IPM). Two models were defined, one with competitive structure, and one without. Model projections were tested using independent data, and results show that the IPM with competitive structure better predicts annual size distribution. Implementation of the IPM presents technical challenges: IPMs must be numerically discretized, and the choice of integration scheme may lead to accuracy or efficiency loss. I analyzed several quadrature schemes for representative IPMs in the third part of the thesis. Results show that the midpoint method is often sufficient, but an Adjusted Gauss-Legendre method leads to higher accuracy. In the final part of the thesis I considered how climate is related to annual growth of chestnut oak in the the Eastern United States. Previously, trees growing in closed-canopy forests were not thought to produce ring-widths useable in climate reconstruction. However, by employing more advanced mathematical tools I used a network of oak forests to identify a strong enough precipitation signal to extend

the current meteorological record back 150 years. My thesis illustrates the importance of careful model formulation, implementation and validation in resolving climate and competition effects in forest dynamics.

## Acknowledgements

First and foremost, I would like to thank my supervisors Mark Lewis and Ken Stadt. I am so fortunate and grateful to have had the opportunity to work with two outstanding mentors with such complimentary areas of expertise. Not only do Mark and Ken excel as scientists, but they serve as excellent role models to their students, colleagues, and children. I have learned so much more from them than what is captured by this thesis.

I thank Mark for leading a supportive and successful research group. This environment has contributed in great part to my growth, and has helped me develop my confidence and communication skills, especially in science. To all the Lewis Research Group members, past and present, who have helped me along the way: I thank you. In particular, I would like to thank: Hannah MacKenzie, Caroline Bampfylde, Tomas de Camino Beck, Ulrike Schlägel, and Stephanie Peacock.

I thank Ken for having enough confidence in me to teach me the ways of field work. Your faith in me gave me the opportunity to do things I never anticipated doing with a math background, namely yielding a chainsaw for the sake of science.

I would not be where I am today without my supervisory committee which includes Narasimha Prasad, Peter Blenis, Phil Comeau, Ken Stadt and Mark Lewis. Thank you for taking time out of your busy schedules to provide guidance, feedback, and support over the years. Your experience and wisdom is much appreciated.

Thanks to the Jim Clark and the entire Clark Lab Group at Duke University where I spent a good part of the last two years. You all welcomed me without hesitation, and I will truly miss our lively discussions and your passion for ecological research.

Finally, I would like to thank those closest to me: my steadfast husband Matthew Emmett, and our daughter Sadie Emmett. You have provided me with endless support throughout this process. You are a constant reminder that there is greatness in life.

# Table of Contents

<b>1</b>	<b>Introduction</b>	<b>1</b>
<b>2</b>	<b>Predicting white spruce mortality from retrospective data: competition versus recent growth</b>	<b>12</b>
2.1	Introduction . . . . .	12
2.2	Methods . . . . .	15
2.2.1	Study area . . . . .	15
2.2.2	Sampling . . . . .	16
2.2.3	Identification of death year using Dendrochronological methods . . . . .	18
2.2.4	Stand density reconstruction . . . . .	18
2.2.5	Variables . . . . .	20
2.2.6	Mortality modeling . . . . .	22
2.2.7	Model assessment . . . . .	24
2.3	Results . . . . .	27
2.3.1	Stand and tree characteristics . . . . .	27
2.3.2	Dendrochronological methods . . . . .	29
2.3.3	Mortality rates . . . . .	30
2.3.4	Model fitting and interpretation . . . . .	30
2.3.5	Model validation and prediction . . . . .	31
2.4	Discussion . . . . .	33

<b>3</b>	<b>A multi-species integral projection model for the prediction of forest structure</b>	<b>58</b>
3.1	Introduction . . . . .	58
3.2	Materials and Methods . . . . .	63
3.2.1	Data . . . . .	63
3.2.2	Two-species IPM formulation . . . . .	64
3.2.3	Competitive interactions . . . . .	66
3.2.4	Fitting the redistribution kernel . . . . .	66
3.2.5	Assessing model projections . . . . .	70
3.2.6	Mixedwood forest scenarios . . . . .	71
3.3	Results . . . . .	72
3.3.1	Data summary . . . . .	72
3.3.2	Model selection . . . . .	73
3.3.3	Goodness of fit and model validation . . . . .	74
3.4	Discussion . . . . .	76
<b>4</b>	<b>A guide to efficient integration schemes for integral projection models (IPMs)</b>	<b>103</b>
4.1	Introduction . . . . .	103
4.2	Integration schemes . . . . .	106
4.2.1	Point based discretizations . . . . .	107
4.2.2	Cell based discretizations . . . . .	109
4.3	Sample IPM kernels . . . . .	112
4.3.1	Virtual kernel . . . . .	112
4.3.2	Shrub kernel . . . . .	113
4.3.3	Tree kernel . . . . .	113
4.4	Numerical results . . . . .	115
4.4.1	Virtual kernel . . . . .	116
4.4.2	Shrub kernel . . . . .	116

4.4.3	Tree kernel . . . . .	118
4.5	Discussion . . . . .	118
4.6	Acknowledgements . . . . .	122
<b>5</b>	<b>A tree-ring based reconstruction of early summer precipitation in southwestern Virginia (1750-1981)</b>	<b>133</b>
5.1	Introduction . . . . .	133
5.2	Materials and Methods . . . . .	135
5.2.1	Tree ring data . . . . .	135
5.2.2	Principal component analysis . . . . .	137
5.2.3	Climate data . . . . .	138
5.2.4	Reconstruction methods . . . . .	138
5.2.5	Model calibration and verification . . . . .	139
5.2.6	Reconstruction assessment . . . . .	140
5.3	Results . . . . .	140
5.4	Discussion . . . . .	143
<b>6</b>	<b>Discussion</b>	<b>172</b>
6.1	Retrospective data collection . . . . .	173
6.2	Management implications . . . . .	174
6.3	Forest competition . . . . .	175
6.4	The Importance of Interdisciplinary Collaboration . . . . .	176
6.5	Closing Remarks . . . . .	177
<b>A</b>	<b>Numerical considerations for the multi-species IPM</b>	<b>180</b>
1.1	Numerical implementation of the IPM and model projections . . . . .	180
1.2	Assessing domain eviction . . . . .	181

# List of Figures

2.1	Map of Alberta indicating the transect locations throughout the sampled natural subregions. Out of the 40 transects sampled, 21 fell in the Central Mixedwood Natural Subregion, 10 in the Lower Foothills, 5 in the Dry Mixedwood, and 4 in the Lower Boreal Highlands. . . . .	36
2.2	<b>A</b> Boxplots of tree diameters at breast height (DBH) for both the live and dead spruce groups. Note that on average the dead spruce DBH is smaller than the DBH of the live spruce. <b>B</b> Histogram of live tree diameters. Note that the distribution is positively skewed. <b>C</b> Histogram of dead tree diameters. Although this distribution is again positively skewed, not as much weight appears in the tail relative to the DBH distribution of the live trees. . . . .	37
2.3	Boxplots of the local competition measurements including only neighbors thicker than the subject tree for live and dead trees. Upper panel depicts spruce competition measured by the basal area of thicker spruce (SWBAGR), the number of thicker spruce (SWNGR), and the sum of diameters of thicker spruce (SWSDGR). Bottom panels depicts the competition from aspen measured by the basal area of thicker aspen (AWBAGR), the number of thicker aspen (AWNCR), and the sum of diameters of thicker aspen (AWSDCR). Note that there is little difference in experienced aspen competition between the live and dead groups relative to the difference seen in the experienced spruce competition. . . . .	38
2.4	Mortality rates for both stand reconstruction methods averaged over all years by latitudinal degree band. There appears to be only minor differences between the reconstruction methods, and both show increased mortality at higher latitudes. Despite this positive correlation between mortality rate and latitude, latitude was not found to be a significant predictor of spruce mortality. . . . .	39
2.5	Boxplots of <b>A</b> the average radial increase over the last two years (ARWI2) and <b>B</b> the average basal area increase over the last two years (ABAI2) for both live and dead trees. For both measures, on average the size increase of dead spruce is less than that of live spruce.	40

2.6	<b>A</b> Histogram showing the distribution of death years for sampled dead trees from all transects. The number of tree deaths decreased with decreasing year of death. <b>B</b> Histogram showing the time from stand establishment to tree death. Note that more than half of all trees deaths occurred 42-55 years after stand establishment. . . . .	41
2.7	Mortality rates averaged over all years by transect are shown with the 95% upper quantile. Error bars provide some indication of year-to-year variation within a given transect, while relative bar heights represent variation of the mean mortality among transects. Transects which had no dead spruce are those for which no error bars are visible. . . . .	42
2.8	Aggregate fit plot showing the survival probabilities for the data (black circles) plotted against decile bin midpoints of the average basal area increment over the last two years (ABAI2). Median model performance for the competition model (blue solid), and the growth model (red dashed) are indicated by the bold lines, while shading indicates the 95 % credible interval. Credible intervals are narrow, and the competition model provides a better fit across the ABAI2 covariate domain. . . . .	43
2.9	Aggregate fit plot showing the survival probabilities for the data (black circles) plotted against decile bin midpoints of the diameter at breast height (DBH). Median model performance for the competition model (blue solid), and the growth model (red dashed) are indicated by the bold lines, while shading indicates the 95 % credible interval. Except for the first decile, the data falls within the credible intervals of both models. . . . .	44
2.10	Aggregate fit plot showing the survival probabilities for the data (black circles) plotted against decile bin midpoints of the local number of larger trees per hectare (ALLNGR). Median model performance for the competition model (blue solid), and the growth model (red dashed) are indicated by the bold lines, while shading indicates the 95 % credible interval. Except in the case of very few competitors, data falls well within the credible intervals of both models. . . . .	45
2.11	Aggregate fit plot showing the survival probabilities for the data (black circles) plotted against decile bin midpoints of the June climate moisture index (juneCMI). Median model performance for the competition model (blue solid), and the growth model (red dashed) are indicated by the bold lines, while shading indicates the 95 % credible interval. Data falls well within the credible intervals of both models. . . . .	46

2.12	Aggregate fit plot showing the survival probabilities for the data (black circles) plotted against decile bin midpoints of the local basal area of larger spruce (SWBAGR) measured in m <sup>2</sup> /ha. Median model performance for the competition model (blue solid), and the growth model (red dashed) are indicated by the bold lines, while shading indicates the 95 % credible intervals. Data falls within the credible intervals of both models, except for the last decile, which falls outside the credible intervals of both models. . . . .	47
2.13	Odds ratios for parameters in the local competition survival model (DBH, SWBAGR, ALLNGR, and juneCMI; denoted by circles) and the recent growth survival model (logABAI2; denoted by squares). The 95% predictive intervals are indicated by error bars. An odds ratio greater than one indicates that an increase of a single unit in the considered covariate leads to an increase in survival odds, while a odds ratio value less than one indicates a unit increase of covariate leads to a decrease in survival odds. . . . .	48
2.14	ROC curves for the growth (solid line) and competition (dashed line) based survival models. The optimal thresholds identified are indicated by asterisks, with values of 0.983 (sensitivity of 0.74, specificity of 0.83) for the growth-based model, and 0.979 (sensitivity of 0.75, specificity of 0.71) for the competition-based model. The area under the curve (AUC) and associated 95% confidence intervals (CI) are 0.859 [0.841, 0.876] for the growth-based survival model, and 0.795 [0.772, 0.817] for the competition-based survival model, indicating excellent and good discrimination between live and dead classes respectively. . . . .	49
3.1	Provincial map of Alberta indicating the locations of retrospective sample plots and PSP location, with pertinent natural subregions indicated. . . . .	84
3.2	Spruce and aspen sample plot densities in stems per hectare for the retrospective data set, as measured at year of sampling. . . . .	85
3.3	Diameter distributions for spruce (left panel) and aspen (right panel) for the entire retrospective data set. . . . .	85
3.4	Spruce and aspen sample plot densities in stems per hectare for the PSP data set, as measured at initial year of sampling. Note that spruce densities are in general not as high as those in the retrospective data set, which is largely a reflection of the older stand ages of the PSP stands. . . . .	86

3.5	Diameter distributions for spruce (left panel) and aspen (right panel) for the entire PSP data set. The range of diameters is larger than those seen in the retrospective data set, and on average both spruce and aspen diameters are larger. This is again likely a result of the older stand ages of the PSP stands. . . . .	87
3.6	Spruce growth model summary plots for the model with (left panels) and without (right panels) competitive structure. Top panels show spruce size (DBH) as predicted by the best-fit linear growth model plotted against observed spruce size (points), as well as the reference line $y = x$ (grey line). Middle figures show histograms of the frequency of growth model residuals. Bottom panels show the growth variance $\sigma^2$ against size (points). The best-fit line is indicated (grey line), indicating that in both cases variance does not show significant size-dependence. . . . .	88
3.7	Average survival probabilities from the data (grey triangles) and best-fit model (open circles) plotted against survival model covariates for each of the twenty covariate data quantiles. Left panel shows the survival model with competitive interactions, while the right panel shows the survival model without. Average survival probability is plotted against: diameter at breast height ( $x$ ) in upper panel; sum of diameters of thicker spruce ( $S_1^*$ ) in middle panel; and basal area of thicker aspen ( $A_2^*$ ). . . . .	89
3.8	Aspen growth model summary plots for the model with (left panels) and without (right panels) competitive structure. Top panels show aspen size (DBH) as predicted by the best-fit linear growth model plotted against observed size (points), as well as the reference line $y = x$ (grey line). Middle figures show histograms of the frequency of growth model residuals. Bottom panels show the growth variance $\sigma^2$ against size (points). The best-fit line is indicated (grey line), indicating that in both cases variance does not show significant size-dependence. . . . .	90
3.9	Empirical and predicted size distributions (top panels) and cumulative density functions (bottom panels) for the IPMs with and without competitive structure for PSP 237 for the year 2000 based on model initialization using the 1988 empirical distribution. Note that visually there is little difference between the projection from the IPMs with and without competitive structure. In the case of aspen, constant mortality was assumed and therefore we do not expect a large difference between the two models – the only change between the two IPMs occurs in the kernel growth function. . . . .	91

3.10	Predicted and observed numbers of spruce and aspen for PSP 291. Model is reinitialized at each year for which there is data available. As expected, the IPM with competitive structure predicts higher spruce mortality than the IPM without competition. Aspen mortality is constant in both models, which is why aspen population numbers remain the same regardless of the model. . . . .	92
3.11	White spruce Kolmogorov-Smirnov (KS) statistic values for the IPM with competition plotted against those from the IPM without competition (grey points). Darker regions indicate dense regions of points. Reference line $y = x$ also shown. In 138 out of 154 cases, the KS statistic for the IPM with competition was smaller than for the IPM without competition, indicating that the IPM with competition performs better according to this metric. . . . .	93
3.12	Aspen Kolmogorov-Smirnov (KS) statistic values for the IPM with competition plotted against those from the IPM without competition (grey points). Darker regions indicate dense regions of points. Reference line $y = x$ also shown. In 142 out of 154 cases, the KS statistic for the IPM with competition was smaller than for the IPM without competition, indicating that the IPM with competition performs better according to this metric. . . . .	94
3.13	Observed versus number of spruce predicted by the model with competition, measured in stems per hectare. Solid blue line shows the line $y = x$ , and dashed red line shows the best-fit regression line. For a perfect model, all the points would fall along the dashed red line. . . . .	95
3.14	Observed versus number of aspen predicted by the model with competition, measured in stems per hectare. Solid blue line shows the line $y = x$ , and dashed red line shows the best-fit regression line. . . . .	96
3.15	Predicted stems per hectare shown for 30 years post-initialization year based on the IPM model with competitive structure. Predictions are made for each of the four cover classes: conifer (C), deciduous-conifer (DC), deciduous (D), and conifer-deciduous (CD). Note that the C and CD scenarios experience the highest spruce mortality. As indicated by the total population, after 30 years the DC stand has the highest density, followed by the CD and C which have approximately equal densities. . . . .	97

3.16	Predicted basal area in $m^2/ha$ shown for 30 years post-initialization year based on the IPM model with competitive structure. Predictions are made for each of the four cover classes: conifer (C), deciduous-conifer (DC), deciduous (D), and conifer-deciduous (CD). Here we see that although the C stand experiences the largest increase in spruce basal area over 30 years, it still has the smallest total basal area. The CD and D stands have the largest total basal area after 30 years as a result of the larger sizes of the aspen relative to the spruce. . . . .	98
4.1	Typical error vs mesh size / computational cost / runtime plot and how to interpret them. . . . .	123
4.2	Diagram of the GL( $k = 3$ ) discretization method with $N = 5$ sub-intervals on the interval $[L, U]$ . The dotted vertical lines depict the edges of the $N$ sub-intervals. The solid vertical ticks depict the locations of the quadrature points within each sub-interval (which in this case are the Gaussian quadrature points for $k = 3$ ). Increasing $k$ would result in more quadrature points within each sub-interval, while increasing $N$ would result in more sub-intervals across the domain. The entries of the projection matrix $A$ are determined by evaluating the kernel at the quadrature points and weighting them appropriately (eg, here $w_2$ is the second quadrature weight of the standard three-point Gaussian quadrature scheme). . . . .	124
4.3	Diagram of bin-to-bin discretization methods with $N = 5$ cells on the interval $[L, U]$ . The dotted vertical lines depict the edges of the $N$ bins/cells. Each particular bin-to-bin method (MP, INTB2B, GENB2B, Zuidema) has a particular way of approximating the double-integral to obtain the entries of the projection matrix $A$ . . .	124
4.4	Error of the total population and growth rate after 5 years vs computational cost for various integration methods and the Exact kernel. Note that the cell based methods (GENB2BGL(9), INTB2BGL(9), MidPoint and Zuidema) exhibit first order convergence and are much less accurate than the point-based methods, which are exceptionally accurate here. For a given level of accuracy, the MidPoint method is the fastest cell-based method (even if a larger mesh is required). . . . .	125
4.5	Error of the total population and growth rate after 5 years vs computational cost for various integration methods and the SHRUB kernel. Note that in all cases, except for the Adjusted Gauss Legendre method, each method performs poorly until a sufficiently large mesh is used due to the discontinuity in the fecundity term. . . . .	126

4.6	Error of the total population and growth rate after 5 years vs run time for various integration methods and the SHRUB kernel. Note that although the point based methods are easily vectorized and often exhibit faster run times than most of the cell based methods even though their computational complexity is similar. . . . .	127
4.7	Error of the total population and growth rate after 5 years vs computational cost for various integration methods and the SHRUB kernel with modified growth parameters. Note that even after modifying the growth parameters to simulate a slow-growing species, the midpoint method still performs quite well once the discontinuity is resolved, and that the Adjust Gauss Legendre method is still extremely accurate. . . . .	128
4.8	Error of the total population and growth rate after 5 years vs computational cost for various integration methods and the TREE kernel. Note that the bin-to-bin methods (except the Zuidema method) perform well for small mesh sizes as they are able to resolve slow growth more effectively than the MidPoint method. . . . .	129
4.9	Code snippets for computing only the dominant eigen-value of a matrix $A$ using ARPACK. . . . .	130
5.1	Regional chronology sample locations. . . . .	152
5.2	Plots of the five chronologies used in the principal component analysis. The top panel shows the chronology built from the sample data at Brush Mountain (BM), while the others are the regional chronologies from Lynn Hollow (LH), watchdog Mountain (WD), Craig Creek (CC), and Otter Creek (OC). . . . .	153
5.3	Top: Scatter plot of the loadings for the five chronologies analyzed in the first PCA which covered the period 1845-1981. Bottom: Scatter plot of the loadings for the five chronologies analyzed in the second PCA which covered the period 1750-1981. . . . .	154
5.4	Sample depth by each year for the growth proxy obtained from the nested principal component analysis. The dashed line indicates the principal component which contained the years 1750-1844 with only four chronologies (WD, LH, CC, and OC), while the solid line indicates the principal component resulting from the analysis which used all five chronologies (BM, WD, LH, CC, and OC) and covered the years 1845-1981. . . . .	155

5.5	Top: Correlation between the growth proxies (BM or PC1) and the monthly precipitation from previous April (pA) through December (D) as well as for average May and June (aMJ). Middle: Correlation between the growth proxies (BM or PC1) and average PDSI from previous April (pA) through December (D) as well as for average June and July (aJJ). Bottom: Correlation between the growth proxies (BM or PC1) and average monthly temperature from previous April (pA) through December (D). . . . .	156
5.6	Correlation map showing the correlation between the first principal component and averaged May-June precipitation. Stars indicate the locations of the sites where the tree-rings used to develop the contributing chronologies were sampled. . . . .	157
5.7	A 31-year windowed correlation plot showing the correlations between each growth proxy (chronologies and first principal component) and mjPR. Correlation points are plotted above the window centers. The dashed line indicates the 95% significance level of 0.355.	158
5.8	Average May-June precipitation (mjPR) reconstruction (grey curve), smoothed estimate showing decadal-scale variable (black curve), and the reconstruction 95% credible interval (shaded grey region).	159
5.9	Periodogram showing periodicity of high amplitude at approximately 11, 17, and 24 years. . . . .	160
5.10	Time series plots showing annual- and decadal-scale variability for the mjPR and six compared moisture reconstructions for the period 933-2008. . . . .	160
5.11	Time series plots showing annual- and decadal-scale variability for the mjPR and six compared moisture reconstructions for the period 1745-1985. . . . .	161
5.12	The standardized mjPR (black lines) and Cook PDSI (grey lines) reconstructions are plotted against time to highlight both the similarities and the differences. The top panel shows the standardized reconstructions at an annual scale, while the bottom panel shows 5-year smoothed time series to better highlight the decadal-scale variability. Particularly notable differences include the year 1774, and the interval 1855-1863. . . . .	162
5.13	The mjPR reconstruction (top panel) and the mjPR instrumental record (bottom panel). Lines show the best-fit regression line through the time series data to indicate any dominant trends. Areas falling above the best-fit lines and the time series data are shaded grey to indicate periods of higher precipitation. Note the correspondence of wetter and drier years between the top and bottom panels. . . . .	163

5.14	A representation of how the mjPR reconstruction and the mjPR instrumental record are changing with respect to each other. Top panels show a black dot if both time series were increasing or decreasing from the previous year to the year indicated, while the grey dots indicate that the time series changes are not synchronous. Time series show synchronous behavior with respect to this measure in 72% of the years. Bottom panel shows a black dot if both time series are either above or below their respective best-fit trend lines, while the grey dots indicate asynchronous behavior. Time series show synchronous behavior with respect to this measure in 65% of the years. . . . .	164
5.15	A 31 year windowed correlation plot between the mjPR and Cook PDSI reconstructions shows the discrepancy during the 1855-1863 interval. In the top panel correlation values are plotted about window centers, while the bottom panel shows the corresponding p-value (black) as well as the line of significance (dashed). . . . .	165
5.16	A 31 year windowed correlation plot between each of the chronologies and the Cook PDSI reconstruction. Note the interval of abrupt poor correlation during the years 1855-1863. . . . .	166

# List of Symbols and Abbreviations

## Field measurements and tree mortality

MGM	Mixedwoot Growth Model .....	3
GYPSY	Growth and Yield Projection System .....	3
PSP	Permanent Sample Plot .....	4
GDD	Growing degree days .....	16
DBH	Diamter at breast height .....	16
H	Height .....	16
BAF	Basal area factor .....	17
$t$	Time (year) .....	20
ARWI	Average ring width increment .....	21
ABAI	Average basal area increment .....	21
CMI	Climate moisture index .....	22
PET	Potential evapotranspiration .....	22
PDF	Probability density function .....	23
$w_i$	Sampling weight (transect) .....	24
DIC	Deviance information criterion .....	24
PL	Predictive loss .....	24
ROC	Receiver operator curve .....	24
HL	Hosmer-Lemeshow statistic .....	24
AUC	Area under the ROC curve .....	25
BAGR	Basal area (greater than) .....	31
SDGR	Sum of diameters (greater than) .....	31
NGR	Density (greater than) .....	31
BA	Basal area .....	31
SD	Sum of diameters .....	31
N	Density .....	31
SWBAGR	Spruce basal area in thicker trees .....	31
ALLNGR	Density of all thicker species .....	31
cmiJune	June climate moisture index .....	31
logABAI2	Logarithm of ABAI over the past two years .....	31

## Integral projection models

IPM	Integral Projection Model	4
$n_m(x, t)$	Density of species $m$ individuals of size $x$ at time $t$	61
$x$	Individual size (DBH)	61
$y$	Individual size (DBH)	61
$k_m$	IPM kernel for species $m$	61
$L$	Lower bound of IPM (smallest individual size)	61
$U$	Upper bound of IPM (largest individual size)	61
$\mathbf{n}_m^t$	Discrete density of species $m$ individuals at time $t$	65
$S_1^*$	Sum of diameters of thicker spruce	68
$N_m^*$	Density of thicker species $m$	68
$A_2^*$	Area of thicker aspen	69
KS	Kolmogorov-Smirnov statistic	70
MSEP	Mean square error of predictions	70
MC	MSEP bias error	71
SC	MSEP model and observation variances	140
RC	MSEP random error	71
C	Conifer group	71
D	Deciduous group	71
CD	Conifer and deciduous group	71
CD	Deciduous and configer group	71
$N$	Mesh size	106
$A$	Discrete projection matrix	106
$GL(k)$	Sub-interval based Gauss-Legendre method	108
$CC(k)$	Sub-interval based Clenshaw-Curtis method	109
$AGL(k)$	Self-adjusting sub-interval based Gauss-Legendre method	109
MP	Midpoint method	140
$INTB2BGL(k)$	Integrable bin-to-bin Gauss-Legendre method	111
$GENB2BGL(k)$	Generalized bin-to-bin Gauss-Legendre method	111
ZB2B	Zuidema bin-to-bin method	112

## Climate reconstruction

PCA	Principle component analysis	135
ARMA	Autoregressive and/or moving average	136
BM	Brush Mountain	137
EPS	Expressed population signal	137
PDSI	Palmer Drought Severity Index	138
MCMC	Markov Chain Monte Carlo	138
MSE	Mean squared error	139
RE	Reduction of error	139
CE	Coefficient of efficiency	139
$r^2$	Squared correlation	139

GLK	Gleichläufigkeit score .....	139
NADA	North American Drought Atlas .....	140
JT	July PDSI reconstruction for Virginia and North Carolina	140
NC	North Carolina .....	140
SC	South Carolina .....	140
GA	Georgia .....	140
MP	Early summer anomalies .....	140
mjPR	May-June precipitation .....	140
jjPDSI	June and July PDSI .....	140
LH	Chronology .....	140
WD	Chronology .....	140
CC	Chronology .....	140
OC	Chronology .....	140

# Chapter 1

## Introduction

Climate models predict that by the end of the 21st century there will be substantial warming in temperature extremes (IPCC, 2007). Heavy rainfall events are also predicted to increase on a global scale (IPCC, 2007). How this changing climate will affect the earth's ecosystems has been a prominent question in the scientific community since the acknowledgement of global warming (Walther et al., 2002; Falkowski et al., 2000). However, there is no consensus on the implications that a changing climate can have on forest and animal communities (Malcolm et al., 2002; Scheller and Mladenoff, 2005; Zhu et al., 2012).

While many have shown that it is likely that increased temperatures will cause organisms to migrate in the polar directions, others studies show home range contractions (Walther et al., 2002; Zhu et al., 2012). In particular, the earth's forested landscape plays a significant role in this unraveling story – published averages for combined above and below ground carbon are about 400 tons per hectare (t/ha) in boreal forests, 150 t/ha in temperate forests, and 250 t/ha in tropical forests (Dixon et al., 1994). Globally, the carbon sequestered by forests amounts to approximately 90% of all above-ground terrestrial carbon, and 40% of all below-ground terrestrial carbon (Waring et al., 1985). Whether the combination of increased atmospheric carbon dioxide, deforestation, and increased tree mortality risks will amplify or dampen climate change is still undetermined (Bonan, 2008). For this reason, it is necessary for the scientific community to work towards a deeper understanding of forest ecosystems. This endeavor requires the use and interfacing of ecological, mathematical, and statistical tools. This thesis focusses on the application of mathematical and statistical tools to further our understanding of forest systems, and on the importance of the correct application of such tools.

The majority of this thesis deals with the mixedwood boreal forests of Alberta. The boreal forest is the world's largest biome, which comprises 29% of the world's forest cover (ECE, 1985). Approximately 300 million hectares of this boreal biome lies within Canada (McCullough et al., 1998), a country which boasts the largest area of certified forest in the world, and is considered an international leader in sustainable forest management planning (Canadian Council of Forest Ministers, 2013). The forest industry is of particular importance in Alberta, where it remains the third largest economic sector (Alberta Forest Products Association, 2013). Of the forested land falling within the province, the mixedwood boreal forests are the most fertile and productive, and are composed primarily of white spruce and trembling aspen, although stands may also contain a variety of other native boreal species (Chen and Popadiouk, 2002). Managers are typically focussed on the preservation of the long-term productivity and natural diversity occurring in these mixtures, and rely on growth and yield models to help them achieve this goal.

Forest models are a great asset to managers because they provide the ability to not only predict yield outcomes, but to assess the outcomes of different silvicultural treatments. In addition to helping managers plan for the future, forest models can also be used to address questions in forest ecology. To make use of a forest growth and yield model, some initial data that provides a description of the focus stand is required. In Alberta, this data is typically available from performance surveys conducted in every cutblock, and, in most jurisdictions, in the ground survey data supporting regular inventories. There are many different approaches that have been used to construct forest growth models, but they are commonly grouped as being individual tree, whole stand, or size class models (Vanclay, 1994). Individual tree models consider the tree as the basic model unit, and require a list of tree sizes as the minimum initial input. Individual tree models range in complexity: some include detailed sub-models describing tree architecture and carbon allocation, while some model growth at a coarser scale. Whole stand models consider the modelling unit to be the stand, and model components predict stand basal area and volume over time, as well as more basic measures such as tree density and canopy height. Individual trees are not tracked in this type of model, but some information about size distributions may be inferred. Size class models focus on modelling structural stand changes, and the idea is to separate trees into classes based on size, where submodels determine movement between classes. For a more detailed introduction to forest models, I refer readers to Vanclay (1994).

Most models consist of several components which describe the demographic pro-

cesses of growth, mortality, and recruitment. Growth and mortality can be easily measured in the field, while recruitment data is more difficult to collect and therefore recruitment functions differ widely in their level of process detail: some models include seed production through to germination, while some consider only the rate of ingrowth of juvenile trees.

The purpose of a model may be for the purpose of prediction or of understanding, or some combination therein, and the model purpose can help determine the complexity required (Vanclay, 1994) . Prediction models may allow for the omission of some process details, whereas these details may be required in a model built to improve understanding. Typically forest managers are concerned with prediction accuracy to support calculation of sustainable timber supply.

Forest models are generally species or region specific, and in the Alberta mixed-wood boreal forest, the region of focus for Chapters 2 and 3 in this thesis, there are two forest models that are commonly used by managers. The Mixedwood Growth Model (MGM) is an individual tree, distance-independent growth and yield model applicable to both pure and mixed stands composed primarily of aspen and spruce in the western boreal forest (Bokalo et al., 2013). MGM also has the ability to generate yield tables, where volume is equal to the sum of tree volumes. According to sub-models developed for juvenile, mid-rotation, and old-growth classes, growth and survival are determined by species and social class of each tree. MGM requires a stand or tree list containing tree-level measurements of height, diameter, age, and expansion factor (1/plot size) from a representative plot as well as site index as user-defined initial conditions. In the case that a tree-list is not available, one may be simulated according to desired conditions. MGM also includes tools to thin, herbicide or partially harvest stands, and a routine to evaluate shade cast by surrounding stands (to deal with strip-cut harvest systems), using the spatial info from a block layout file (eg. a list of polygons and what trees are in them).

GYPSY is used more routinely to model forest development in the mixedwood boreal, and is considered a whole-stand model because it does not track individuals (Huang et al., 2009). Both spatial and non-spatial variants of GYPSY exist, and at a minimum require site index, age, density, and percent stocking (number of 10 m<sup>2</sup> plots with the presence of a species is a measure of spatial pattern when coupled with density) to run the model. As with MGM, GYPSY is composed of sub-models that predict top height, density, basal area increment, and volume. Since it is a whole-stand model, GYPSY is designed to produce unbiased stand volume estimates for a given stand-age. However, it is less able to deal with complex stands created by partial cutting, pulsed herbicide application, thinning,

or with partial overstory death due to insects such as the mountain pine beetle.

Other theoretical approaches used to model forest dynamics that are relevant to this thesis include size class models. The most familiar size class model is the matrix model, where trees are categorized into discrete classes based on size (Silvertown et al., 1993; Lytle and Merritt, 2004). In this thesis I consider an extension of the matrix model referred to as the integral projection model (IPM) where tree demography depends continuously on size. This model has previously been applied to tree populations (Zuidema et al., 2010), but not to the boreal forest. Other approaches previously taken include the use of a Fokker-Plank drift-diffusion partial differential equation to model structural changes in a population (Kohyama, 1991), and integral-differential equations formulated as an optimization problem to determine the optimal forest management scenario after considering intra-specific competition and carbon sequestration (Hritonenko et al., 2008).

Both MGM and GYPSY are based on permanent sample plot (PSP) data which currently lacks data in the mid-rotation 30-70 year range. This implies limited confidence in the predictive abilities of these models for forests developing through this age bracket. In particular, white spruce mortality data within this age range is lacking. This thesis addresses this issue through targeted collection of data to fill this gap and the construction of mortality and multi-species size class models based on this new data.

The key questions addressed in this thesis are:

- What is the strength and importance of competition in a closed-canopy forest with complex structure?
- Does competition in the mixedwood boreal forest impact spruce and aspen demography?
- What are the repercussions of using a sub-optimal integration scheme to implement an IPM?
- Do stand dynamics (i.e. competitive interactions) obscure the relationship between annual growth and climate?

In particular, Chapter 2 of this thesis was motivated by a pressing need to better quantify mid-rotation spruce mortality in the mixedwood boreal. Previous studies have estimated background spruce mortality, but these estimates are typically based on limited PSP data (Feng et al., 2006). The lack of age-appropriate data

has prevented confirmation of these estimates. A goal of this project was to address the lack of data through a large-scale sampling effort, and to use this data to generate overall spruce mortality estimates.

Traditionally, growth and yield data collection has been limited to PSP sampling, which involves the designation of a fixed sample plot, and collection of successive measurements on all individuals in the plot area. Re-measurements are typically completed every 5-10 years, which makes it difficult to identify mortality events at an annual scale. Here, I use a sampling approach based on the principles of dendrochronology referred to as retrospective sampling. Trees growing in regions with seasonal variation produce annual rings, and ring formation is directly affected by climatic variation. When trees grow close together, they experience the same weather conditions, and therefore produce rings that are similar in terms of relative magnitude. For example, trees that experience a growing season with lower than average precipitation may all exhibit reduced growth. This common response to climate allows us to identify favorable and unfavorable growth years among individuals, and in particular to determine the year of death of a dead tree given a representative time series of ring widths from nearby live trees. By taking samples from trees to obtain ring width time series in a defined transect, and using methods in dendrochronology, I am able to reconstruct the stand history. In addition to the data obtained via dendrochronological methods, I record local neighborhood competition for a randomly selected group of live trees in each transect, as well as for all the dead spruce in a transect. These competitive neighborhoods can also be retrospectively estimated. Sampling and data processing protocol are discussed in greater detail in Chapter 2.

The new retrospective data set was subsequently used to fit two spruce mortality models, also described in Chapter 2. Tree mortality is difficult to characterize because it is often the result of cumulative complicated mechanisms (Franklin et al., 1987). Ultimately a tree dies when the balance between photosynthesis and respiration is negative for too long, or if growing buds are removed or killed, all of which leads to diminished carbohydrate production. Specific physiological mechanisms leading to tree mortality are still poorly understood, although carbon starvation and hydraulic failure theories have been debated in recent literature (McDowell, 2011).

Mortality is often the culmination of prolonged stress, during which carbohydrate allocation priorities typically shift away from radial thickening (Waring, 1987). As a result, it is not surprising that reduced radial growth has been shown to be an indicator of increased mortality risk (Kobe and Coates, 1997; Bigler and Bugmann,

2003; Wyckoff and Clark, 2000). One of the causes of stress is competition for resources between neighbors, and this local competition has also been shown to be a predictor of mortality risk in some regions (Dawson et al., 2013).

One of the questions addressed in Chapter 2 is whether a survival model based on local neighborhood predictors is as effective as a survival model based on recent growth. Additionally, I test the significance of the effects of climate on spruce mortality using climate data interpolated from weather station data using the BioSim model (Régnière et al., 1995). Drought has been shown to lead to increased mortality in the boreal forest (Peng et al., 2011), therefore in addition to temperature and precipitation, I also test the climate moisture index (CMI) (Hogg, 1994, 1997). CMI can be thought of as the site water balance, determined roughly by precipitation minus evapotranspiration.

Tree size has also been shown to be a predictor of individual demographic rates, although stand composition and structure, edaphic characteristics, and climate also influence these rates (Kunstler et al., 2009; Hurst et al., 2011). A key question in the mixedwood boreal is how competition both between and within species affects stand composition and structure. More specifically, can species be modelled independently of each other? Or, are the complex ecophysiological processes so interdependent that they must be modelled simultaneously?

In Chapter 3 I build a two-species IPM to determine if this population model holds promise for the boreal forest, and to test the importance of competitive interactions. The IPM models change in population structure and density over time given an initial population size distribution, and is particularly attractive because it allows growth, survival, and fecundity (if included), to be modelled as a continuous function of tree size, while time is kept discrete. Discrete time works well for boreal tree species, where growing seasons are distinctly demarked by the formation of annual rings. In an IPM, how a population changes through time is determined by the redistribution kernel. In Chapter 3, two types of kernels are considered: those which include competitive structure which leads to a coupled pair of IPMs (one for aspen and one for spruce), and those which depend only on size of an individual. The latter kernels equate to using a single-species model with the assumption that the presence of other species has no effect on the subject species. What is particularly novel in Chapter 3 is the ability to use two independent data sets to fit and test the models respectively.

The projection and analysis of the IPM requires that the model be numerically implemented, which can pose challenges that stem from the numerical quadrature

scheme employed. Challenges include computational inefficiency and lack of accuracy. The midpoint method has often been the method of choice in previous numerical implementations of the IPM. The midpoint method is relatively easy to implement, and in most cases will provide sufficiently accurate results if an appropriate mesh size is chosen. However, some kernels present problems and may require alternative numerical schemes. The challenges of numerical implementation have been recognized in the literature (Easterling et al., 2000; Rees and Ellner, 2009), although no comprehensive analysis of suitable methods has been performed. Zuidema et al. (2010) recognized this issue when working with a kernel used to model long-lived slow-growing trees, and overcame the issues by employing a modified scheme using subintervals to approximate function values within bins with edges defined by mesh points. In Chapter 4, the efficiency and accuracy of a variety of integration schemes is assessed for three different kernels, two of which are inherently difficult to integrate. Recommendations that specify the appropriateness of different schemes for kernels that exhibit certain mathematical features are presented.

In Chapter 5, the focus returns to methods in dendrochronology and dendroclimatology. As established above, tree ring width formation is influenced by the weather experienced, and trees which grow in close proximity to one another experience similar weather. If the relationship between a driving weather variable and tree ring growth is sufficiently strong, it is possible to exploit this relationship and use the tree ring data to make inference about past climate. The actual climate drivers that correlate most strongly with ring width increments vary by species and by region. However, climate is not the only factor which determines radial increment. As shown in Chapters 2 and 3, competitive interactions can influence tree demography, and in particular radial growth. Trees that are most limited by climate are deemed to be the best candidates for climate reconstructions. As such, trees growing in a closed-canopy stand where stand dynamics play an important role in the development of stand structure are frequently not considered as candidates for climate reconstructions. However, if the climate signal can be identified, at least in part, then climate reconstructions based on closed-canopy stands are possible. Chapter 5 focusses on the oak-dominated mixedwood forests in the Eastern US. Using data from several sites throughout the Eastern US, I show that there is a strong relationship between early summer precipitation and ring width size, and use this relationship to reconstruct average May-June precipitation for 150 years prior to the available instrumental record.

Finally, in Chapter 6, the main results of the preceding thesis chapters are sum-

marized and discussed, and future directions as well as general concluding remarks are presented.

Throughout the thesis, I address questions in applied forest ecology using mathematical and statistical tools to analyze and interpret data. In the first portion of the thesis (Chapter 2 and 3), key questions about competition, growth, and mortality processes in the Alberta mixedwood boreal forest are addressed. In Chapter 2, the retrospective data set is used to parametrize two competing spruce mortality models – one based on recent growth, and one on local competition. The performance of both models is assessed and compared, and shows that local competition can indeed be used as a predictor of spruce mortality. In Chapter 3 I formulate and analyze a two-species IPM and its effectiveness as a forest modelling tool, and consider the importance of competition. As expected, competition does play an important role in determining forest structure, but perhaps not as a great a role as one would think. Models are fitted and validated using independent data sets using methods that have not previously been used to assess IPM validity. The dependence of results from an IPM on the numerical implementation is investigated in Chapter 4. The importance of the choice of numerical integration scheme has been recognized by IPM users, and this chapter provides a thorough analysis and comparison of several integration methods for selected kernels that contain inherent numerical difficulties. Chapter 4 shows that the integration scheme used may matter in some cases, but in many cases the commonly used midpoint method with a sufficiently large mesh will perform as well as other methods. Finally, in Chapter 5 I show that annual growth data from trees in a closed-canopy oak forest data can be linked to early summer precipitation, and that the link is strong enough to allow me to reconstruct early summer precipitation for 150 years prior to initial year of the meteorological record.

Ultimately, the goal of this thesis is to further our understanding of forest processes, and their relation to competition and climate, using mathematical and statistical modeling. Models developed in this thesis will provide forest managers with improved tools for prediction of stand development, and are a step towards disentangling and quantifying complex forest processes with the hope of being able to eventually mitigate the effects of climate change on the earth's forests.

# Bibliography

- Alberta Forest Products Association. Facts and figures. [http://www.afpa-courses.com/industry/facts\\_figures.aspx](http://www.afpa-courses.com/industry/facts_figures.aspx), 2013. Accessed: 01/02/2013.
- Bigler, C. and Bugmann, H. Growth-dependent tree mortality models based on tree rings. *Canadian Journal of Forest Research*, 33(2):210–221, 2003.
- Bokalo, M., Stadt, K.J., Comeau, P.G., and Titus, S.J. The validation of the mixedwood growth model (MGM) for use in forest management decision making. *Forests*, 4(1):1–27, 2013.
- Bonan, G. Forests and climate change: forcings, feedbacks, and the climate benefits of forests. *Science*, 320(5882):1444–1449, 2008.
- Canadian Council of Forest Ministers. Integrated forest land-use planning. <http://www.sfmcanada.org/english/pubs.asp>, 2013. Accessed: 01/02/2013.
- Chen, H. and Popadiouk, R. Dynamics of North American boreal mixedwoods. *Environmental Reviews*, 10(3):137–166, 2002.
- Dawson, A., Stadt, K., and Huang, J. Predicting white spruce mortality from retrospective data: competition versus recent growth. *In preparation*, 2013.
- Dixon, R., Brown, S., Houghton, R., Solomon, A., Trexler, M., et al. Carbon pools and flux of global forest ecosystems. *Science*, 263(5144):185–189, 1994.
- Easterling, M., Ellner, S., and Dixon, P. Size-specific sensitivity: applying a new structured population model. *Ecology*, 81(3):694–708, 2000.
- ECE, U. *The Forest Resources of the ECE region (Europe, the USSR, North America)*. ECE, FAO, 1985.
- Falkowski, P., Scholes, R., Boyle, E., Canadell, J., Canfield, D., et al. The global carbon cycle: a test of our knowledge of earth as a system. *Science*, 290(5490):291–296, 2000.
- Feng, Z., Stadt, K.J., and Lieffers, V.J. Linking juvenile white spruce density, dispersion, stocking, and mortality to future yield. *Canadian Journal of Forest Research*, 36:3173–3182, 2006.

- Franklin, J., Shugart, H., and Harmon, M. Tree death as an ecological process. *BioScience*, pp. 550–556, 1987.
- Hogg, E. Climate and the southern limit of the western Canadian boreal forest. *Canadian Journal of Forest Research*, 24(9):1835–1845, 1994.
- Hogg, E. Temporal scaling of moisture and the forest-grassland boundary in western Canada. *Agricultural and Forest Meteorology*, 84(1):115–122, 1997.
- Hritonenko, N., Yatsenko, Y., Goetz, R.U., and Xabadia, A. Maximum principle for a size-structured model of forest and carbon sequestration management. *Applied Mathematics Letters*, 21(10):1090–1094, 2008.
- Huang, S., Meng, S., and Yang, Y. A growth and yield projection system (GYPSY) for natural and post-harvest stands in Alberta. Tech. rep., Alberta Sustainable Resource Development, Edmonton, Alberta, 2009.
- Hurst, J., Allen, R., Coomes, D., and Duncan, R. Size-specific tree mortality varies with neighbourhood crowding and disturbance in a montane *nothofagus* forest. *PLoS One*, 6(10):e26670, 2011.
- IPCC. Climate change 2007: the physical science basis. In S. Solomon, D. Qin, M. Manning, Z. Chen, M. Marquis, K. Averyt, M. Tignor, and H. Miller (eds.), *Contribution of Working Group I to the Fourth Assessment Report of the Intergovernmental Panel on Climate Change*. Cambridge University Press, 2007.
- Kobe, R. and Coates, K. Models of sapling mortality as a function of growth to characterize interspecific variation in shade tolerance of eight tree species of northwestern British Columbia. *Canadian Journal of Forest Research*, 27(2):227–236, 1997.
- Kohyama, T. Simulating stationary size distribution of trees in rain forests. *Annals of Botany*, 68(2):173–180, 1991.
- Kunstler, G., Coomes, D., and Canham, C. Size-dependence of growth and mortality influence the shade tolerance of trees in a lowland temperate rain forest. *Journal of Ecology*, 97(4):685–695, 2009.
- Lytle, D. and Merritt, D. Hydrologic regimes and riparian forests: a structured population model for cottonwood. *Ecology*, 85(9):2493–2503, 2004.
- Malcolm, J., Markham, A., Neilson, R., and Garaci, M. Estimated migration rates under scenarios of global climate change. *Journal of Biogeography*, 29(7):835–849, 2002.
- McCullough, D., Werner, R., and Neumann, D. Fire and insects in northern and boreal forest ecosystems of North America. *Annual Review of Entomology*, 43(1):107–127, 1998.
- McDowell, N. Mechanisms linking drought, hydraulics, carbon metabolism, and vegetation mortality. *Plant physiology*, 155(3):1051–1059, 2011.

- Peng, C., Ma, Z., Lei, X., Zhu, Q., Chen, H., et al. A drought-induced pervasive increase in tree mortality across Canada's boreal forests. *Nature Climate Change*, 1(9):467–471, 2011.
- Rees, M. and Ellner, S. Integral projection models for populations in temporally varying environments. *Ecological Monographs*, 79(4):575–594, 2009.
- Régnière, J., Cooke, B., and Bergeron, Y. BioSIM: user's manual. 1995.
- Scheller, R. and Mladenoff, D. A spatially interactive simulation of climate change, harvesting, wind, and tree species migration and projected changes to forest composition and biomass in northern Wisconsin, USA. *Global Change Biology*, 11(2):307–321, 2005.
- Silvertown, J., Franco, M., Pisanty, I., and Mendoza, A. Comparative plant demography—relative importance of life-cycle components to the finite rate of increase in woody and herbaceous perennials. *Journal of Ecology*, pp. 465–476, 1993.
- Vanclay, J.K. *Modelling forest growth and yield: applications to mixed tropical forests*. CAB International, 1994.
- Walther, G., Post, E., Convey, P., Menzel, A., Parmesan, C., et al. Ecological responses to recent climate change. *Nature*, 416(6879):389–395, 2002.
- Waring, R. Characteristics of trees predisposed to die. *BioScience*, pp. 569–574, 1987.
- Waring, R., Schlesinger, W., et al. *Forest ecosystems: Concepts and management*. Academic Press, 1985.
- Wyckoff, P. and Clark, J. Predicting tree mortality from diameter growth: a comparison of maximum likelihood and Bayesian approaches. *Canadian Journal of Forest Research*, 30(1):156–167, 2000.
- Zhu, K., Woodall, C., and Clark, J. Failure to migrate: lack of tree range expansion in response to climate change. *Global Change Biology*, 2012.
- Zuidema, P., Jongejans, E., Chien, P., During, H., and Schieving, F. Integral projection models for trees: a new parameterization method and a validation of model output. *Journal of Ecology*, 98(2):345–355, 2010.

## Chapter 2

# Predicting white spruce mortality from retrospective data: competition versus recent growth<sup>1</sup>

### 2.1 Introduction

Mortality is one of several key processes in forest stand development, yet it is difficult to quantify and model robustly from establishment to old-growth. Mortality can lead to changes in tree demography, which in turn can initiate changes in carbon, energy, and water budgets at both site and regional levels (Peng et al., 2011). Mortality is also one of the drivers of forest succession, which is particularly important in mixed-species stands. Causes of mortality include exogenous factors such as fire, insect outbreak, disease, and environmental change, as well as endogenous factors such as competition for resources or senescence (Hogg et al., 2008; Peng et al., 2011). In the Canadian boreal forest, competition among individuals plays a key role in establishing forest structure in the mid-aged stem exclusion and canopy transition phases (Chen and Popadiouk, 2002). This competition among individuals manifests itself as reduced radial and height growth (Lieffers and Stadt, 1994; Wright et al., 1998), and continued tree suppression puts an individual at a higher risk of mortality (Kobe et al., 1995; Kobe and Coates, 1997). In this study,

---

<sup>1</sup>A modified version of the chapter titled “Predicting white spruce mortality from retrospective data: competition versus recent growth” is in preparation for submission to *Ecological Modelling*.

I further our understanding of mixedwood dynamics by examining the effects of mixedwood competition, growth, and climate on spruce mortality in mid-aged boreal forests of Canada.

Competition is generally considered to be a major contributor to tree mortality in the Canadian boreal forest (Yang et al., 2003). In addition, drought has been shown to be another major cause (Hogg and Wein, 2005; Peng et al., 2011). With potential future climate warming, tree mortality rates in western Canada are predicted to be more severe than those in eastern Canada (Peng et al., 2011). These potentially high mortality rates cause local changes in ecosystem processes including compositional, structural, and productivity changes which may lead to global repercussions from the change in boreal carbon storage capabilities (Pachauri and Reisinger, 2007). To mitigate these potential effects, it is critical to understand how both competition and climate affect stand structure in the boreal mixedwood forests.

In the mixedwood boreal, the limited understanding of tree mortality can be largely attributed to the lack of data, especially for mid-aged forests. Considerable effort has been placed on the development and maintenance of permanent sample plots (PSP), but the data obtained from these plots is not ideal for the understanding and modeling of tree mortality. Most of the plots in the western Canadian boreal are either in near-mature to old-growth stands of natural origin, established to guide the choice of harvest age for optimal productivity (e.g. ASRD (1995a)), or in young stands of harvest-origin with various regeneration treatments, established to demonstrate early post-harvest stand development (e.g. ASRD (1995b)). As a result, there are few plots in the 25 to 50 age range. Further, the resolution of PSP re-measurements is not annual, but follows a 2-15 year cycle in the boreal (Yang et al., 2003). Older plots are measured less frequently to ensure growth exceeds measurement error (Vanclay, 1999). Mortality is often assumed to be constant throughout the re-measurement interval (Yang et al., 2003), which may lead to a misinformed understanding of the processes causing mortality. Critical climate events, for instance, may have a shorter cycle than the re-measurement interval.

To address the lack of mid-age mortality data on white spruce and overcome shortcomings encountered with traditional PSP sampling, I employed a retrospective sampling approach (Biondi, 1999; Metsaranta and Lieffers, 2009). This approach makes use of crossdating techniques to estimate year of death of dead individuals, thereby allowing us to reconstruct past spruce density as well as individual annual growth increment. Using this retrospective technique has the advantage that it is fairly quick – sampling a transect can be completed in 1-2 days, and sample pro-

cessing can be completed over a few weeks depending on the size of the transect. One shortcoming of this method is that it is difficult to define precisely how far back in time one can reconstruct because of variable stem decomposition rates. A recent study has suggested that it is possible to reconstruct conifer stand structure for approximately 50 years prior to the current year in the boreal (Metsaranta et al., 2008).

Typical moist upland sites in the western mixedwood boreal forest are dominated by two tree species, white spruce [*Picea glauca* (Moench) Voss] and trembling aspen [*Populus tremuloides* Michx.], whose long-term growth interactions have been quantified using primarily older PSP data (Huang et al., 1992; Meng et al., 2008; Nunifu, 2009; Kabzems and García, 2004; Osika et al., 2013). After disturbance, aspen is quick to colonize the site, and usually dominates the stand for extended periods. White spruce establishment is dependent on several factors, including the occurrence of a mast-year and seedbed receptivity (Peters et al., 2005). In the appropriate conditions, the shade-tolerant spruce establish in the understory, and can spend many years there until they emerge into the upper canopy. Mortality during this understory phase is low with little sensitivity to competition variables. Feng et al. (2006) showed that in the juvenile stage, dead spruce were more likely to have more spruce neighbors, whereas having aspen neighbors did not seem to be correlated with spruce mortality. A more robust model of spruce mortality from the juvenile stage to maturity is clearly required.

Previous studies have modeled probability of survival as a function of recent growth (Bigler and Bugmann, 2004; Kobe and Coates, 1997; Wyckoff and Clark, 2000). Although competition for resources is manifested through changes in radial growth, it is not the only factor which influences secondary growth. Many other factors affect radial increase, such as climate and small scale disturbances (ground fires, herbivory, etc.), while most forest models only consider site quality and competition. Attributing growth rates to these two factors, while separately attributing mortality to low growth creates a disconnect which may bias the mortality estimates. Ring width measurements are also more difficult to obtain in routine surveys conducted during stand development. Since density and size structure are simpler to measure, mortality may be better linked to these predictors, even though ring measurements may be useful in calibrating such a model.

In this Chapter, I develop and compare two models for spruce mortality based on tree growth, stand characteristics, and climate metrics. The first model considers mortality as a function of recent growth, while the second predicts mortality as a function of local competition. These models are compared to determine if there

is a significant price in terms of ability to predict individual mortality events in the case where ring width measurements are not used. In addition, the effects of temperature, precipitation, and the water balance carried from the previous year through the current growing season were tested to determine if spruce mortality is significantly affected by inter-annual moisture or temperature variation.

I hypothesize that:

1. Retrospective data collection is a viable alternative to permanent sample plot data collection for determining white spruce survival rates in the mixedwood boreal;
2. Recent growth is a better predictor of spruce survival than local competition;
3. Competition from conspecifics will have a greater effect on spruce survival than will inter-specific competition, particularly from deciduous species;
4. In the absence of recent growth data, using local competition as a mortality predictor will still allow us to make reasonable survival predictions; and
5. Site moisture availability affects the probability of survival of white spruce.

## **2.2 Methods**

### **2.2.1 Study area**

This study was conducted in the mixedwood boreal forest of Alberta, Canada. The topography of the region varies from the steeper lower foothills of the Rocky Mountains to rolling hills and plains, shaped by retreating glaciers 10,000 years ago. In this region, climate is characterized by short, generally moist summers and long, cold, drier winters. High elevation sites are generally cooler and more moist. This region is composed of intimate and patchy mixtures of white spruce, trembling aspen, balsam poplar, white birch, balsam fir, jack and lodgepole pine, and black spruce (Beckingham et al., 1996; Beckingham and Archibald, 1996).

Forty sites located throughout the Central Mixedwood, Dry Mixedwood, Lower Boreal Highlands and Lower Foothills Natural Subregions were sampled (Figure 2.1). Sites were randomly chosen from the last comprehensive provincial forest inventory (Alberta Phase 3 inventory) based on the criteria that they were of mixedwood to pure spruce composition (at least 20 % cover of white spruce in

either the overstory or understory), photo-interpreted as being 20-100 years of age, and accessible (less than 800 m from a road, trail, or cutline). Only natural origin sites were considered for this study. Site elevation ranged from 266 to 1288 m above sea level. According to site-specific climate data generated through the application of the BioSIM climate forecasting model (Régnière and Saint-Amant, 2008), site mean annual precipitation ranged from 388 to 613 mm/yr, mean annual temperature ranged from  $-1.47$  to  $2.66$  °C, and growing degree days (GDD  $> 5$  °C) ranged from 880.1 to 1419.3.

## 2.2.2 Sampling

Data was collected using a transect-based approach. Each site was surveyed prior to sampling to determine stand boundaries, to ensure that sampling occurred within a single stand type with respect to species composition, size, and ecosite (Beckingham and Archibald, 1996; Beckingham et al., 1996). A minimum 10 m forest buffer was maintained between the sampling region and any potential interfering features (such as other stands, cut lines, roads, etc.) to discount the effects of edges on stand structure. The direction and centerline of each transect was set by a compass person carrying a distance-measuring hip chain. Searchers ranged on either side of the compass person, flagging dead spruce and tallying all live trees. Live spruce were tallied in three size categories, small, medium, and large. The small category included trees with heights (H) greater than 1 m and less than 3 m; the medium category included tree with heights greater than 3 m but with a diameter at breast height (DBH) less than 10 cm; and the final large category included all trees with a DBH greater than 10 cm. Aspen were also sampled, although less intensively. Approximately 16 dominant aspen were sampled at each site to determine approximate age of the site, and were used for analysis in a parallel study looking at growth rates of aspen and spruce (Huang et al., 2013).

Transect size was variable, and depended on the density of the stand as well as the number of dead spruce encountered. The goal was to sample approximately 5-10 dead spruce per transect, but in practice the number of dead spruce in any given stand was quite variable and this was not always possible. Once a sufficient number of dead spruce were identified, or when the transect size was at least 60 m<sup>2</sup>, transect length was cut off at the next length divisible by 5. Variable transect sizes may introduce sampling bias, but I assume this effect is negligible. Sampled transect width varied from 4 - 20 m; narrower widths were used in denser stands or stands with more brush to ensure no dead spruce were missed. In the case of

borderline trees, a sonic rangefinder with the transponder (1% accuracy) aligned at right angles to the transect centerline were used to confirm if the trees fell within the transect strip. Transect length ranged from 5 - 785 m. In very low density stands, several non-overlapping transect segments were run within the stand to ensure that a sufficiently large population was sampled. Transect size ranged from 40 to 12,560 m<sup>2</sup> with an average area of 835 m<sup>2</sup>. Transects typically included 5-20 dead spruce, although transects with no dead individuals as well as a transect with 31 dead individuals were sampled.

The position at the start and end of each transect or transect segment was recorded with a global positioning system (Garmin GPS Map60CSx) with approximately 10 m accuracy. After transversing the transect, a random sample of five to ten live spruce (at least five; otherwise approximately equal to the number of dead trees) was selected from all live spruce within the transect. As a quality control check, a second pass over the transect area was made in the reverse direction to flag the randomly chosen live trees to be sampled and to ensure all dead spruce had been identified. Decay state of dead spruce was assessed as the degree of needle loss, twig suppleness, and bark loss (Kobe et al., 1995; Kruys et al., 1999). The dead and selected live spruce were then felled, and their heights as well as diameters at both stump (0.3 m) and breast (1.3 m) height were measured. Stem cross-sections were cut at stump height (0.3 m). Several aspen cross-sections were also taken at stump height to determine stand age, while increment cores were taken from the remaining sampled aspen.

To determine the year of death of dead spruce through crossdating, site chronologies were constructed from the ring-width series of 8 - 10 dominant spruce trees (defined as those trees with no over-topping competitors) situated within or near the transect and in the same ecosite. Two cores per dominant tree were taken at breast height, at 180 degrees to one another and perpendicular to any slope.

For all sampled trees, two measures of competition were collected. A “variable radius” sample of local competition was obtained by performing a prism sweep centered at the sample tree using a metric basal area factor (BAF) 2 prism (Husch et al., 2003). In preliminary sampling I observed higher mortality among smaller trees in dense spruce patches but found that the prism sampling missed much of this observed local competition, particularly in stands with abundant small spruce. To capture this observed local density effect I added a small-plot assessment of “fixed radius” competition, where the DBH and species of all trees and shrubs taller than 1.3 m within a 1.78 m radius (10 m<sup>2</sup>) of each sample tree was recorded.

In the laboratory, core samples and small disks were mounted on strips of wood.

All samples were air dried in a 70 °C fan-circulated oven, then sanded using a series of grits (120, 220, 320, and 400). Growth radii were carefully measured from bark to pith under a binocular microscope with a precision ( $\pm 0.001$  mm) sliding stage micrometer (Velmex Inc., Bloomfield, NY). Many of our samples were taken mid-way through the growing season; in these cases the current, partially-formed ring was not included. All trees had two radii measured for additional data quality control. A large number of samples showed some decay or compression wood so radial paths were chosen to avoid these regions.

### **2.2.3 Identification of death year using Dendrochronological methods**

Master chronologies were constructed for each site from the ring width measurements from both the dominant and randomly selected spruce samples. Chronologies were used only to crossdate dead trees, therefore, only ring-width series from trees which showed a strong common climate signal were kept in the chronology. Ring width time series were detrended using smoothing splines with a 50 % cutoff at 30 years to remove both the age related growth trend as well as the effects of stand dynamics, and were then converted to tree-ring indices prior to inclusion in the master chronology (Cook and Peters, 1981). Unusually large and small annual rings identified in a site chronology were noted as marker years. The two radii taken from a single dead spruce were first compared against each other, and subsequently compared to the master chronology. Crossdating was performed visually using identified site marker years, and confirmed with PyDendro (Emmett, pers. comm.) and COFECHA (Holmes, 1983). Tree decay characteristics (needle, twig, and bark loss) were compared with determined year of death to further validate the year of death determination. In all further analysis, raw ring-width values were used.

### **2.2.4 Stand density reconstruction**

Identifying the year of death of all individuals within a transect and combining this information with the tally of live trees allowed me to reconstruct the stand density of spruce for a period of time prior to the sampling year. The simplest approach is to add dead trees on to the tree count for years prior to their death. However, in order to obtain a reasonable mortality rate estimate using this method, we need to either: ensure that all live and dead trees within the sampling frame were present for the entire period of reconstruction, or account for those younger

trees which may have only recently entered the sampling frame. In addition, the estimate of competition should be relevant to these mortality events. Since deciduous competition generally peaks at about a stand age of 20 years (which occurs prior to the stand age of our data) (Lieffers et al., 2002), we expect it to be stable or slowly declining. However, spruce competition at this time may be increasing (Lieffers and Stadt, 1994).

Spruce density was reconstructed in two ways, as enumerated below, to better understand the uncertainty associated with different simplifying assumptions.

1. In the first case, I assume all individuals in the sampling frame were present for the entire period of reconstruction. The age at stump height of the youngest spruce in a transect determines the valid period of reconstruction. The ages of the youngest spruce ranged from 16 to 65 years across transects, with a median age of 34 years. A total of 12 spruce trees were between 16 and 20 years of age, and since it takes several years for spruce to reach stump height (the height at which the samples were taken), it seems reasonable to reconstruct for 20 years prior to the year of sampling. Although for many transects it might be possible to extend the reconstruction further back in time, I limit uncertainty by restricting the reconstruction period.
2. In the second case, I consider that younger individuals in a transect may not have been present throughout the entire period of reconstruction. To account for these individuals, I combine the tally and tree size distribution data to populate transects with individuals of various sizes. For each size class tallied (small, medium, and large), I randomly assign a tree height from a uniform distribution with limits defined by the size class (intervals are as previously defined: heights greater than 1 m and less than 3 m for small trees, heights greater than 3 m but DBH less than 10 cm for medium trees, and DBH greater than 10 cm for large trees). Measured radial increments were grouped by size class for each transect. Then, for each year that I step back in time, a randomly sampled radial increment from the corresponding size class was subtracted from the radius of each individual in the populated transect. The year in which tree diameter at stump height passed 0 determined the year that individual entered the sampling frame, and would therefore determine that the individual be excluded from the stem count prior to the year in which it entered the sampling frame. To estimate the error involved with this stochastic estimate, I repeated this computation 1,000 times per transect and report the interval in which 95% of the resulting estimates lie. Note that if the

empirical increment distributions for each size class had been approximately normal, subtracting a mean increment for each size class would have been a simpler alternative to the subtraction of randomly sampled increments.

Both methods were used to reconstruct spruce density for 20 years prior to the year of sampling.

Estimating annual stand density allows us to compute site-specific annual mortality rates. The mortality rate for year  $t$  is given by  $\gamma(t) = \frac{\mu(t)}{N(t)}$  where  $\mu(t)$  is the number of individuals that died in the interval  $(t, t + 1)$ , and  $N(t)$  is the total number of live individuals at time  $t$ . This gives the proportion of spruce which died that year relative to the total spruce in the previous year. Mortality is the complement of survival, where annual survival rate is calculated from survival over  $t$  years as  $S(t) = (N(t)/N(0))^{1/t}$ . For both of the methods used to reconstruct spruce density I computed annual mortality rates for each transect for 20 years prior to the year of sampling.

### 2.2.5 Variables

The covariates and life status of each spruce were retrospectively determined for twenty years prior to the year of sampling. The resulting data set is analogous to traditional PSP data with the added benefit of having annual resolution in the diameter growth data. Covariates were classified as tree, stand, and climate variables. Trees were classified as live or dead at the end of each annual growth interval using a binary variable where 1 indicated a live tree, and 0 a dead tree. Trees that were dead at time of sampling were classified as dead in only the identified year of death, and live for all years from the time they entered the 20-year retrospective reconstruction period to the year of death.

Tree variables were broken down into three groups: individual variables, growth variables, and competition variables. Individual variables considered were diameter at breast height outside bark, height, and age. Age was taken to be age at stump height (0.3 m) and was determined by the number of rings from pith to cambium. Total age of white spruce, particularly in fire-origin stands, is difficult to determine because the impact of falling snags on seedlings during time of fire (Peters et al., 2002). Huang et al. (Huang et al., 2009) suggested planted spruce are 4 years old when they reach 0.3 m height, but Peters et al. (Peters et al., 2002) reports that in natural fire-origin stands, as many as 6 years of spruce growth are buried in accumulated litter (since the fire) in 20 yr old stands and as much as 10 yr are

buried in 38 yr old stands. Regardless, age at stump height underestimates the true age, and I suspect that my natural origin trees are similar in growth pattern to those considered by Peters et al.

Competition variables were determined from the measured fixed radius neighborhoods. These values provide an approximation to the competition present in a local niche for each individual. Neighborhood sampling was strictly relevant only for the year it was sampled, while competition covariates are needed for the previous 20 years. Local neighborhood competition was reconstructed through the subtraction of plot-specific average annual growth increments for each spruce and aspen tree in the measured neighborhood, with the stipulation that trees were “removed” from the fixed radius neighborhood once their DBH reached 0. For spruce, plot-specific average annual growth increments were computed for three size classes from the live spruce sampled within the corresponding transect. For aspen, these average growth rates were computed based on the sampled dominant trees within the transect. The reconstructed local neighborhood data, which consists of a list of species with their diameters at breast height, was then used to compute total, spruce, and aspen competitor counts, basal area, and sum of diameters.

Growth variables were used to describe the recent growth of individual spruce. The average ring width increment (ARWI, mm/yr), average basal area increment (ABAI, mm<sup>2</sup>/yr), and log transformed values of both of these measures (logARWI, logABAI), over the last 2, 3, 5, 7 and 10 years were all considered as candidate predictors. Basal area increment may be a less biased measure of growth because it removes the natural decline in ring width increment with tree size (a larger tree may put on the same basal area as a smaller tree, but the radial increment will be smaller when it is spread over a larger perimeter, e.g. (Dang and Lieffers, 1989)). Not all samples contained the pith year, so inside bark diameter, which is needed to compute ABAI, could not be computed in all cases. To overcome this issue, for all samples ABAI was determined by first converting stump-height diameter outside bark to stump-height diameter inside bark using Alberta conversion equations (Huang, 1994), and then computing the annual basal area increment based on the assumption that each annual ring had a thickness equal to the average of the ring width measurements for that year for that individual.

Stand variables were defined as those which describe forest structure and composition. In particular, I considered stems per hectare, basal area, and sum of diameters per hectare for spruce, broadleaf, and all species. These values were calculated for a given transect for a specific year. Due to the developmental stage of the mid-aged forests considered, I do not expect large changes in stand basal

area or the sum of diameters per hectare over a twenty-year timescale (Yang et al., 2009). Regardless, I avoid assuming that stand basal area is constant (as described in 2.2.4) so that I can assess the influence of small changes in both local neighborhood and stand characteristics.

Both temperature and precipitation were computed at a monthly resolution for each transect according to geographical location using the BioSIM forecasting model (Régnière and Saint-Amant, 2008). I considered mean monthly temperature and monthly precipitation as model covariates. Additionally, I computed the climate moisture index (CMI), the difference between precipitation and potential evapotranspiration (PET), as described in Hogg et. al (Hogg, 1994, 1997). PET is the expected rate of moisture loss when moisture is not limiting, and was computed using the simplified Penman-Monteith method which requires only mean monthly maximum and minimum temperatures and site elevation (Hogg, 1997). Monthly values for temperature, precipitation, and CMI from the previous April through the current month of September were tested as predictors. I also considered covariates that represented aggregated climate data, such as the average values during the growing season of the previous year as well as the current year, mean annual temperature, total precipitation measured from May of the previous year through April of the current year, and CMI for a tree water year (measured from August 1 of the previous year to July 31 of the current year, E.H. Hogg, pers. comm., 2012).

### 2.2.6 Mortality modeling

The annual survival probability of an individual was modeled using a logistic regression model, which allows a dichotomous response variable to be modeled as a function of covariates (Hosmer and Lemeshow, 2000). In our case the binary response is tree survival status, where  $Y_i = 1$  if tree  $i$  is alive at the end of an annual growth interval, and  $Y_i = 0$  if tree  $i$  is dead at the end of the interval. The general form for the logistic regression model which predicts the probability of survival of an individual is given by

$$P(\mathbf{Y} = 1|\mathbf{X}) = \frac{e^{\mathbf{X}\boldsymbol{\beta}}}{1 + e^{\mathbf{X}\boldsymbol{\beta}}} \tag{2.1}$$

where  $\mathbf{X}$  is a matrix of independent variables and  $\boldsymbol{\beta}$  is a vector of the regression coefficients.

Trees within a given transect are expected to exhibit more similar survival proba-

bilities than those between transects, as a result of spatial autocorrelation which is not accounted for in the model covariates (e.g. unknown differences in soil properties among transects). To account for differences in variation between and within transects I modeled transect random effects using a hierarchical Bayesian framework (Clark, 2007). Genetic and small-scale microsite variation also inherently affects an individual’s survival probability, but is difficult to measure in a large-scale study such as this. To assess the presence of individual variation, I test for individual random effects by evaluating whether the estimated effects are different from zero.

Regression coefficients were fit using an adaptive random walk Metropolis algorithm with diffuse normal priors on all parameters. In a Bayesian regression formulation it is assumed that the true parameter values are distributed according to a probability distribution function (PDF), and that these distributions express the degree of belief about where the true values lie. In a Bayesian framework, the PDFs are approximated by the posterior distribution, which is proportional to the likelihood multiplied by a prior. Posterior distributions can either be sampled directly if a closed-form solution exists, or can be indirectly sampled using a random walk Metropolis algorithm. Due to the absence of prior information, parameters are assigned uninformative priors. These uninformative priors indicate that we assign approximately equal weight to all possible parameters values because we have no reason to assume any specific value is more likely than another. The algorithm was implemented using the PyMC framework and was run for 100,000 iterations with a burn-in of 50,000 (Patil et al., 2010; Clark, 2007). Posterior distributions were used to compute parameter medians and 95% credible intervals using the 0.025, 0.5 and 0.975 quantiles (the Bayesian analogue to the 95% confidence interval). Further details about the Bayesian methods used can be found in Clark (Clark, 2007) and in Gelman et al. (Gelman et al., 2003).

The explicit model formulation for tree  $i$ , from transect  $j$ , in year  $k$ , is given by

$$y_{ijk} \sim \text{Bernoulli}(\mu_{ijk}) \tag{2.2}$$

$$\mu_{ijk} = \frac{e^{g(x_{ijk})}}{1 + e^{g(x_{ijk})}} \tag{2.3}$$

$$g(x_{ijk}) = x_{ijk}\beta + \alpha_i + \gamma_j \tag{2.4}$$

where  $\beta$  denotes the fixed effects coefficients,  $\alpha$  the individual random effects, and  $\gamma$  the transect effects. The fixed and random effects were each assigned uninformative

Normal priors, given by

$$\beta \sim \text{Normal}(\text{mean} = 0, \text{var} = 1e6) \tag{2.5}$$

$$\alpha_i, \gamma_j \sim \text{Normal}(\text{mean} = 0, \text{precision} = \tau) \tag{2.6}$$

$$\tau \sim \text{Gamma}(\text{shape} = 1e-3, \text{rate} = 1e-3). \tag{2.7}$$

To ensure that parameter posterior distributions are representative of the true population values, sampling weights were defined. These weights address the concern that for a given transect the entire dead tree population was sampled, whereas only a subset of the live tree population was sampled. In this analysis, sampling weights determine the appropriate weight that the likelihood of an observation is given. Since I sampled all dead trees, their weights are all equal to 1, whereas for the more numerous (and sub-sampled) live trees in transect  $k$ , the weight is defined as  $w_k = \frac{N_T}{N_S}$ , where  $N_T$  is the total number of live trees in transect  $k$ , and  $N_S$  is the number of live trees sampled in transect  $k$  (i.e. each observation for a live tree represents  $w_k$  live trees in the stand). Note that as described in Section 2.2.5, the retrospective sampling method used reveals each subject tree’s size and status (live vs. dead) for each year. This allowed me to generate tree records for each year that a tree was alive. Dead trees were live for all years in the sampling frame until their year of death, and are only identified as dead in the single year of death (after which they were then removed from the data).

### 2.2.7 Model assessment

Models were evaluated based on two criteria: how well they performed relative to other candidate models and how well they were able to predict reality. Candidate models were compared using the deviance information criterion (DIC). DIC is a generalization of AIC and BIC that allows one to evaluate a hierarchical model without having to explicitly compute the number of parameters as needed in AIC and BIC (Spiegelhalter et al., 2002). This measure is used to assess relative model performance, but is only able to identify the best model out of the candidate models, which may still be a poor fit to the data. To quantify how well models predict the data I evaluated the predicted loss (PL), the area under the receiver operator curve (ROC), and the Hosmer-Lemeshow (HL) statistic. PL answers the question of how well the model predicts the data that I actually observed, and incorporates both a goodness-of-fit and predictive variance measure (Gelfand and Ghosh, 2011). The PL goodness-of-fit measure is the weighted error sum of

squares,

$$G_m = \sum_{i=1}^n (w_i(p_i - y_i))^2 \quad (2.8)$$

where  $p_i$  is the predicted survival probability for a tree with survival status  $y_i$  with corresponding sampling weight  $w_i$ . The PL penalty term is the predictive variance

$$P_m = \sum_{i=1}^n w_i p_i (1 - p_i), \quad (2.9)$$

which is a measure of the spread of predicted values for a given data point, summed over all data points. The posterior predictive loss function is then given by the sum of these two measures,  $D_m = G_m + P_m$ . The model with the lowest predicted loss is then said to have the best predictive capability (Gelfand and Ghosh, 2011).

The ROC is a graphical representation of the true positives (sensitivity) versus the false negatives (specificity) for every possible threshold that could be used to classify predicted outcomes (Krzanowski and Hand, 2009). Model sensitivity relates to the ability of the model to identify positive results, while model specificity relates to the ability of the model to identify negative results. There is often a tradeoff between these two measures, so modelers have to consider the consequences of incorrect positive and negative predictions. The area under the ROC curve (AUC) provides a measure of the model discrimination between those individuals who experience the outcome of interest (in our case survival) and ranges from 0.5 for no discrimination, to 1 for perfect discrimination. ROC curves for both the growth-based model and the survival-based model are generated. The AUC for each curve is computed, and associated confidence intervals are generated using bootstrapped replicates. The two ROC curves are then compared using the correlated DeLong test as implemented in the R language pROC package to determine if the curves are significantly different based on their respective AUCs (DeLong et al., 1988).

The ROC is also used to help determine an appropriate threshold for classifying outcomes into groups (in our case live and dead). An optimal threshold can be chosen based on the importance of true positives versus false negatives. Here I assume that the goal is to maximize the overall correct classification of trees (true positives plus false negatives), and accordingly use two of the more commonly used methods to select the optimal threshold: the Youden and closest-to-top-left methods. The Youden method maximizes the distance to the diagonal line, formally maximizing the overall correct classification rate, while the closest-to-top-left method identifies the cutoff which is the closest to the top left corner,

formally maximizing the sum of the squares of the true positives and the false negatives. Using these identified cutoff values allows me to classify individuals as live or dead, allowing the continuous survival probabilities to be translated to dichotomous outcomes in order to make predictions about numbers of trees in the live or dead class (Bigler, 2004). In this case, a tree is predicted to die if the survival probability is less than the threshold. Classifications tables which depict the proportion of trees correctly and incorrectly classified as either live or dead are presented for both models.

To test the hypothesis that the model is a good fit to the observed data, I calculated the HL  $C$  statistic for both models (Hosmer and Lemeshow, 2000). This statistic is based on the predicted survival probabilities from the logistic model, which are divided into  $g$  groups based on percentiles of survival probabilities. Then the test statistic  $C$  can be calculated as

$$C = \sum_{k=1}^g \frac{(O_k - n_k * \bar{p}_k)^2}{n_k \bar{p}_k (1 - \bar{p}_k)} \quad (2.10)$$

where

$O_k$  = observed number of trees in class  $k$ ,

$n_k$  = total number of trees in class  $k$ ,

$\bar{p}_k$  = mean of the predicted survival probabilities for group  $k$ , and

$g$  = total number of groups.

This statistic is approximated by the chi-square distribution with  $g - 2$  degrees of freedom. To account for the individual tree weighting in our data, the total number of trees in class  $k$ ,  $n_k$ , is replaced by the sum of the weights  $\sum w_k$  associated with all trees in class  $k$ .

The model fitting and selection procedures were carried out for both the local competition and recent growth survival models. In both cases, the stand and tree level covariates described above were tested. Additional covariates considered for the competition model were local neighborhood and plot-scale counts of competitors, basal area, and sum of diameters, for spruce, deciduous, and all species combined. Competition indices were computed for all individuals of a given species as well as for only those trees of thicker diameter than the tree in question (Stadt et al., 2007). Growth model covariates tested were ARWI, ABAI, logARWI, and logABAI averaged over 2, 3, 5, 7, or 10 years, although only a single recent growth variable under one averaging period was permitted in the final model.

Odds ratios were calculated to interpret the change in predicted survival probability with respect to changes in covariates. The odds ratio is defined as the ratio of the probability of an event occurring relative to the probability that that event does not occur (Hosmer and Lemeshow, 2000). When the odds ratio is larger than 1, survival is more likely with an increase in the corresponding covariate, whereas an odds ratio less than 1 indicates that survival is less likely with an increase in a given covariate. The odds ratio is typically taken to be a measure of the change in the odds of survival when an increment of 1 unit is added to a given predictor, holding all else constant, and I use this definition.

Aggregated fit plots showing predicted survival probabilities relative to covariates allow the comparison of model predictions with data, and help identify regions in covariate space where the model may not perform well. These plots are made by first dividing the data for a single covariate into deciles, and then computing the average observed and predicted survival probabilities for each decile. For each covariate that appears in either of the final growth- or competition-based models, average predicted probabilities are computed for each covariate decile (even when that covariate does not appear in a given model). The data are plotted at decile bin midpoints, and the predicted probabilities and their 95% credible interval values, though also plotted at bin midpoints, are connected with lines for ease of visual interpretation. These plots allow us to gain insight with respect to model performance that may not be apparent through other methods due to the fact that mortality events are quite rare.

## 2.3 Results

### 2.3.1 Stand and tree characteristics

A total of 40 transects across the Alberta mixedwood boreal forest were sampled. A summary of the site characteristics is provided in Table 2.1. Out of the 40 transects sampled, 21 fell in the Central Mixedwood Natural Subregion, 10 in the Lower Foothills, 5 in the Dry Mixedwood, and 4 in the Lower Boreal Highlands. Spruce density ranged from 163 to 14400 stems per hectare (sph), hardwood density from 625 to 6866 sph, and total density from 1550 to 17200 sph. Stand age was estimated by aging the pioneering aspen within the transect at stump height, and ranged from 30 to 128 years with a median age of 63 years. Six of the transects were sampled prior to the addition of this aging protocol, and therefore stand age was not available for these transects. For each transect, I determined minimum and

maximum spruce stump height (0.3 m) ages, excluding any trees that appeared to be veterans (rare trees not killed in the stand-initiating fire). Minimum spruce ages for each transect ranged from 16 to 65 years with a median of 34 years, while maximum spruce ages ranged from 27 to 74 years, with a median of 54 years. For some of the transects the maximum spruce age exceeded the stand-age by several years, but I attribute this discrepancy to the fact that these dates were based on stump height data as opposed to root collar data, and assume that establishment of these oldest trees occurred at approximately the same point in time. Hardwood basal area was estimated using the aggregated local competition plot data, and ranged from 3.65 to 41.1 m<sup>2</sup>/ha.

Only trees which were over 1 m in height were sampled, thereby excluding all spruce currently in the highly variable juvenile growth phase. A total of 793 spruce trees were sampled, including 443 live and 350 dead spruce. Tree DBH at time of sampling ranged from 0 (those trees with a height in the interval (1, 1.3)) to 364 mm, with a median of 53.4 mm.

Using ring widths to retrospectively determine tree data for twenty years prior to sampling, I obtained a data set analogous to that obtained from PSP sampling, but with an annual resolution. The inclusion of this retrospective information resulted in a total of 13969 annual live tree measurements. There were 350 dead tree measurements; prior to death, these trees were part of the live population. Tree status (live or dead) was assigned depending on the condition of that tree at the end of the annual interval. This expanded data set formed our modeling data. As noted in Section 4.2, I did not track the other species (chiefly deciduous) in the stands using these retrospective techniques. Rather, competition from these was simulated by growing the current live deciduous trees backwards without considering their mortality.

As shown in in Figure 2.2, there was a significant difference in DBH between live and dead spruce ( $p \ll 0.01$ ). This indicates that small trees may be at a higher risk of mortality, likely due to increased competition (i.e. shade from taller competitors) resulting from their smaller stature.

Local competition data indicated that there were also significant differences between the intra-specific competition experienced by live and dead spruce, as shown in Figure 2.3. According to a Mann-Whitney non-parametric test, spruce BA, count, and sum of DBH competition measures for live and dead spruce all led to a rejection of the null hypothesis that the true location shift is for live vs. dead spruce is 0 ( $p \ll 0.01$ ). While deciduous competition also showed significant

differences between the live and dead spruce groups ( $p < 0.01$ ), the observed differences in mean deciduous competition between live and dead groups were smaller than those of the spruce competition measures. Note that observations from trees within a transect may violate the assumption of independence, so Mann-Whitney test results should be interpreted with caution.

Radial increase was much smaller in the years leading up to death for ARWI and ABAI averaged over the last 2, 3, 5, and 7 years. The greatest reduction in radial growth occurred during the two years prior to death in both ARWI and ABAI, as shown in Figure 2.5.

### 2.3.2 Dendrochronological methods

Construction of the transect-specific master chronologies was straightforward. Common marker years within a transect were identified using the list method (Yamaguchi, 1991). Crossdating results were verified using COFECHA, and interseries correlations suggested that the common transect signal was quite strong. Dating dead spruce required more effort because these trees showed periods of suppression, and in many cases compression wood caused the ring structure to be highly asymmetric. These irregular growth patterns led to spurious correlations with the master chronology, which was developed from the larger competition-free spruce. Despite these challenges, a combination of skeleton plotting and the list method allowed us to identify enough marker years to date these samples.

A total of 370 dead spruce trees were crossdated to determine year of death. Only a single dead tree had experienced rot severe enough to prevent dating. In the case of this single individual, year of death was estimated based on decay state. Partial cambial death was commonly observed, and in this case year of death was taken as the year of the last partial increment. Year of death ranged from 1978 to 2011, with both mean and median year of death equal to 2001 (Figure 2.6). Age at stump height of the oldest non-veteran spruce determined the estimated year of establishment of the first spruce cohort. Time from the transect year of establishment to year of death of each dead tree located within that transect was computed to assess if there was a common time-frame across transects in which mortality occurred. The time from establishment of the first spruce cohort to year of death ranged from 20 to 79 years, with a median of 49, as shown in Figure 2.6. More than half of all death events occurred 42 to 55 years after the establishment of the first spruce cohort, which suggests that this is a critical mixedwood successional phase for white spruce.

### 2.3.3 Mortality rates

The annual mortality rate, when averaged over all transects and all years, was equal to 0.77 % spruce per year when I assume all spruce were present for the entire sampling frame, and 0.81 % in the case where I approximated the age at which younger spruce may have entered our retrospective 20 year sampling frame. In both cases, the range of average transect mortality rates were similar: in the first case the range was [0, 2.93] %, while in the second case, where I allowed for ingress, the range was [0, 3.01] %. As expected, when I account for the possibility of young spruce entering the sampling frame later than the initial year considered, I obtain higher mortality (fewer spruce present means that one death represents a greater proportion of the population). These average mortality rates are similar to the previous estimate of 0.7 % for mid-aged spruce suggested by Feng et al. (2006) using limited PSP data. The average mortality rates for each transect in the case when ingress is considered are shown in Figure 2.7, and illustrate the variation in mortality. There were 6 transects in which no dead spruce were found – these account for the zero mortality rates. The difference in mortality rate estimates between the no ingress and ingress datasets is small (0.04 % per year); in a stand stocked with 2500 spruce stems per hectare, the difference in estimates would be equivalent to 1 tree per hectare per year.

Although I did not find latitude to be a significant explanatory variable in the survival models fitted, I did observe that mortality increased with latitude, as shown in Figure 2.4, and hypothesize that this is a result of latitudinal climate gradients.

### 2.3.4 Model fitting and interpretation

In both the growth-based and competition-based models, individual random effects were not found to be significant (95% credible intervals for the effects contained zero and therefore they could not be assumed to be statistically different from zero), and were therefore not included in the models. For ten of the forty transects, the transect random effects 95% credible intervals did not contain zero, and I therefore determined the random effects to be significant and as such they were henceforth included in both models.

The growth-based survival model identified as the best-fit model according to both the DIC and PL included the log of the average basal area increment over the previous two years ( $\log\text{ABAI}_2$ ) and the June climate moisture index ( $\text{cmiJune}$ ).

Estimated parameter values and their credible intervals are shown in Table 2.2, while the model fit statistics are shown in Table 2.4.

For the competition model, competition indices (basal area, sum of DBH, density) which were computed on trees thicker than the subject tree (BAGR, SDGR, NGR) were much more effective than the total index values (BA, SD, N). Spruce basal area in thicker trees was a better predictor of survival probability than number of spruce competitors or sum of diameters. The total density of competitors that were thicker diameter (including all species) also proved to be a better predictor than any of the alternate measures of aspen or total competition. The best-fit model included subject tree DBH (DBH), spruce basal area in thicker trees (SWBAGR), density of all species in thicker trees (ALLNGR), and June climate moisture index (cmiJune). Estimated parameter values and their credible intervals are shown in Table 2.3, while the model fit statistics are shown in Table 2.4.

Aggregated fit plots shown in Figures 2.8, 2.9, 2.10, 2.11, 2.12 show the survival response trends of both models throughout covariate space. Credible intervals, determined by the interval defined by the 0.025 and 0.975 quantiles, were narrow for ABAI2 and DBH (see Figures 2.8 and 2.9), but were much larger for the remaining covariates. The growth model provided a better fit with respect to the ABAI2 covariate space deciles, as shown in Figure 2.8. Both models were able to describe the data with respect to the remaining covariate decile groups, except in the case of high basal area of larger spruce competitors where both models overpredict the probability of survival (see Figure 2.12).

The odds ratios for all parameters are shown in Figure 2.13. In the local competition model, both local spruce basal area (SWBAGR) and local density (ALLNGR) showed negative effects on the survival probability, while DBH showed a positive effect. In the recent growth model, the log of the average basal area increment over the last two years (logABAI2) showed a large effect on the survival probability. This indicates that increasing logABAI2 by 1 causes the risk of mortality versus the likelihood of survival to be 3.3 times lower. In both models, the June climate moisture index had a small positive effect on survival probability indicating that survival improves with increasing moisture availability (and declines with increasing drought).

### 2.3.5 Model validation and prediction

The Hosmer-Lemeshow C statistic was 0.8 for the growth-based survival model, and  $6.4 \times 10^{-6}$  for the competition-based survival model. This suggests that there

is little evidence to support the rejection of the recent growth model, but the local competition model exhibited a significant lack-of-fit despite my best efforts to transform the predictors and test interactions. However, Li et al. (2012) showed that large sample sizes such as ours could lead to erroneous C statistic values and therefore need to be used with caution. Additionally, in cases where the binary outcome data is very skewed as in our case where very few records represent dead trees, the HL statistic may not be the best metric to evaluate lack of fit.

Figure 2.14 shows the ROC curve for both models. The area under the ROC curve was 0.794 with 95% CI [0.772, 0.817] for the local competition model which suggests acceptable discrimination, and 0.859 with 95% CI [0.841, 0.876] for the recent growth model, which suggests excellent discrimination. Note that the confidence intervals do not overlap, which suggests that there may be a true difference in AUC among the two models. The Delong test was used to formally compare the AUC from competition and growth based ROC curves, and the resulting test statistic and corresponding p-value ( $Z = -7.67$ , p-value  $< 0.001$ ) indicated that the true difference in the area under the ROC curves is not equal to zero. Therefore I conclude that the growth-based ROC curve results in significantly better discrimination according to this measure. Both the Youden and closest-to-top-left threshold selection methods resulted in the same cutoff value for a given model. The identified threshold for the competition-based model was 0.979, resulting in a sensitivity of 0.75 and a specificity of 0.71. The threshold for the growth-based survival model was 0.983, which corresponds with a sensitivity of 0.74 and a specificity of 0.83. For each respective model, trees with predicted survival probabilities obtained from the logistic model that are above the threshold values are classified as live trees, and all others are classified as dead. For the optimal thresholds, both models are able to correctly classify live trees, although the ability of the growth-based model to correctly identify dead trees exceeds that of the competition-based survival model by 12%. Threshold values for both models are very close to 1 as a result of the infrequent occurrence of mortality events in the data.

The classification tables for both models were computed using the threshold of 0.981, the mid-point between the identified ideal thresholds for each of the models, and are shown in Table 2.5. The growth model had the ability to classify 75 % of live trees correctly and 81 % of dead trees correctly, with an overall classification of 76 % live and dead trees correctly classified. Out of the live trees which were incorrectly predicted as dead, 83 % of those were trees that did indeed die, but did so prior to the sampling year. The competition model had the ability to classify

75 % of live trees and 71 % of dead trees correctly with an overall classification ability of 75 %. Again, 77 % of the trees which were incorrectly predicted as dead were trees which were found dead at time of sampling. Clearly the models would classify live versus dead trees very well if I allowed more leeway than the precise year of death.

## 2.4 Discussion

In this study I find that the log of the average basal area over the last two years of growth (logABAI2) is the best predictor of spruce probability of survival according to the PL and DIC statistics. The growth-based model included logABAI2 and cmiJune as predictors, and resulted in an HL statistic equal to 0.83, thereby supporting the conclusion that the model is a good fit to the data. Recent growth has been well established to be a good indicator of mortality, although there is variability in the estimates of the length of growth decline prior to death (Wyckoff and Clark, 2000; Kobe and Coates, 1997; Bigler and Bugmann, 2004).

Despite my finding that recent growth is a better indicator of mortality, local competition also serves as an effective indicator of survival probability. The PL and DIC statistics were both larger than in the case of the recent growth survival model, indicating the poorer relative fit and predictive ability of the competition-based model. The HL C statistic was also close to zero, which typically indicates lack-of-fit between model and data. However, as described above, this test statistic may be misleading, especially for large data sets which include discrete predictors such as ALLNGR. Although the model statistics were lower for the competition-based model than the growth-based model, classification ability of the competition-based model was still high – trees were classified correctly with 75% accuracy. This suggests that, in the mixedwood boreal, competition may be the single largest factor affecting changes in annual increment size. Despite these promising results, neither model adequately predicted the average survival probabilities observed for trees experiencing extreme competition from local larger spruce, as measured by basal area of thicker spruce (SWBAGR). For both the growth- and competition-based survival models, average probability of survival was overpredicted for these extreme values, and the data suggests that there may be evidence of a non-linear relationship between survival and SWBAGR.

Overall, I found that intraspecific (spruce-on-spruce) competition had the greatest impact on spruce mortality, while interspecific competition, in particular competition from deciduous neighbors, had little effect on survival probability. Feng et al.

(2006) also noted no effect of deciduous neighbors. The limited competitive effect of broadleaf neighbors on spruce compared to the effect of spruce-on-spruce could perhaps be attributed to the open canopy of the aspen and balsam poplar trees relative to a spruce canopy (Constabel and Lieffers, 1996; Stadt and Lieffers, 2005). White spruce has been shown to tolerate light levels as low as 10% of the above canopy light (Lieffers and Stadt, 1994). Light levels below this spruce light tolerance are not found under aspen canopies, but are found under spruce (Filipescu and Comeau, 2007; Lieffers and Stadt, 1994; Pinno et al., 2001). Additionally, spruce height growth at intermediate light levels has been shown to be at least half of what it would be in full sunlight (Eis et al., 1970). Differences in rooting depth may also result in a limited competitive effect of deciduous neighbors on spruce. Strong and La Roi (1983) showed that on average, the aspen rooting depth was greater than that of the white spruce, which produced mostly surficial roots. This niche separation in terms of light requirements and rooting habit may explain why spruce has a stronger competitive effect than the deciduous species do.

It is important to reiterate that mortality of species other than spruce (chiefly aspen) was not measured in this study. Past local neighborhoods were simulated from current neighborhoods by growing them backwards in time, without considering mortality of the neighbors. This is not ideal, but for the timescales considered (20 years) I don't expect that this will create a significant problem.

In both the competition- and growth-based mortality models June CMI was identified as a significant climate predictor. This is consistent with previous results in McGuire et al. (2010), where summer drought stress was identified as being negatively correlated with growth of white spruce in Alaska. In the boreal, June is a critical time for cambial activity and tracheid formation (Zhai et al., 2012), so it is not surprising that moisture availability during this time is growth and survival limiting. It has been observed that the last decade has been drier than normal in the western boreal (Mbogga et al., 2009), and concurrently Peng et al. (2011) noted increased tree mortality in a survey of boreal PSPs. An increase in mortality events in the last decade is also seen in our data (see Figure 2.6). Thorpe and Daniels (2012) were able to account for apparent increases in mortality for western PSPs in recent decades due to stand age and structure alone, with no climate signal. Our study accounted for age and structure, yet still found a late spring drought signal. It is important that we work towards understanding how changes in moisture availability affect the vast boreal region. Significant increases in mortality resulting from increased drought stress have the potential to shift

the region from a CO<sub>2</sub> sink into a source, exacerbating the effects of a changing climate.

I found that the retrospective sampling approach lends itself well to the boreal mixedwood. The ability to reconstruct stand dynamics is in part determined by decomposition rates of both standing and downed woody debris, which are slow in the Alberta boreal due to the short growing season, cool temperatures, moderate precipitation, and (in particular for conifers) the decay-resistant nature of the wood. Additionally, this method is attractive because it can save substantial time and investment compared to PSP methods. PSPs are inefficient at sampling mortality in tolerant species like white spruce because they require that every tree be sampled at each re-measurement. The retrospective technique devoted the most sampling energy to the rare mortality events, while sub-sampling the frequent live “events”. A particular advantage of the retrospective sampling method is that annual mortality rates can be more easily estimated than with PSP data. Annual resolution allows us to link mortality to climate events, which is much more difficult when using PSPs, which typically have a remeasurement interval of 5-10 years.

I found some decay in my spruce samples from the pith outward as well as from the bark inward. Additionally, partial cambial death occurred frequently several years before death. This required collection of disks to allow us to clearly identify paths from bark to pith, although often these paths were not direct. It would therefore be difficult to use increment cores for consistent crossdating of dead spruce. Another difficulty I encountered arose when trying to crossdate dead individuals with our live site chronologies. Many of the dead samples were from trees which had experienced severe suppression, which made verification of crossdating results using time series correlation difficult if at all possible.

The estimated mortality rates (as well as the variability estimates) provide critical information to managers who need to plan for future yield quotas. For example, using our computed mortality rates, we can determine the proportion of trees at establishment which remain alive through to harvest. If an establishment survey is conducted at age 5, and harvest occurs at age 100, and the mortality rate lies in the interval 0.77 - 0.81 % , then we expect that 46 - 48 % of the established trees remain at harvest.

Our overall average spruce mortality rate was consistent with previous estimates, however I did find that there was variability in mortality rates between transects, and across years even within a transect. Subregions and covariates did not provide further insight into the patterns observed in the data, which indicates that

mortality is outcome of the interaction of many factors. However, the abilities of the models to discriminate live and dead trees was remarkable – both the growth- and competition-based survival models did so with approximately 75% accuracy. The unexplained variation ( 25%) is due to factors not included in the model, but the models were able to capture the majority of the mortality dynamics. This is a significant improvement over the previous mortality estimate by Feng et al. (2006) based on limited PSP data.

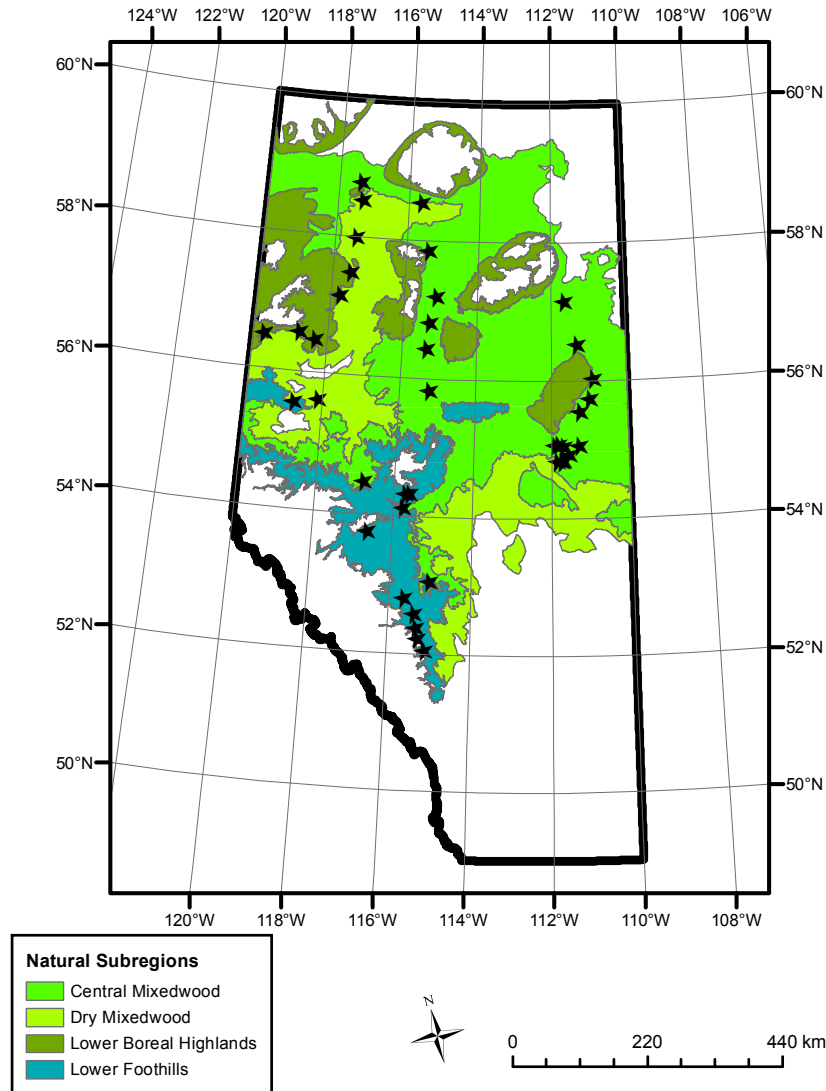


Figure 2.1: Map of Alberta indicating the transect locations throughout the sampled natural subregions. Out of the 40 transects sampled, 21 fell in the Central Mixedwood Natural Subregion, 10 in the Lower Foothills, 5 in the Dry Mixedwood, and 4 in the Lower Boreal Highlands.

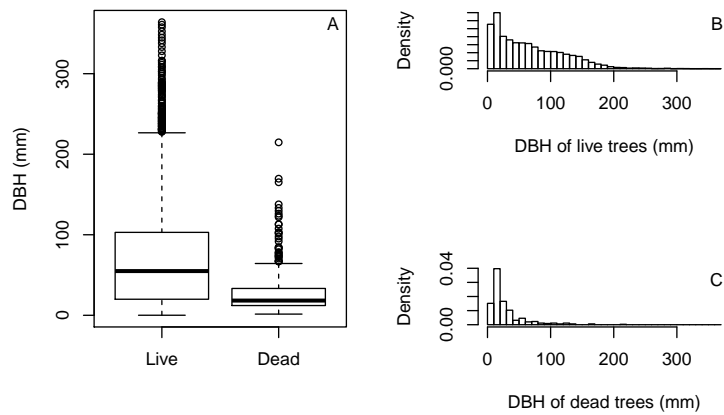


Figure 2.2: **A** Boxplots of tree diameters at breast height (DBH) for both the live and dead spruce groups. Note that on average the dead spruce DBH is smaller than the DBH of the live spruce. **B** Histogram of live tree diameters. Note that the distribution is positively skewed. **C** Histogram of dead tree diameters. Although this distribution is again positively skewed, not as much weight appears in the tail relative to the DBH distribution of the live trees.

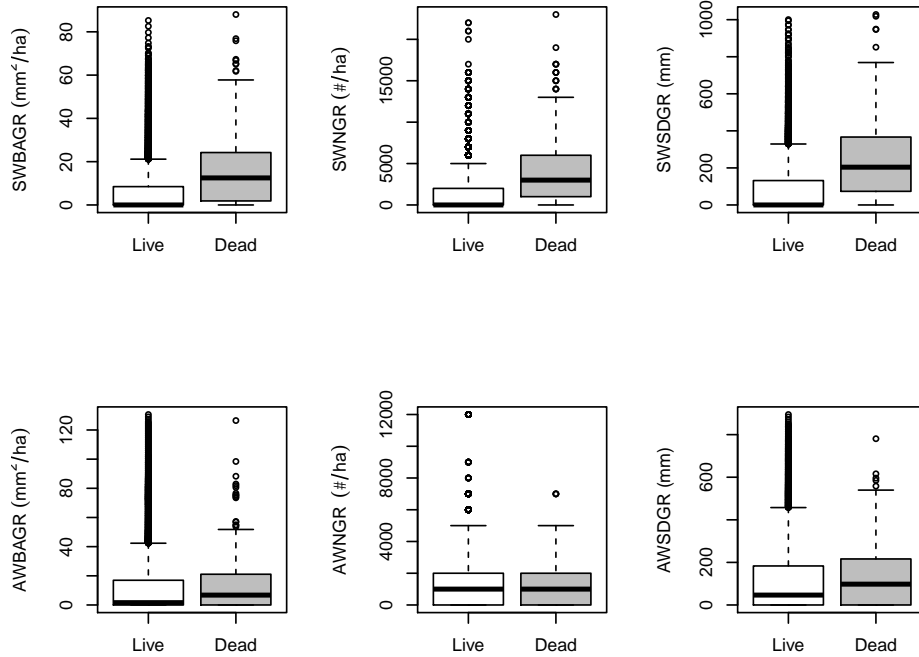


Figure 2.3: Boxplots of the local competition measurements including only neighbors thicker than the subject tree for live and dead trees. Upper panel depicts spruce competition measured by the basal area of thicker spruce (SWBAGR), the number of thicker spruce (SWNGR), and the sum of diameters of thicker spruce (SWSDGR). Bottom panels depicts the competition from aspen measured by the basal area of thicker aspen (AWBAGR), the number of thicker aspen (AWNGR), and the sum of diameters of thicker aspen (AWSGDGR). Note that there is little difference in experienced aspen competition between the live and dead groups relative to the difference seen in the experienced spruce competition.

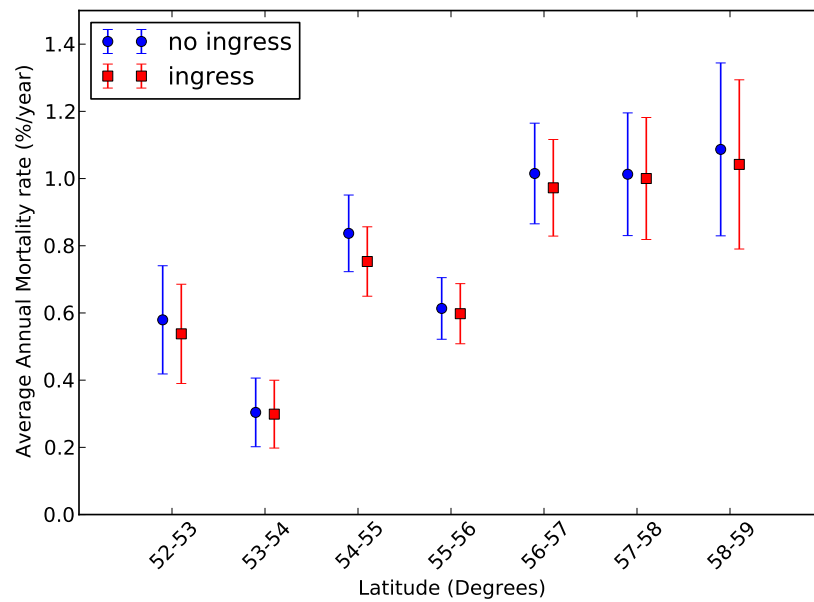


Figure 2.4: Mortality rates for both stand reconstruction methods averaged over all years by latitudinal degree band. There appears to be only minor differences between the reconstruction methods, and both show increased mortality at higher latitudes. Despite this positive correlation between mortality rate and latitude, latitude was not found to be a significant predictor of spruce mortality.

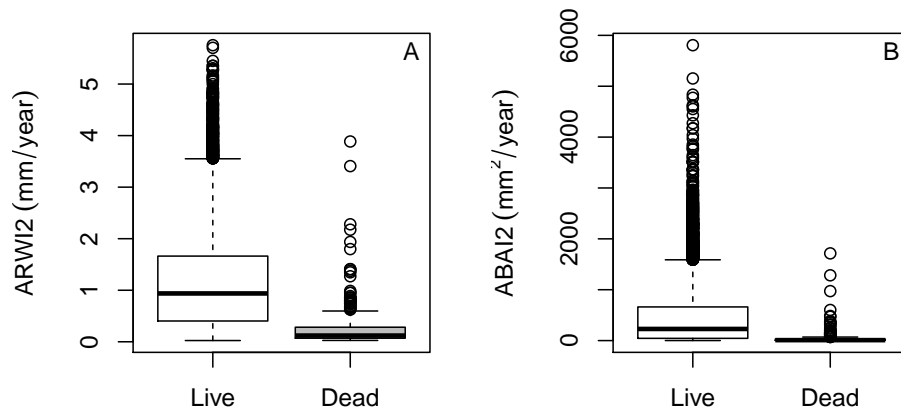


Figure 2.5: Boxplots of **A** the average radial increase over the last two years (ARWI2) and **B** the average basal area increase over the last two years (ABAI2) for both live and dead trees. For both measures, on average the size increase of dead spruce is less than that of live spruce.

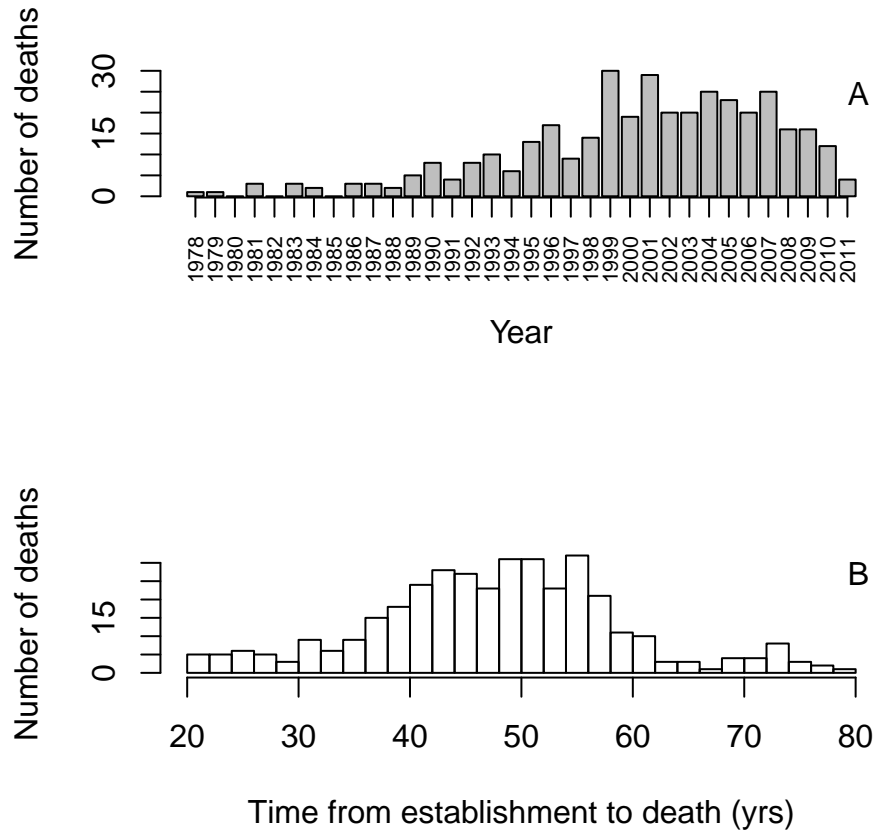


Figure 2.6: **A** Histogram showing the distribution of death years for sampled dead trees from all transects. The number of tree deaths decreased with decreasing year of death. **B** Histogram showing the time from stand establishment to tree death. Note that more than half of all trees deaths occurred 42-55 years after stand establishment.



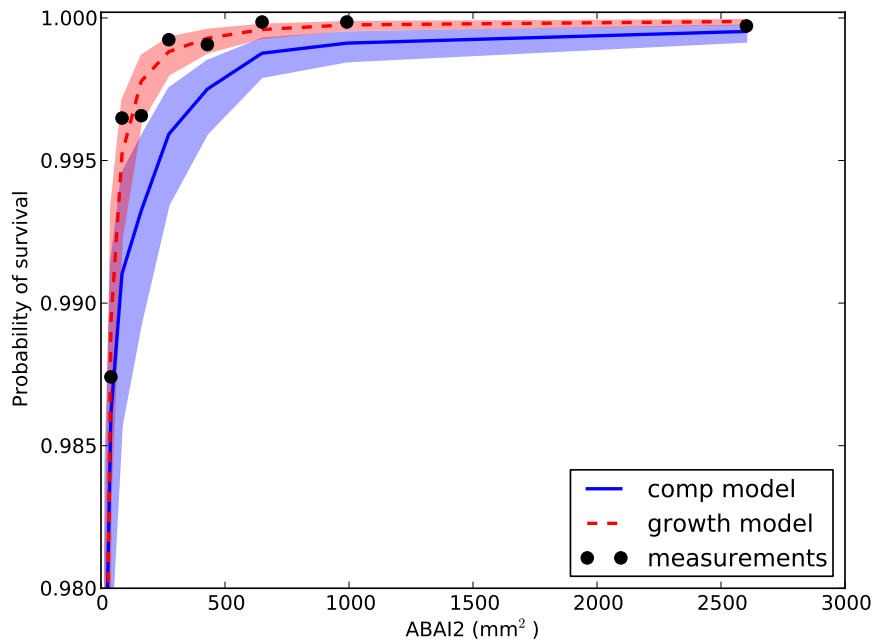


Figure 2.8: Aggregate fit plot showing the survival probabilities for the data (black circles) plotted against decile bin midpoints of the average basal area increment over the last two years (ABAI2). Median model performance for the competition model (blue solid), and the growth model (red dashed) are indicated by the bold lines, while shading indicates the 95 % credible interval. Credible intervals are narrow, and the competition model provides a better fit across the ABAI2 covariate domain.

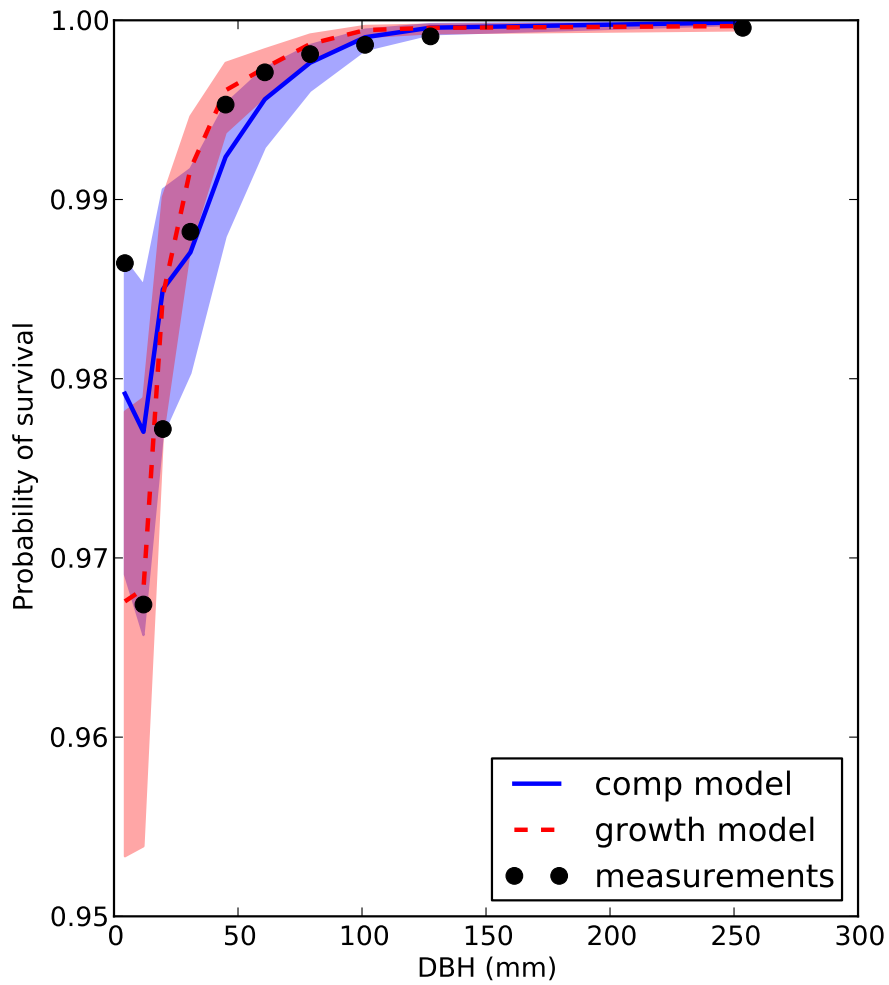


Figure 2.9: Aggregate fit plot showing the survival probabilities for the data (black circles) plotted against decile bin midpoints of the diameter at breast height (DBH). Median model performance for the competition model (blue solid), and the growth model (red dashed) are indicated by the bold lines, while shading indicates the 95 % credible interval. Except for the first decile, the data falls within the credible intervals of both models.

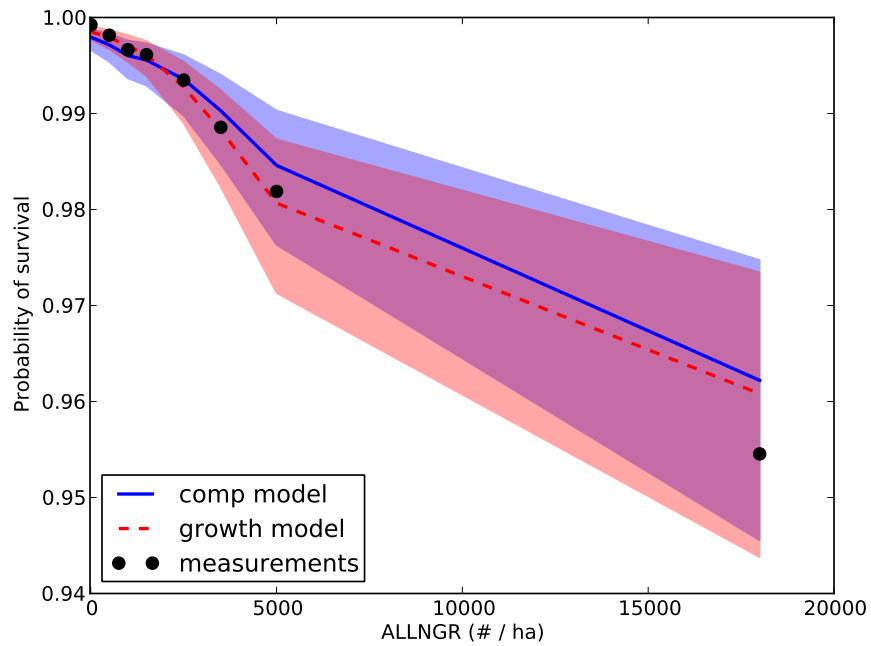


Figure 2.10: Aggregate fit plot showing the survival probabilities for the data (black circles) plotted against decile bin midpoints of the local number of larger trees per hectare (ALLNGR). Median model performance for the competition model (blue solid), and the growth model (red dashed) are indicated by the bold lines, while shading indicates the 95 % credible interval. Except in the case of very few competitors, data falls well within the credible intervals of both models.

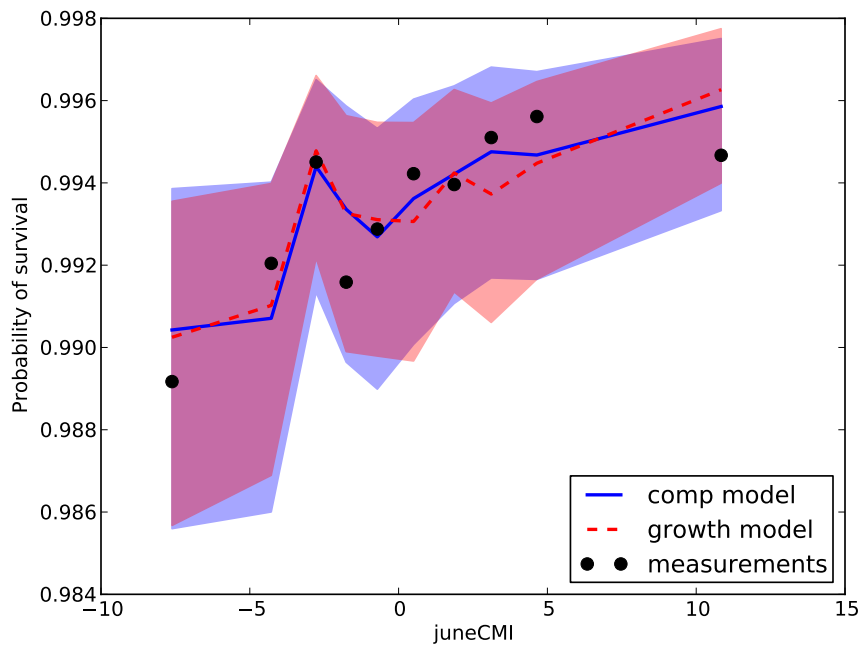


Figure 2.11: Aggregate fit plot showing the survival probabilities for the data (black circles) plotted against decile bin midpoints of the June climate moisture index (juneCMI). Median model performance for the competition model (blue solid), and the growth model (red dashed) are indicated by the bold lines, while shading indicates the 95 % credible interval. Data falls well within the credible intervals of both models.

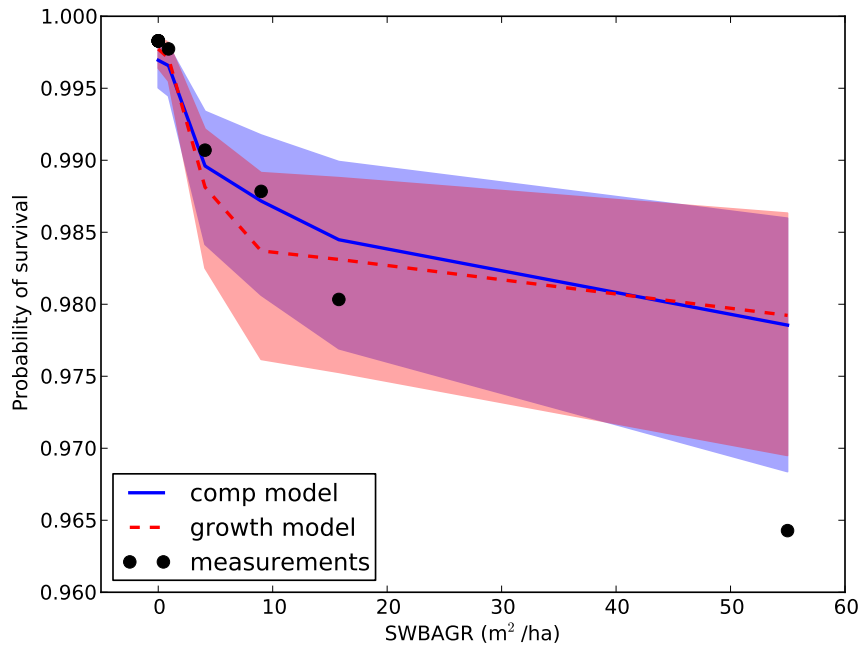


Figure 2.12: Aggregate fit plot showing the survival probabilities for the data (black circles) plotted against decile bin midpoints of the local basal area of larger spruce (SWBAGR) measured in m<sup>2</sup>/ha. Median model performance for the competition model (blue solid), and the growth model (red dashed) are indicated by the bold lines, while shading indicates the 95 % credible intervals. Data falls within the credible intervals of both models, except for the last decile, which falls outside the credible intervals of both models.

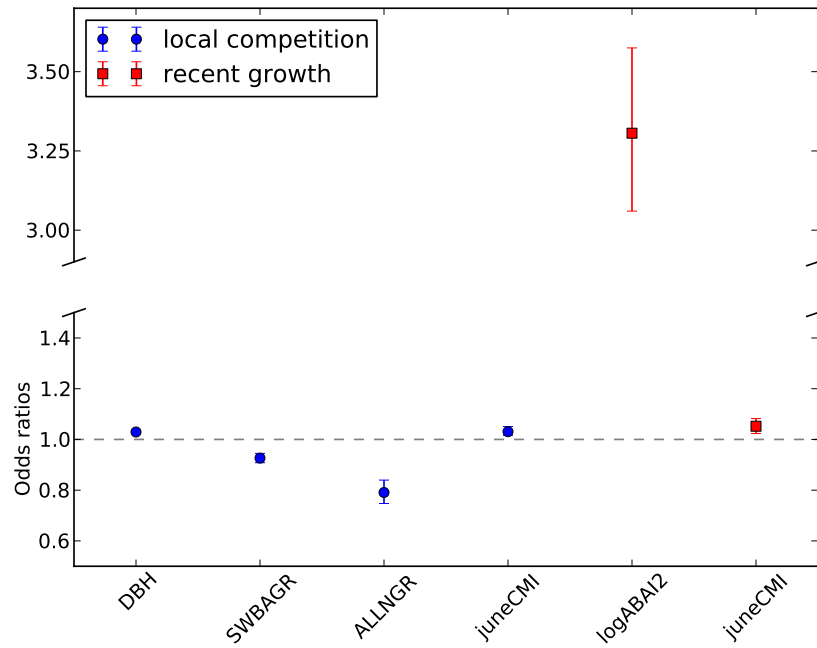


Figure 2.13: Odds ratios for parameters in the local competition survival model (DBH, SWBAGR, ALLNGR, and juneCMI; denoted by circles) and the recent growth survival model (logABAI2; denoted by squares). The 95% predictive intervals are indicated by error bars. An odds ratio greater than one indicates that an increase of a single unit in the considered covariate leads to an increase in survival odds, while a odds ratio value less than one indicates a unit increase of covariate leads to a decrease in survival odds.

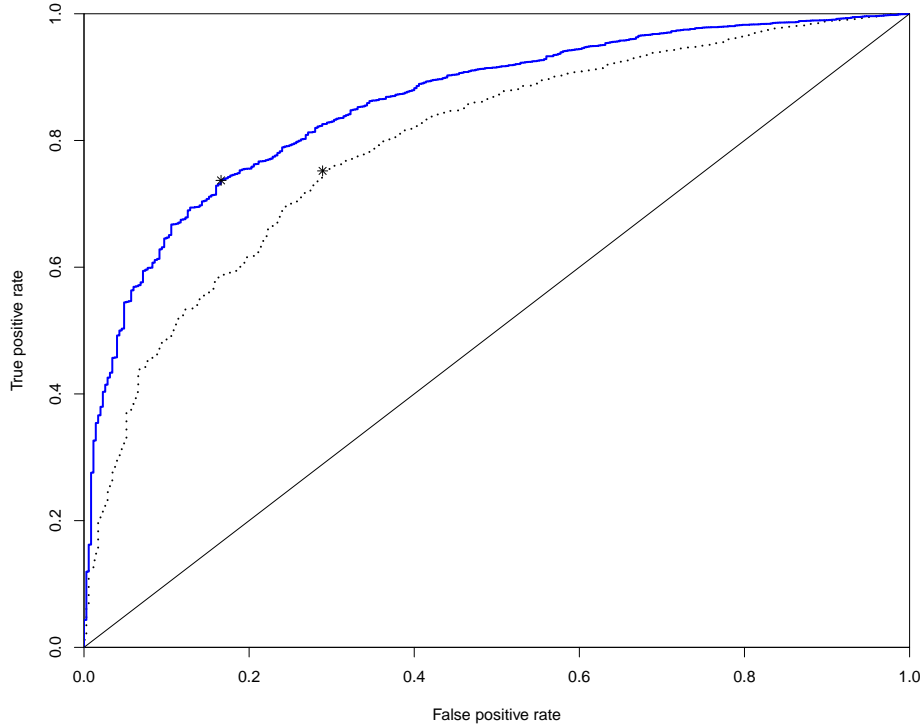


Figure 2.14: ROC curves for the growth (solid line) and competition (dashed line) based survival models. The optimal thresholds identified are indicated by asterisks, with values of 0.983 (sensitivity of 0.74, specificity of 0.83) for the growth-based model, and 0.979 (sensitivity of 0.75, specificity of 0.71) for the competition-based model. The area under the curve (AUC) and associated 95% confidence intervals (CI) are 0.859 [0.841, 0.876] for the growth-based survival model, and 0.795 [0.772, 0.817] for the competition-based survival model, indicating excellent and good discrimination between live and dead classes respectively.

Transect	Coords	NSR	min(SA)	max(SA)	Sw Sph	Hw Sph	Hw ba	Stand age
6	54.83 ° N, 111.71 ° W	CM	19	53	500	1875	14.46	60
7	54.84 ° N, 111.68 ° W	CM	16	66	163	2520	22.04	62
8	54.93 ° N, 111.54 ° W	CM	44	56	505	2777	19.09	NA
9	54.83 ° N, 111.84 ° W	CM	22	56	1600	1575	17.79	67
A	55.03 ° N, 111.68 ° W	CM	30	59	244	2166	18.52	NA
AA	55.73 ° N, 110.98 ° W	CM	53	57	5977	2423	31.42	63
B	55.05 ° N, 111.27 ° W	CM	49	63	513	1025	21.23	NA
CC	55.82 ° N, 115.21 ° W	CM	62	66	5524	2657	22.54	71
DD	56.80 ° N, 115.26 ° W	CM	54	57	5333	3166	39.54	69
EE	57.19 ° N, 115.11 ° W	CM	52	58	6106	2389	10.45	64
F	55.07 ° N, 111.81 ° W	CM	34	54	360	2388	11.48	NA
FF	56.44 ° N, 115.33 ° W	CM	44	45	8631	1894	12.37	51
G	55.56 ° N, 111.24 ° W	CM	26	58	646	625	7.81	NA
H	55.06 ° N, 111.90 ° W	CM	20	55	575	1055	6.47	NA
HH	58.53 ° N, 117.29 ° W	DM	65	74	5473	1684	41.06	83
JJ	57.85 ° N, 115.38 ° W	CM	55	58	2444	2333	27.26	68
KK	57.99 ° N, 117.42 ° W	DM	50	54	6894	1736	24.18	64
MM	53.75 ° N, 116.62 ° W	LF	40	44	10459	5057	10.77	51
N	53.04 ° N, 115.01 ° W	LF	27	42	4666	2000	6.41	35
PP	58.78 ° N, 117.38 ° W	CM	56	62	14400	2800	24.99	66
Q	54.10 ° N, 115.75 ° W	LF	23	62	872	911	6.74	70

Continued on next page...

Continued from previous page...

QQ	58.54 ° N, 115.62 ° W	DM	34	55	2444	3111	16.27	68
R	56.57 ° N, 118.75 ° W	LBH	42	59	6092	2384	16.50	128
RR	57.48 ° N, 117.50 ° W	DM	18	27	3255	4883	16.94	34
S	56.49 ° N, 119.69 ° W	LBH	21	28	1733	6866	3.66	63
SS	57.14 ° N, 117.73 ° W	LBH	26	37	2731	3512	18.47	44
T	55.54 ° N, 118.74 ° W	LF	22	54	983	1650	29.16	64
TT	52.58 ° N, 115.35 ° W	LF	27	36	4678	2573	17.24	42
U	56.47 ° N, 118.31 ° W	LBH	41	52	5000	1333	4.84	63
UU	52.22 ° N, 115.25 ° W	LF	25	30	1368	2052	17.65	30
V	55.60 ° N, 118.11 ° W	DM	39	54	661	2430	22.49	66
VV	52.37 ° N, 115.30 ° W	LF	20	32	6815	1179	12.25	51
W	54.32 ° N, 115.59 ° W	LF	22	31	7101	5579	13.71	33
WW	52.05 ° N, 115.08 ° W	LF	30	44	3025	2762	25.03	87
X	54.32 ° N, 115.70 ° W	LF	42	63	866	966	38.01	64
XX	56.52 ° N, 111.30 ° W	CM	39	44	3910	1368	26.36	55
Y	54.48 ° N, 116.79 ° W	CM	33	64	733	1583	30.95	60
YY	57.15 ° N, 111.64 ° W	CM	39	48	5234	2538	18.35	57
Z	53.04 ° N, 115.01 ° W	CM	16	54	1233	3850	6.82	51
ZZ	56.03 ° N, 110.88 ° W	CM	48	54	5169	1336	15.40	67

Table 2.1: Transect characteristics including: Coords (lat, long), natural subregion (NSR), minimum spruce age (min(SA)), maximum spruce age (max(SA)), spruce stems per hectare (Sw Sph), hardwood stems per hectare (Hw Sph), hardwood basal area (Hw ba) in m<sup>2</sup>/ha, and stand age determined by the oldest aspen in the stand (Stand age). Note that stand age was not determined for several transects that were sampled earlier on in the study.

Parameter	Mean	0.025	0.975
Intercept	0.134	-0.131	0.390
logABAI2 [log(mm <sup>2</sup> /yr)]	1.196	1.118	1.274
cmiJune [cm]	0.051	0.023	0.079

Table 2.2: Recent growth survival model parameter estimates and 95% credible intervals.

Parameter	Mean	0.025	0.975
Intercept	5.055	4.728	5.389
DBH [mm]	0.030	0.024	0.034
SWBAGR [m <sup>2</sup> /ha]	-0.076	-0.096	-0.057
ALLNGR [# /ha]	$-2.35 \times 10^{-5}$	$-2.91 \times 10^{-5}$	$-1.75 \times 10^{-5}$
cmiJune [cm]	0.030	0.016	0.050

Table 2.3: Local competition survival model parameter estimates and 95% credible intervals.

Model	PL	DIC	HL
Growth-based	498	2863	0.83
Competition-based	534	3125	$6.4 \times 10^{-6}$

Table 2.4: Model fit statistics for the recent growth and local competition survival models.

<b>A. Recent growth</b>		
	Predicted live	Predicted dead
Live	0.75	0.25
Dead	0.19	0.81
<b>B. Local competition</b>		
	Predicted live	Predicted dead
Live	0.75	0.25
Dead	0.28	0.71

Table 2.5: Classification tables for the recent growth (A) and local competition (B) survival models. Using a threshold of 0.981 for both models, the predicted survival probabilities obtained from the fitted logistic models were used to classify trees as live or dead. Trees with predicted survival probabilities greater than 0.981 were classified as live, while all others were classified as dead. These predictions can be compared with the data, to determine the proportion of live and dead trees that were correctly classified. Overall, the percent of trees correctly classified was 76% for the growth-based model and 75% for the competition-based model.

# Bibliography

- ASRD. *Permanent Sample Plot (PSP) Field Procedures Manual*. Public Lands and Forests Division, Forest Management Branch, Alberta Sustainable Resource Development, Edmonton, Alberta, Canada, 1995a.
- ASRD. *Stand Dynamics System Field Remeasurement Manual*. Public Lands and Forests Division, Forest Management Branch, Alberta Sustainable Resource Development, Edmonton, Alberta, Canada, 1995b.
- Beckingham, J. and Archibald, J. *Field guide to ecosites of northern Alberta*, vol. 5. University of British Columbia Press, 1996.
- Beckingham, J., Corns, I., and Archibald, J. *Field guide to ecosites of west-central Alberta*, vol. 9. University of British Columbia Press, 1996.
- Bigler, C. Assessing the performance of theoretical and empirical tree mortality models using tree-ring series of Norway spruce. *Ecological Modelling*, 174(3):225–239, 2004.
- Bigler, C. and Bugmann, H. Predicting the time of tree death using dendrochronological data. *Ecological Applications*, 14(3):902–914, 2004.
- Biondi, F. Comparing tree-ring chronologies and repeated timber inventories as forest monitoring tools. *Ecological Applications*, 9(1):216–227, 1999.
- Chen, H.Y.H. and Popadiouk, R.V. Dynamics of North American boreal mixed-woods. *Forest Research*, 166:137–166, 2002.
- Clark, J. *Models for ecological data: an introduction*. Princeton University Press Princeton, New Jersey, USA, 2007.
- Constabel, A. and Lieffers, V. Seasonal patterns of light transmission through boreal mixedwood canopies. *Canadian Journal of Forest Research*, 26(6):1008–1014, 1996.
- Cook, E. and Peters, K. The smoothing spline: a new approach to standardizing forest interior tree-ring width series for dendroclimatic studies. *Tree-Ring Bulletin*, 41:45–53, 1981.
- Dang, Q.L. and Lieffers, V.J. Assessment of patterns of response of tree ring growth of black spruce following peatland drainage. *Canadian Journal of Forest Research*, 19:924–929, 1989.

- DeLong, E., DeLong, D., and Clarke-Pearson, D. Comparing the areas under two or more correlated receiver operating characteristic curves: a nonparametric approach. *Biometrics*, pp. 837–845, 1988.
- Eis, S. et al. *Root-growth relationships of juvenile white spruce, alpine fir, and lodgepole pine on three soils in the interior of British Columbia*. Department of Fisheries and Forestry, Canadian Forestry Service, 1970.
- Feng, Z., Stadt, K.J., and Lieffers, V.J. Linking juvenile white spruce density, dispersion, stocking, and mortality to future yield. *Canadian Journal of Forest Research*, 36:3173–3182, 2006.
- Filipescu, C.N. and Comeau, P.G. Competitive interactions between aspen and white spruce vary with stand age in boreal mixedwoods. *Forest Ecology and Management*, 247(1):175–184, 2007.
- Gelfand, A.E. and Ghosh, S.K. Model choice : A minimum posterior predictive loss approach. *Biometrika*, 85(1):1–11, 2011.
- Gelman, A., Carlin, J., Stern, H., and Rubin, D. *Bayesian data analysis*. Chapman & Hall/CRC, 2003.
- Hogg, E. Climate and the southern limit of the western Canadian boreal forest. *Canadian Journal of Forest Research*, 24(9):1835–1845, 1994.
- Hogg, E. Temporal scaling of moisture and the forest-grassland boundary in western Canada. *Agricultural and Forest Meteorology*, 84(1):115–122, 1997.
- Hogg, E.H.T., Brandt, J.P., and Michaelian, M. Impacts of a regional drought on the productivity, dieback, and biomass of western Canadian aspen forests. *Canadian Journal of Forest Research*, 38(6):1373–1384, 2008.
- Hogg, E.H.T. and Wein, R.W. Impacts of drought on forest growth and regeneration following fire in southwestern Yukon. *Canadian Journal of Forest Research*, 2150:2141–2150, 2005.
- Holmes, R. Computer-assisted quality control in tree-ring dating and measurement. *Tree-Ring Bulletin*, 43(1):69–78, 1983.
- Hosmer, D.W. and Lemeshow, S. *Applied logistic regression*. Wiley series in probability and statistics: Texts and references section. Wiley, 2000.
- Huang, J.G., Stadt, K.J., Dawson, A., and Comeau, P. Modelling growth-competition relationships in trembling aspen and white spruce mixed boreal forests of western Canada. *Submitted to PLoS One*, 2013.
- Huang, S. *Ecologically Based Reference-age Invariant Polymorphic Height Growth and Site Index Curves for White Spruce in Alberta*. Alberta Environmental Protection, Land and Forest Services, Forest Management Division, 1994.

- Huang, S., Meng, S.X., and Yang, Y. A Growth and Yield Projection System (GYPSY) for Natural and Post-harvest Stands in Alberta. Tech. rep., Alberta Sustainable Resource Development, 2009.
- Huang, S., Titus, S., and Wiens, D. Comparison of nonlinear height-diameter functions for major Alberta tree species. *Canadian Journal of Forest Research*, 22(9):1297–1304, 1992.
- Husch, B., Beers, T., and Kershaw Jr, J. Forest mensuration. 2003.
- Kabzems, R. and García, O. Structure and dynamics of trembling aspen - white spruce mixed stands near Fort Nelson, BC. *Canadian Journal of Forest Research*, 34(2):384–395, 2004.
- Kobe, R., Pacala, S., Silander Jr, J., and Canham, C. Juvenile tree survivorship as a component of shade tolerance. *Ecological Applications*, 5(2):517–532, 1995.
- Kobe, R.K. and Coates, K.D. Models of sapling mortality as a function of growth to characterize interspecific variation in shade tolerance of eight tree species of northwestern British Columbia. *Canadian Journal of Forest Research*, 236:227–236, 1997.
- Kruys, N., Fries, C., Jonsson, B., Lämås, T., and Ståhl, G. Wood-inhabiting cryptogams on dead Norway spruce (*Picea abies*) trees in managed Swedish boreal forests. *Canadian Journal of Forest Research*, 29(2):178–186, 1999.
- Krzanowski, W. and Hand, D. *ROC curves for continuous data*. Chapman & Hall, 2009.
- Li, D., Bhariok, R., and Neagu, R. The effect of variant sample sizes and default rates on validation metrics for probability of default models. *The Journal of Risk Model Validation*, 5(4):49–74, 2012.
- Lieffers, V., Pinno, B., and Stadt, K. Light dynamics and free-to-grow standards in aspen-dominated mixedwood forests. *The Forestry Chronicle*, 78(1):137–145, 2002.
- Lieffers, V. and Stadt, K. Growth of understory *Picea glauca*, *Calamagrostis canadensis*, and *Epilobium angustifolium* in relation to overstory light transmission. *Canadian Journal of Forest Research*, 24(6):1193–1198, 1994.
- Mbogga, M.S., Hamann, A., and Wang, T. Historical and projected climate data for natural resource management in western Canada. *Agricultural and Forest Meteorology*, 149(5):881–890, 2009.
- McGuire, A., Ruess, R., Lloyd, A., Yarie, J., Klein, J., et al. Vulnerability of white spruce tree growth in interior Alaska in response to climate variability: dendrochronological, demographic, and experimental perspectives. *Canadian Journal of Forest Research*, 40(7):1197–1209, 2010.
- Meng, S., Huang, S., Lieffers, V., and Yang, Y. Modelling the change in aspen species composition in boreal mixedwoods. *Forestry*, 81(5):575–586, 2008.

- Metsaranta, J., Lieffers, V., and Wein, R. Dendrochronological reconstruction of jack pine snag and downed log dynamics in Saskatchewan and Manitoba, Canada. *Forest Ecology and Management*, 255(3):1262–1270, 2008.
- Metsaranta, J.M. and Lieffers, V.J. Using dendrochronology to obtain annual data for modelling stand development: a supplement to permanent sample plots. *Forestry*, 82(2):163–173, 2009.
- Nunifu, T. Compatible diameter and height increment models for lodgepole pine, trembling aspen, and white spruce. *Canadian Journal of Forest Research*, 39(1):180–192, 2009.
- Osika, D., Stadt, K., Comeau, P., and MacIsaac, D. Sixty-year effects of deciduous removal on white spruce height growth and site index in the western boreal. *Canadian Journal of Forest Research*, 43:139–148, 2013.
- Pachauri, R. and Reisinger, A. IPCC 2007 Synthesis Report: An Assessment of the Intergovernmental Panel on Climate Change. IPCC, Geneva, Switzerland, 2007.
- Patil, A., Huard, D., and Fonnesbeck, C. PyMC: Bayesian stochastic modelling in Python. *Journal of Statistical Software*, 35(4):1, 2010.
- Peng, C., Ma, Z., Lei, X., Zhu, Q., Chen, H., et al. A drought-induced pervasive increase in tree mortality across Canada’s boreal forests. *Nature Climate Change*, 1(9):467–471, 2011.
- Peters, V.S., Macdonald, S.E., and Dale, M.R.T. Aging discrepancies of white spruce affect the interpretation of static age structure in boreal mixedwoods. *Canadian Journal of Forest Research*, 32(8):1496–1501, 2002.
- Peters, V.S., MacDonald, S.E., and Dale, M.R.T. The interaction between masting and fire is key to white spruce regeneration. *Ecology*, 86(7):1744–1750, 2005.
- Pinno, B.D., Lieffers, V.J., and Stadt, K.J. Measuring and modelling the crown and light transmission characteristics of juvenile aspen. *Canadian Journal of Forest Research*, 31(11):1930–1939, 2001.
- Régnière, J. and Saint-Amant, R. *BioSIM 9: User’s Manual*. Laurentian Forestry Centre, 2008.
- Spiegelhalter, D., Best, N., Carlin, B., and Van Der Linde, A. Bayesian measures of model complexity and fit. *Journal of the Royal Statistical Society: Series B (Statistical Methodology)*, 64(4):583–639, 2002.
- Stadt, K., Huston, C., Coates, K., Feng, Z., Dale, M., et al. Evaluation of competition and light estimation indices for predicting diameter growth in mature boreal mixed forests. *Annals of Forest Science*, 64(5):477–490, 2007.
- Stadt, K.J. and Lieffers, V.J. Comparing PAR transmission models for forest understorey vegetation. *Applied Vegetation Science*, 8(1):65–76, 2005.

- Strong, W. and La Roi, G. Root-system morphology of common boreal forest trees in Alberta, Canada. *Canadian Journal of Forest Research*, 13(6):1164–1173, 1983.
- Thorpe, H.C. and Daniels, L.D. Long-term trends in tree mortality rates in the Alberta foothills are driven by stand development. *Canadian Journal of Forest Research*, 42(9):1687–1696, 2012.
- Vanclay, J. Management advice from tree measurements. In *Permanent Sample Plots and Growth Models for Natural Forest Management*, pp. 93–102. 1999.
- Wright, E., Coates, K., Canham, C., and Bartemucci, P. Species variability in growth response to light across climatic regions in northwestern British Columbia. *Canadian Journal of Forest Research*, 28(6):871–886, 1998.
- Wyckoff, P.H. and Clark, J.S. Predicting tree mortality from diameter growth: a comparison of maximum likelihood and Bayesian approaches. *Canadian Journal of Forest Research*, 30(1):156–167, 2000.
- Yamaguchi, D.K. A simple method for cross-dating increment cores from living trees. *Canadian Journal of Forest Research*, 21(3):414–416, 1991.
- Yang, Y., Huang, S., Meng, S.X., Trincado, G., and VanderSchaaf, C.L. A multi-level individual tree basal area increment model for aspen in boreal mixedwood stands. *Canadian Journal of Forest Research*, 39(11):2203–2214, 2009.
- Yang, Y., Titus, S.J., and Huang, S. Modeling individual tree mortality for white spruce in Alberta. *Ecological Modelling*, 163(3):209–222, 2003.
- Zhai, L., Bergeron, Y., Huang, J.G., and Berninger, F. Variation in intra-annual wood formation, and foliage and shoot development of three major Canadian boreal tree species. *American Journal of Botany*, 99(5):827–837, 2012.

## Chapter 3

# A multi-species integral projection model for the prediction of forest structure

### 3.1 Introduction

The Boreal forest is the most extensive ecosystem type on earth, and for this reason is important in terms of the global terrestrial carbon cycle (Plaut, 2002). In Canada, the Boreal forest covers approximately 77 % of the forested landscape, and is of national economic, societal, and ecological importance (Natural Resources Canada, 2009; Murphy et al., 1993). The mixedwood Boreal subregion forms the largest managed subregion, and is dominated by trembling aspen (*Populus tremuloides*) and white spruce (*Picea glauca*), although other species coexist in smaller numbers. Species interactions in mixedwood forests play an important role in determining future forest composition and structure (Man and Lieffers, 1999). The Alberta mixedwood forest demonstrates the structural and compositional complexity that can arise from competitive and successional dynamics. Typically, the pioneering aspen are first to appear after a large stand-replacing disturbance. The more shade-tolerant spruce subsequently appear, although their understory establishment depends on the interaction of seedbed receptivity, location of seed source, time since fire, and occurrence of a mast year (Peters et al., 2005). Aspen canopy closure typically occurs at a stand-age of approximately 20 years (Lieffers et al., 2002), and is soon after followed by the initiation of aspen break-up, during which the aspen begin to senesce resulting in gap creation (Chen and Popadiouk, 2002).

These gaps allow the understory spruce to intercept increased amounts of solar radiation, which is often sufficient to trigger growth increase, sometimes referred to as a growth release. Throughout these successional stages, ecological interactions continuously affect the growth, survival, and reproductive abilities of individuals.

With the increased awareness of complex ecosystem interactions, whole ecosystem management has become increasingly important (Kneeshaw et al., 2000). These management practices make an effort to retain varied composition, structure, and processes representative of those typically present in an unaltered landscape. These practices are implemented with the goal of preserving biodiversity at the landscape scale, although the impact of regenerating mixed stands on productivity has been favored by both scientists and managers alike (Man and Lieffers, 1999; MacPherson et al., 2001). Regardless of the implications of whole ecosystem management, managers are required to abide by certain practices when developing forest management plans as defined in the Canadian Council of Ministers' criteria for sustainable forest management (CCFM 2005). Effective sustainable management that meets all necessary obligations requires careful planning and the use of accurate predictions. Here, mathematical and statistical models of forest growth are essential to the planning process. As government standards become more rigid, questions regarding the growth and yield implications of planting mixtures as opposed to mono-cultures have become forefront in the Alberta forest management community (Alberta Reforestation Standards Science Council, 2001; Lieffers et al., 2008; Lieffers and Beck, 1994).

Although many studies have considered how competition affects tree growth and mortality, the lack of mid-rotation data for the mixedwood boreal has prevented a more complete understanding of the mechanisms of forest evolution and coexistence. In this study, I investigate the importance of competitive interactions through the application of a structured population model to a large-scale mixedwood boreal forest data set.

Structured population models have been successfully used to model populations of trees (Silvertown et al., 1993). The matrix modelling approach is most commonly used, and has been used to not only understand species demographics and make predictions about the long-term fate of a population, but also to compare the importance of different life-cycle stages with respect to long-term growth rates (Silvertown et al., 1993). This modelling framework was originally presented by Leslie in 1945 as an age-structured matrix model (Leslie, 1945), but was later modified to capture size-structure in forest populations by Usher in 1966 (Usher, 1966). Several modifications of these basic age or size structured matrix models

have been implemented for tree populations. For example, Lytle and Merritt used a matrix model to stratify a cottonwood population by age and capture the demographic dependence on river hydrology by allowing transition matrices to vary according to the hydrograph (Lytle and Merritt, 2004). In tree populations where species interactions drive population demographics, density dependent transition matrices have been used (Freckleton et al., 2003). Although in many cases matrix models have been used to effectively model tree populations, Van Mantgem and Stephenson (2005) found that matrix models offered only marginal improvements when compared to demographic models without size structure, indicating that size alone may not always be sufficient to predict growth and survival rates.

Other structured population approaches have also been considered. Kohyama (1991) used a Fokker-Plank drift-diffusion partial differential equation to model population distribution changes, where population demography continuously depended on tree size. In this case, although species differences were not considered, competition for light was included in demographic rate functions using an index based on the basal area of thicker trees. Most recently, Zuidema et al. (2010) used an integral projection model (IPM) to describe tree populations, but encountered difficulties when performing numerical integration resulting from the slow-growing long-lived nature of trees (which results in a “tall and skinny” kernel that is near-discontinuous in nature). In this work I use the IPM.

The IPM provides an attractive modeling alternative to other aforementioned structured population modelling approaches (Easterling et al., 2000). For a population whose demography and therefore structure can be modelled as a function that is continuously dependent on another variable, such as size, the IPM modeling formulation addresses some of the challenges that arise from a more traditional matrix modeling framework. In particular, the IPM overcomes the challenge of having to arbitrarily divide a continuous variable into discrete classes, where the determination of class endpoints is difficult and subjective, and all individuals in a class are considered equal (homogenization within classes). A natural step towards dealing with continuous structure is to partition the continuous domain into arbitrarily small classes - in theory this concept works in a matrix modeling framework, but the practical application of a model with a large number of structural classes requires the determination of a large number of parameters. In most cases the available data is not sufficient to obtain parameter estimates for these models. The development of an IPM for a given population allows one to make predictions about change in structure and population numbers (both on a short-term and longer term scale), and to learn about the sensitivity of these predictions to

parameters and inputs. A straightforward IPM considers growth, survival, and fecundity of a particular species, typically as a function of size.

Here I implement a coupled two-species IPM with and without competition to address questions about the importance of competition in the mixedwood boreal. The multi-species IPM is a natural extension of the single-species model, and it enables modelers to predict changes on a landscape of coexisting individuals interacting with each other. These interactions are typically manifested as reductions in predicted values from demographic functions, such as reduced survival probability, reduced growth, or reduced fecundity (although note that competitive interactions may also have positive effects on survival, growth, and fecundity). Adler et al. (2010) used multi-species IPMs among other modelling tools to identify the effects of niche differences on coexistence by considering growth rates and population size for the stable stage distributions. Further work by Adler et al. (2012) used the same modelling framework to identify the relative importance of niche differences in order to determine when it is necessary to use multi-species models as opposed to single species models which do not explicitly include interspecific interactions.

Other extensions of the basic IPM have been developed, for example Ellner and Rees (2006) included complex demography through kernel dependence on other variables affecting demography such as age and individual quality or vigor. Another natural extension is the incorporation of stochasticity to allow for a varying environment. Environmental stochasticity can be incorporated by allowing a kernel to dependent on available climate data. To project forward in time, kernels or climate data that inform a redistribution function can be randomly be drawn at each iteration (Rees and Ellner, 2009; Childs et al., 2004).

In a simple IPM formulation for a single-species, population is assumed to depend on continuous variable  $x$ , where the domain of  $x$  is  $[L, U]$  and is typically defined by limits of known processes or by the data. The model maps a population distribution  $n(x, t)$  to the next time  $t + 1$  using an integral operator

$$n(y, t + 1) = \int_L^U k(x, y)n(x, t)dx. \quad (3.1)$$

The kernel  $k(x, y)$  mathematically describes how individuals transition from size  $x$  to size  $y$  in a single time step and can take many forms depending on the nature of the system and the characteristics of the data set. In general, there are two ways that individuals can transition from size  $x$  to size  $y$  in a year: 1) by growing from size  $x$  to  $y$  and surviving from time  $t$  to time  $t + 1$ ; and 2) through the

production of new individuals of size  $y$  by individuals of size  $x$ . More formally, the kernel is written as  $k(x, y) = f(x, y) + p(x, y)$ , where  $f(x, y)$  describes the production of size  $y$  individuals by size  $x$  adults, and  $p(x, y)$  describes the growth and survival associated with a size  $x$  individuals transitioning to become size  $y$ . Using integral operator theory, conditions for which stable stage distributions exist can be derived. The conditions are typically satisfied for IPMs which describe living populations because of the assumption that the defined redistribution kernel satisfies a power-positivity condition. For example, in Rebarber et al. (2011), stability conditions for an IPM with density-dependent fecundity are derived using feedback control system methods. For a more thorough overview of the IPM, I suggest the excellent introduction to integral projection modeling by Briggs et al. (2010).

In this work my goal is to assess the viability of the IPM as a tool for prediction of structural changes in a mixedwood forest, and to investigate the strength of competitive interactions. To do this, my model is built and validated using independent data sets from the mixedwood boreal forest of Alberta. The approach is to use the IPM framework to construct a two-species model, both with and without competitive interactions, to understand the dynamics of the mixedwood forest. There are several features that the IPMs should reflect as emergent properties in order to conclude that they are reasonable and realistic models that can be used for forest management. The model should be able to not only capture the dynamics of the changing size distribution, but should also be able to predict the number of individuals (i. e. the balance of mortality and fecundity).

In this Chapter, after describing the two independent data sets used, I introduce the two species IPM. Redistribution kernels for the two-species IPM are then fitted with and without competitive structure in order to assess the importance of competition. Both IPMs are assessed according to several metrics to inform about their performance when compared to data, allowing me to draw conclusions about the importance of species interactions. Then, using the IPM with competitive structure, projections for four canopy cover classes are made using initial conditions defined by data from a post-fire natural-origin mixedwood forest report. These projections are used to discuss the relative productivity of mixed stands relative to mono-cultures. Lastly, I highlight the contributions of this modeling approach, and suggest possible future extensions.

## 3.2 Materials and Methods

### 3.2.1 Data

In this Chapter I use two independent mixedwood boreal forest data sets: one to fit the model, and one to assess the ability of the model to make out-of-sample predictions. I refer to these data sets as the retrospective and permanent sample plot (PSP) data. Both data sets are comprised of data from a large number of sample plots from across the mixedwood boreal forest in Alberta, Canada (see Figure 3.1). The topography of the region varies from the lower foothills of the Rocky Mountains to rolling hills and plains, shaped by retreating glaciers some 10,000 years ago. In this region, climate is characterized by short, generally moist summers and long, cold, drier winters. The high elevation sites are generally cooler and more moist. This region is composed of intimate and patchy mixtures of white spruce, trembling aspen, balsam poplar, white birch, balsam fir, jack and lodgepole pine, and black spruce.

The retrospective data set is unique in that sample plots were visited only once, but the dendrochronological data collected allowed sample plot density and tree growth to be reconstructed for the previous 20 years as described in Chapter 2. This sampling protocol included the determination of year-of-death of dead spruce based on crossdating techniques, and the resulting data set included survival information for this species. Reconstructed data included measures of competition including plot basal area, number of individuals, and sum of diameters, for both spruce and aspen. For each sampled tree, these measures were determined for all competitors and for only competitors that were thicker in diameter. This data set was used to fit the redistribution kernel demographic models, as described in Section 3.2.4. The retrospective data consisted of measurements from forty mixedwood sites across Alberta. Out of the forty sites sampled, 21 fell in the Central Mixedwood Natural Subregion, 10 in the Lower Foothills, 5 in the Dry Mixedwood, and 4 in the Lower Boreal Highlands (Alberta Sustainable Resource Development, 2005). A total of 1318 trees were sampled, including 443 live spruce, 350 dead spruce, and 525 aspen. Using ring widths to retrospectively determine tree data for 20 years prior to sampling, the data set obtained was analogous to one obtained from PSP sampling, but with an annual resolution. The inclusion of this additional information resulted in a total of 13969 annual tree measurements.

The PSP data set comes from a long-term program established by the Alberta Government in 1960 to better understand stand dynamics and establish a sus-

tainable yield program, and now consists of re-measurements on over 650 PSPs (Public Lands and Forests Division, Forest Management Branch, 2005). Plots are re-measured every 5 or 10 years according to stand type and age (in general, intervals are 5 years for younger stands, 10 years for mature stands). For the purpose of this study, I only considered mixedwood plots composed primarily of trembling aspen and white spruce, and required that each species represent at least 20% of the total tree population, and that any additional species present account for a maximum of 30% of the population. In some PSPs, new individuals were tagged and measured as they appeared. In this work, I focus on the development of an established cohort, and do not consider any new trees present in measurement years subsequent to the first. The exclusion of new individuals is supported by previous work that suggests that competitive interactions for a given tree are best captured by indices based on trees that are thicker in diameter than a subject tree (Stadt et al., 2007; Filipescu and Comeau, 2007). In total, 58 PSPs met the requirements that spruce and aspen each represent a minimum of 20% of the total population, and that any additional species not make up more than 30% of the population. The sample plots were distributed among the natural subregions as follows: 18 in Central Mixedwood; 16 in Lower Foothills; 8 in Dry Mixedwood; 8 in Lower Boreal Highlands; 2 in Northern Mixedwood; 1 in Upper Foothills; and 1 in Montane.

### 3.2.2 Two-species IPM formulation

Here I describe the general functional form of the two-species IPM, which is written as two equations that are coupled through inter-dependent redistribution kernels. The distribution function which describes the state of a species is  $n_m(x, t)$  for  $m = 1$  (spruce), 2 (aspen), where  $n_m(x, t)dx$  is the number of individuals that are in the size range  $[x, x + dx]$  and  $n_m$  is a piecewise continuous function of size, which in our case is tree DBH. How the population moves through time is determined by the projection kernel

$$k_m(x, y, n_1(\cdot, t), n_2(\cdot, t)) : \Omega_m \times \Omega_m \times C(\Omega_m) \times C(\Omega_m) \rightarrow R^+. \quad (3.2)$$

The projection kernel defines how a size  $x$  individual transitions to become a size  $y$  individual in a year. The kernel depends not only on  $x$  and  $y$ , but on the forest size structure for both species ( $n_1$  and  $n_2$ ). This allows for size-structured competitive intra- and inter-specific interactions. Mathematically  $k_m$  is assumed to be a bounded piecewise continuous functional. The general form of the coupled

IPM is:

$$\begin{aligned} n_1(y, t + 1) &= \int_{\Omega_1} k_1(x, y, n_1(\cdot, t), n_2(\cdot, t)) n_1(x, t) dx \\ n_2(y, t + 1) &= \int_{\Omega_2} k_2(x, y, n_1(\cdot, t), n_2(\cdot, t)) n_2(x, t) dx \end{aligned} \tag{3.3}$$

where the domain  $\Omega_m$  contains all possible tree sizes for species  $m$ .

In this model, I consider only the trajectory of the cohort of individuals present at the initial time. Although in the long run new individuals may impact the forest structure, in the short-term these smaller individuals can be ignored since it has been shown, and confirmed by the retrospective data set, that competition is most effective as a predictor of growth or mortality when measured as a function of trees that are thicker in diameter (Dawson et al., 2013; Stadt et al., 2007). Because this model is designed to follow a cohort of trees, the fecundity  $f_m$  is set to zero. The growth and survival term  $p_m$  has two subcomponents,  $g_m$  and  $s_m$ . In our case the kernels are therefore defined as  $k_m(x, y, n_1(\cdot, t), n_2(\cdot, t)) = g_m(x, y, n_1(\cdot, t), n_2(\cdot, t)) s_m(x, n_1(\cdot, t), n_2(\cdot, t))$ , where  $g_m(x, y, n_1(\cdot, t), n_2(\cdot, t))$  defines how a size  $x$  individual transitions to become a size  $y$  individual in a single time-step as a function of the current forest structure, and  $s_m(x, n_1(\cdot, t), n_2(\cdot, t))$  denotes the probability that a tree of size  $x$  will survive to the next time-step given the current forest structure. Here I consider kernels  $k_m$  that are continuous in  $y$  over the domain, and therefore the resulting population densities  $n_m(y, t + 1)$  will be continuous if the population densities  $n_m(y, t)$  are continuous. <sup>1</sup>

The coupled IPM in (3.3) is evolved through time numerically (see Appendix 1.1 for details). For simplicity I consider a common size ( $x$ ) domain, measured in  $mm$ , for spruce and aspen such that  $\Omega_1 = \Omega_2 = [L, U]$  where  $L = 0$  and  $U = 800$ . Note that  $L$  and  $U$  are chosen in order to bound the range of tree sizes observed in the data, as well as to minimize the domain eviction rate. This domain is discretized using  $N$  uniform mesh points. The midpoint rule is used to discretize the integral operators in (3.3), and hence the population distributions  $n_m(\cdot, t)$  become  $N$  dimensional vectors denoted by  $\mathbf{n}_m^t$ . The coupled IPM in (3.3) becomes  $\mathbf{n}_m^{t+1} = P_m(\mathbf{n}_1^t, \mathbf{n}_2^t) \mathbf{n}_m$  where the projection matrices  $P_m$  are discrete versions of the integral operators and are determined by sampling the kernels  $k_m$  according to the midpoint rule.

---

<sup>1</sup>For a kernel that is only piecewise continuous with respect to  $y$ , we only achieve piecewise continuity in the resulting population density (for an example of a piecewise continuous kernel, see (Easterling et al., 2000)).

### 3.2.3 Competitive interactions

Resource access is a limiting factor of tree growth and survival. Increasing local forest population size in density or biomass increases resource demand, and can therefore limit the resource supply available to any given individual. However, both species and individual variation play an important role in determining the demographic response among individuals (Clark et al., 2010). More specifically, different species have been found to occupy different niches, have varying resource requirements, and have a range of responses to resource deficiencies (Reich et al., 2002; Kobe and Coates, 1997). Even within a species there exists large variability in niche specificity and tolerance to extreme environments (Clark, 2010).

In the Alberta mixedwood, the coexistence of aspen and spruce has been shown to increase yield through efficient partitioning of the light resource (Man and Lieffers, 1999). The shade tolerant spruce establish in the understory of the shade-intolerant aspen canopy and utilize incoming solar radiation that passes through the relatively open aspen canopy. Additionally, mixedwoods exhibit increased nutrient cycling relative to conifer monocultures resulting from the nutrient rich aspen leaf litter (Man and Lieffers, 1999). It has also been shown that competition from all thicker trees can decrease height increments in both spruce and aspen. However, spruce mortality is more sensitive to competition from conspecifics, whereas aspen mortality has been shown to depend on total density (Feng et al., 2006; Bokalo et al., 2007). Aggregating results is not straightforward, and quantifying complicated interactions at varying spatial scales is difficult if even possible.

In this study I do not incorporate fine-scale spatial dynamics into the model, but consider site-specific proxy measures of competition such as basal area, sum of diameter, and number of stems, for all trees, and for trees thicker in diameter. As shown below, these measures can be determined from  $n_1(x, t)$  and  $n_2(x, y)$  when calculating the growth  $g_m$  and survival  $s_m$  functionals. These indices are straightforward to obtain when sampling, and have been shown to serve as useful measures of competition in previous studies (Stadt et al., 2007). I assess the importance of mixedwood interactions by developing IPMs with and without competitive structure and assessing the validity of these competing models using PSP data.

### 3.2.4 Fitting the redistribution kernel

To include the effects of both inter- and intra-specific competition, I consider different measures of plot competition as covariates. Competition measures considered

were species-specific tree density, basal area, and sum of tree diameters. In the retrospective data set, for each sampled tree these measures were computed for competitors of all sizes as well as for individuals with a DBH larger in magnitude than that of subject tree. Due to high correlation of species-specific competition covariates, only a single measure of the competitive effect was included for each species. Subject tree size (DBH) was also considered as a covariate.

Demographic models were fitted using the linear or generalized linear modeling framework in R. Model covariates were selected step-wise based on the Akaike Information Criterion (AIC) which measures relative goodness-of-fit (see Section 3.3.2). Note that using this relative measure is useful for model selection but provides no information about the absolute fit of a model and how well any given model fits the data. The methods for analyzing this aspect are described in Section 3.2.5.

## Growth

The kernel growth function  $g_m(x, y)$  describes how a size  $x$  tree grows to become a size  $y$  tree in a year. This transition is typically described using a normal distribution probability density function (PDF), where both  $\mu$  and  $\sigma$  are considered functions of  $x$  and any other explanatory variables (Easterling et al., 2000; Briggs et al., 2010). The normal PDF best describes our sample data, where given a size  $x$  at time  $t$ , size at time  $t + 1$  is randomly dispersed around a mean  $\mu(x)$ . Using the Gaussian PDF to model the growth of both aspen and spruce, growth from size  $x$  to size  $y$  we formally write

$$g_m(x, y, n_1(\cdot, t), n_2(\cdot, t)) = \frac{1}{\sigma_m \sqrt{2\pi}} \exp \left( -\frac{\left( y - \mu_m(x, n_1(\cdot, t), n_2(\cdot, t)) \right)^2}{2\sigma_m^2} \right) \quad (3.4)$$

where the expected growth  $\mu_m(x, n_1(\cdot, t), n_2(\cdot, t))$  and variance  $\sigma_m$  still need to be determined. In our case, the relationship between size in consecutive years is approximately linear and therefore size in the next year  $\mu_m(x, n_1(\cdot, t), n_2(\cdot, t))$  is modelled as a linear function of current size and competition using linear regression, fit using least squares. In the competition-free case, only size is considered as a covariate. The variance term  $\sigma_m^2$  which appears in the normal PDF used to define the growth kernel can be determined through examination of the squared residuals from the  $\mu_m(x, n_1(\cdot, t), n_2(\cdot, t))$  regression. In some cases, these residuals have been shown to depend on size, however in the retrospective data set there was no evidence to suggest that  $\sigma_m^2$  changes with  $x$ . Therefore  $\sigma_m^2$  is modelled

as a constant, defined by the mean of the squared residuals. I now introduce the expected growth functions and variances for spruce and aspen, for both the competition-free and competitive structure cases.

When competitive structure is considered, spruce expected size is given by

$$\mu_1(x, n_1(\cdot, t), n_2(\cdot, t)) = a_0^{sw} + a_1^{sw} x + a_2^{sw} S_1^*(x; n_1) + a_3^{sw} (N_1^*(x; n_1) + N_2^*(x; n_2)) + a_4^{sw} x^2 \quad (3.5)$$

where  $x$  is diameter in mm,  $S_1^* = \int_x^U x' n_1(x', t) dx'$  is the sum of diameters of thicker spruce in m/ha, and  $N_m^* = \int_x^U n_m(x', t) dx'$  is the density of thicker trees of species  $m$  in number/ha, and the estimated variance was  $\hat{\sigma}_1^2 = 1.79$ .

In the absence of competition, spruce diameter is modelled as only a function of diameter at the previous year. The best-fit model is given by

$$\mu_1(x, n_1(\cdot, t), n_2(\cdot, t)) = a_0^{sw} + a_1^{sw} x + a_2^{sw} x^2 \quad (3.6)$$

where  $x$  is diameter in mm, and  $\hat{\sigma}_1^2 = 1.97$ .

For aspen, when competitive interactions are considered as covariates, the best-fit model is given by

$$\mu_2(x, n_1(\cdot, t), n_2(\cdot, t)) = a_0^{aw} + a_1^{aw} x + a_3^{aw} S_1^*(x; n_1) \quad (3.7)$$

where  $x$  is diameter in mm, and  $\hat{\sigma}_2^2 = 3.55$ .

In the absence of competition, aspen diameter is only a function of diameter in the previous year and is described by

$$\mu_2(x, n_1(\cdot, t), n_2(\cdot, t)) = a_0^{aw} + a_1^{aw} x + a_2^{aw} x^2 \quad (3.8)$$

where  $x$  is diameter in mm, and  $\hat{\sigma}_2^2 = 3.91$ .

## Survival

Tree survival is an observed binary outcome of dead (0) or alive (1), and these outcomes can be related to continuous predictors using the logistic regression model. Logistic regression is a popular and versatile model that allows dichotomous outcomes to be linked to predictors (Hosmer and Lemeshow, 2004). The binary outcome is assumed to be Bernoulli distributed as  $Y \sim \text{Bernoulli}(\pi)$  and is linked to the predictors via the logistic link function  $\pi(x) = \exp(\beta X) / (\exp(\beta X) + 1)$ , where

$X$  is a matrix with different predictors in each columns and  $\beta$  is a vector of fitted parameters. In this case, the predictor matrix is given by  $X_m(x, n_1(\cdot, t), n_2(\cdot, t))$ . Spruce survival models were fit using logistic regression, while aspen survival required a different approach due to the lack of aspen survival data. Here I introduce the spruce survival models, both with and without competitive structure.

The best-fit spruce survival model with competitive structure is given by

$$\text{logit}\left(s_1(x, n_1(\cdot, t), n_2(\cdot, t))\right) = b_0^{sw} + b_1^{sw}x + b_2^{sw}S_1^*(x; n_1) + b_3^{sw}A_2^*(x; n_2) \quad (3.9)$$

where  $A_2^*(x; n_2) = \frac{\pi}{4} \int_x^U (x')^2 n_2(x', t) dx'$ .

In the absence of competition, spruce survival is modelled by

$$\text{logit}\left(s_1(x, n_1(\cdot, t), n_2(\cdot, t))\right) = b_0^{sw} + b_1^{sw}x. \quad (3.10)$$

Aggregated fit plots of measured and predicted survival probabilities relative to covariates allow for an assessment of model performance and help identify regions in covariate space where the models may not have good predictive ability. These plots are made by dividing the covariate data into vigintiles (twenty groups of equal frequency), and then computing the average measured and predicted probabilities of survival for all trees that fall within group (or vigintile). This is done for all covariates that appear in a given spruce survival model (size, sum of thicker spruce diameters, and basal area of thicker aspen for the competition model; size for the competition-free model). Survival probabilities are plotted at the quantile bin midpoints. These plots provide insight about model performance, and highlight issues that may not be apparent through other methods due to the fact that mortality events are quite rare.

Aspen mortality data was not collected in the retrospective data set, and it was therefore not possible to fit a survival model in this case. I rely on the assumption that the stands being considered are no longer in the juvenile phase, and that the aspen are already well-established. Previous work has suggested that competition indices based on thicker trees are better predictors of demography changes, and therefore it is not likely that the understory spruce crop have a noticeable effect on aspen demography in the short-term (Huang et al., 2013). However, aspen mortality has been shown to depend on the density of conspecifics, especially in stands where aspen density is extremely high where data shows an increased mortality risk (Bokalo et al., 2007). Aspen mortality has also been shown to vary with stand age: in young dense stands aspen mortality is generally about 8%/year

until a stand age of approximately 20 years, then diminishes to about 3-4%/year by maturity, and increases again in the old-growth phase (Yang, 2002). I am primarily interested in mid-rotation stands, and therefore assume that aspen mortality is constant at 4%/year. This is likely an oversimplification of the mortality process, but I assume that this estimate is sufficient at a population-scale.

### 3.2.5 Assessing model projections

To assess whether the model sufficiently represents the real world, I formally test the model using several validation measures. Having a second data set that is independent from the data set used for calibration provides me with an opportunity to stringently test model predictions without having to rely upon data-splitting methods, which violate the assumptions of statistical independence (Kozak and Kozak, 2003). As always, I bear in mind the Popperian principle that favorable validation results do not imply that the model is correct, only that it is defensible (Popper, 1959).

Projections of the IPM generate annual species size distributions, which can be compared with the empirical PSP size distributions for the years where such data is available. To assess the similarity of these distributions, I use the non-parametric Kolmogorov-Smirnov (KS) test which compares the empirical distribution (the sample) with the reference distribution (continuous projected distribution). Formally, I test the null hypothesis that the sample is in fact drawn from the reference distribution by measuring the maximum absolute difference between the two cumulative distribution functions (CDFs) and comparing this statistic to the KS distribution. Resulting large p-values provide some evidence to support the null hypothesis. For each considered PSP, I compute the KS statistic and corresponding p-value for each model/data year pair initialized on the preceding model/data pair.

Species density is another metric which can be used to make model/data comparisons. There are numerous methods that have been proposed to formally test model predictions and observations, with no consensus on a single best method. Here I consider several approaches, including the 1:1 regression test, Pearson's correlation, the paired t-test, Theil's U, and the mean square error of predictions (MSEP) (Haefner, 2005). The 1:1 regression test exploits the knowledge that when perfect model predictions are plotted against observations, all points fall on a line with an intercept of 0 and a slope of 1. Regressing the observations on the model predictions determines both the slope and intercept of the best-fit line, and these

estimated parameters can be simultaneously tested to determine if the best-fit regression line is significantly different from the 1:1 line. Although appealing, the computed F statistic associated with this method has been shown to increase with sample size, making it more likely to reject the null hypothesis that the best fit line is not discernible from the 1:1 line. In addition, an ideal model would be one where observations and predictions are perfectly correlated. However, the correlation value should not be the only measure used to assess fit - observations and predictions may be perfectly correlated without falling along the line  $y = x$ .

The paired t-test tests the null hypothesis that the difference in means between the observations and predictions is 0, and has been found to be less discriminating than the 1:1 regression test. Both Theil's U and MSEP compute indices of inequality. In particular, Theil's U statistic is used to compare the predictions with a naive forecast, and falls between 0 and 1, 0 being a perfect fit, and 1 being that the prediction is not any better than using the last observation as the naive prediction. The MSEP index consists of three components, which help assess the cause of the error in the deviations of model predictions from observations. The three components which can account for error are the bias error (MC), the error associated with the differences in model and observation variances (SC), and the random error (RC). For all measures of model performance, for a given PSP each consecutive set of observations were used as an initial condition and validation pair. For example, for a PSP that was measured in the years 1985, 1990, and 1995, we use the pairs (1985, 1990), (1990, 1995) as initialization-validation pairs.

### 3.2.6 Mixedwood forest scenarios

Data from a recently published report summarizing natural fire-origin stand development for performance survey age stands (8-14 years post-fire) is used to specify initial diameter distributions for the spruce-aspen IPM (Gärtner et al., 2009). I consider four compositional variations defined in the Alberta Vegetation Inventory by the broad cover groups Conifer (C), Deciduous (D), Deciduous and Conifer (DC), and Conifer and Deciduous (CD). These groups were originally defined to be percentage of species crown cover out of the total crown cover, although the definition is loosely used: in PSP sampling, classification is based on basal area, while in regeneration surveys, classification is based on density (Alberta Environment and Sustainable Resource Development, 2012). Regardless of which attribute is used for classification, the relative compositional values used to categorize forested land remain identical and depend on the percent of the total attribute (crown cover, basal area, or density) that is deciduous: 80-100% deciduous is classified as

D; 50-80% deciduous is classified as DC; 20-50% deciduous is classified as CD; and <20% deciduous is classified as C. The data I used for the following mixedwood scenarios is based on cover classification determined by tree density. In the natural-origin mixedwood stand report, sampled stands had experienced large fires in the past 10-20 years, so that when sampled, stands would be roughly at performance survey age (8-14 years). In this work, I am focussed on mid-rotation development, and initial conditions are therefore based on data reported from a stand sampled 20 years post-fire, referred to as the O'Chiese stand. Sub-plots within the O'Chiese stand were sampled, and were distributed throughout the four cover groups. For each of these cover groups, I use the reported average density to determine the initial number of individuals, and the reported average diameter and its standard deviation, and the minimum and maximum diameter values to determine the diameter distribution. In the case of spruce, sample size for the diameter distribution data was small so all available spruce DBH values were pooled and an identical normal size distribution was used for all cover classes (although for each cover class a separate initial population was drawn). Diameter distributions and densities used to specify initial conditions are given in Table 3.3. By projecting these mixedwood scenarios forward through time, I can determine if the model predicts increased mortality for mixedwood stands as a result, and therefore address the question that asks which composition is most productive according to the IPM.

## 3.3 Results

### 3.3.1 Data summary

Spruce density ranged from 163 to 14400 stems per hectare (sph), aspen density from 625 to 6867 sph, and total density from 1550 to 17200 sph (Fig. 3.2). All plot densities are reported for year of sampling. Stand age at stump height was estimated by ageing the pioneering aspen within the transect, and ranged from 30 to 128 years with a median age of 63 years. Over the complete data set, spruce DBH ranged from 0 (those trees with a height in the interval (1, 1.3)) to 361 mm, while aspen DBH ranged from 1 to 415 mm (Fig. 3.3).

For the PSP data set, I computed density for the first measurement year, and

found that spruce density ranged from 210 to 6613 sph, aspen from 145 to 4960 sph, and total density from 400 to 9644 sph (Fig. 3.4). Over the PSP data set, spruce DBH ranged from 10 to 782 mm, while aspen DBH ranged from 11 to 782 mm (Fig. 3.5).

### 3.3.2 Model selection

Demographic models included in the redistribution kernels for both spruce and aspen were chosen from a list of ecologically plausible models based on their AIC. For each species, two models were selected to represent both the competition-free and competition dependent scenarios. For all candidate models, subject tree size was considered as a covariate. For kernels dependent on competitive interactions, density, sum of diameters, and basal area of competing trees were considered as covariates, for all trees and trees of thicker diameter than the subject tree.

For spruce, the best competition-free mean growth model included subject tree size and squared subject tree size as covariates. When competitive interactions were included, the best mean growth model included the sum of diameters of thicker spruce ( $S_1^*$ ), the total density ( $N_1^* + N_2^*$ ), in addition to the covariates from the competition-free model. In both cases the squared residuals did not show a significant size-dependent trend, and therefore the growth variance was determined to be constant with a value of 1.00 for the competition-free model, and a value of 3.55 for the competitive interactions model. Spruce growth model summary plots are shown in Figure 3.6.

For aspen, the best mean growth competition-free model included a linear and quadratic size covariate, while the growth model with competitive interactions included size as well as the sum of spruce trees of thicker diameters ( $S_1^*$ ). Summary plots for the aspen mean growth models are shown in Figure 3.8. As with spruce, the squared residuals from both the competition-free and competitive interactions aspen models did not show a significant size-dependent trend, and therefore the growth variance was determined to be constant with a value of 1.00 for the competition-free model, and a value of 3.55 for the competitive interactions model.

For the spruce probability of survival, the best fit competition-free model included only a size covariate, while the model which included competitive interactions contained the sum of diameters of thicker spruce and the aspen basal area of trees thicker than the subject tree as covariates, in addition to size. Aggregated survival plots shown in Figure 3.7 demonstrate how the spruce survival models perform

throughout covariate space. The survival model with competition performs well with respect to size ( $x$ ) and sum of thicker spruce diameters ( $S_1^*$ ), but the relationship between model and data is less clear in the case basal area of thicker aspen ( $A_2^*$ ). The competition-free model performs well with respect to size ( $x$ ), except for the smallest sized trees which show an increased survival probability relative to the survival probabilities for the adjacent quantiles of slightly larger spruce.

Due to the lack of aspen mortality data, aspen probability of survival was fixed to a constant value of 4%/yr.

Parameter estimates for demographic models including competitive interactions are given in Table 3.1, while those for the competition free models are found in Table 3.2.

### 3.3.3 Goodness of fit and model validation

Using the two-species IPMs with empirical data to define an initial condition, size distributions for spruce and aspen were propagated through time. For each PSP, any two consecutive data points form an initialization/validation pair, and a total of 154 such pairs were available. Initial mixedwood size distributions were projected to the validation data year for both the competition-free and competition-dependent cases, and for each species the projected distributions from the IPM were compared to empirical data size distributions for the next year of available data using the KS test. To illustrate the method, Figure 3.9 shows the projected size distributions for both spruce and aspen as well as the associated empirical and predicted CDFs for PSP 237. This model run was initialized using the 1988 empirical size distributions, and was projected to the year 2000 which was the subsequent year for which there was available data. Projections are shown for the IPMs with and without competitive structure. The bottom panels show the empirical and projected CDFs, which are used to perform the KS test. The greater the maximum vertical distance between the empirical and the modelled CDF, the less likely it is that both result from the same distribution.

For white spruce, in 138 out of 154 data/model pairs the KS statistic from the IPM with competition was smaller than for the IPM without competition (Figure 3.11). For aspen, the KS statistic from the IPM with competition was smaller in 142 out of 154 data/model pairs (Figure 3.12). These results indicate that for approximately 90% of the PSP sample, the IPM with competitive structure is better able to predict species distribution changes than the IPM without competitive structure.

Empirical and projected distributions were used to compute species densities, and the ability of the model to accurately predict observed densities was assessed. Figure 3.10 shows the projected density for spruce and aspen for both the competition-free and competition-dependent models for PSP 291, as well as the observed densities for years where such data is available. Note that the jumps in number of individuals in years for which there is data are due to re-initialization - in this assessment I evaluate the ability of the model to predict subsequent measurement years independently. In this example I see that when competition is included in the IPM redistribution kernel, spruce mortality is increased leading to fewer individuals. However, in both scenarios aspen mortality is fixed to a constant mortality rate leading to no difference in aspen densities between the with- and without-competition cases. Predicted densities were compared to observed densities using several metrics to help assess goodness-of-fit of the IPM, and results from these statistical tests are given in Table 3.4. Plots of observed against predicted numbers of individuals for the IPM with competition for both spruce and aspen demonstrate that the model performs well according to visual inspection (Figs. 3.13, 3.14). However, for both spruce models the linear regression slope-intercept test generates p-values greater 0.01 (0.0135 for the model with competition, and 0.0134 for the model without competition) which do not allow me to confidently draw conclusions about whether the best-fit regression line is different from a line with an intercept of zero and a slope of one. I consider this to be a positive result, given that the linear regression test has been shown to have properties which can affect its usefulness as a goodness-of-fit metric for good models fit to a large data-set. The linear regression test for aspen resulted in a p-value slightly less than 0.01 (0.00992), indicating that there is more evidence against the null hypothesis that in the case of spruce, but not much.

The paired t-test used to test the difference in means resulted in large p-values ( $> 0.05$ ) in all cases, indicating that there is evidence in support of the null hypothesis which states that there is no difference in means between the observed and predicted groups. Interestingly, the competition-free model led to a slightly larger p-value than the competition-dependent case, but the difference was small (difference of 0.0010). The inequality coefficients determined by Theil's U test were small in all cases ( $< 0.15$ ), which indicates that the root mean squared error is small relative to the normalizing factor, and suggests a high degree of similarity between the observed and predicted values. The Mann-Whitney U test statistics showed that there is not enough evidence to say that the predicted values and data come from different distributions, and therefore I favor the null hypothesis that both groups are equal. Correlation values between the model/data pair data were

all greater than 0.96, with the strongest correlation for aspen (0.979), followed by the competition-dependent spruce case (0.964), and lastly the competition-free spruce case (0.963). Lastly, the index of model quality suggests that in all three cases random error measured as the deviation in model/data correlation from one (denoted by RC) is the most important component in the MSEP. This suggests that I do need to recognize the possibility of making Type II errors.

Overall, I find that the species density metrics (F, t, U, ...) suggest that both the competition-free and competition-dependent IPMs perform well for both species. These metrics test the overall density of each species at measurement years, but do not test the species structure (ie, diameter distribution). However, as noted above, the species distribution metric (KS) suggests that the competition-dependent IPMs perform better than the competition-free IPMs.

Mixedwood scenarios for four cover classes (D, DC, CD, C) were projected using the IPM with competitive structure with initial conditions based on reported data for a 20 year post-fire mixedwood stand. For each projection year, densities were computed and are shown in Figure 3.15 for all cover classes by species and total. For spruce, the cover classes C and CD which are dominated by conifers showed high spruce mortality (steepest descent), and after 25 years the CD spruce SPH had fallen below the DC spruce SPH. As expected for aspen, none of the trajectories crossed as a result of the constant mortality rate inherent in the kernel. When total SPH was considered, I again see that the cover classes C and CD which are conifer dominated show the highest mortality. Figure 3.16 shows the evolution of basal area for the four cover classes for spruce, aspen, and total. The rate of increase of total basal area is steepest for the mixedwood classes. The projected basal area leads to extremely high values for the aspen and total basal area. For the DC, D, and CD scenarios, projected aspen basal at a stand age of 50 years was between 60 and 110 m<sup>2</sup>/ha, leading to a projected total basal was between 80 and 120 m<sup>2</sup>/ha. In the PSP data set that was used to assess the IPM fit, the 95% quantile of the basal area taken over all plots over all years was 27 m<sup>2</sup>/ha for aspen, and 48 m<sup>2</sup>/ha for all species. Finally, I also note that although all the SPH curves are decreasing with time, the basal area curves are all increasing.

### 3.4 Discussion

This study supports the theory that individual interactions resulting from competition for resource access play an important role in shaping the mixedwood boreal

forest. The importance of these interactions was evaluated through the comparison of two structured population models, one including the effects of competitive structure and one without these effects. Both models were built using an IPM framework, which has been shown to be an effective population model for many perennials as well as some tree species (Ellner and Rees, 2006; Zuidema et al., 2010). To capture the mixedwood system dominated by two species, I developed a two-species system of IPMs, coupled through the redistribution kernels in the competition-dependent case, and decoupled in the competition-free case. An advantage of this study was the access to two independent data sets, the retrospective and PSP data sets, which were used for fitting and validation respectively.

Assessment of model performance was based on the comparison of model predictions and data with respect to two key features: population density and size distribution. The ability to predict both of these features is critical in a forest management setting where the goal is to estimate stand merchantable volume by species. With and without competition dependence, both IPMs performed similarly in their ability to predict population density. According to all metrics except for the simultaneous slope-intercept regression test, which is subject to recognized limitations, there was evidence in favor of the conclusion that the model was a good fit to the data. Most metrics test the null-hypothesis that there is no difference between the model and data, and although there was not evidence to reject the null hypothesis, I am not able to say the model and data are indistinguishable. Nevertheless, our results are promising – I have no evidence to conclude lack of fit. In contrast, the comparison of predicted and empirical size distributions allowed us to distinguish the IPMs with and without competition. The results from the Kolmogorov-Smirnov tests were overwhelmingly in favor of the IPM that included competition dependence.

More specifically, for a cohort of individuals in a mixedwood forest dominated by spruce and aspen, likely uneven-aged, competition from thicker trees influenced species demography. This apparent asymmetric competition has been observed by others in boreal forests (Luo and Chen, 2011; Huang et al., 2013). These findings suggest that in mixedwood boreal stands in Alberta, relative size stature determines the effective competition experienced by a subject tree. However, the IPMs considered here were spatially implicit, meaning competition was measured at a stand level as opposed to a local level. Other work suggests that local interactions may be more useful measures of competitions, and that these need not discount interactions with smaller individuals (Thorpe et al., 2010).

In the diameter growth models for both spruce and aspen, as well as the spruce

mortality model, the sum of thicker spruce diameters was identified as a predictor. Sum of diameters can be thought of as a proxy for sapwood area, determined by the area of the outer annulus of conductive wood (Huang et al., 2013). Assuming that sapwood radial depth is roughly constant over time, then sapwood area is determined by tree diameter. In turn, sapwood area is proportional to leaf area both at the individual and stand level (Waring et al., 1982). Tree leaf area affects light interception and evapotranspiration, and therefore stand leaf area (typically measured using leaf area index) is commonly used as a measure of aboveground productivity for overstory trees or as a measure of competition for understory trees. These relationships suggest that the sum of diameters of thicker spruce may provide a measure of competition for primarily light, but also for resources such as water, and soil nutrients. Total number of thicker competitors was also determined to be a predictor of spruce growth, and easier to interpret because it can be thought of as a measure of density dependence – more larger spruce amounts to increased difficulty accessing resources. Finally, basal area of thicker aspen appeared as a predictor in the spruce mortality model. Basal area is a commonly used competition index, which like sum of diameters incorporates both competitor size and density and is therefore thought of as a measure of stand crowdedness. Although all measures of competition considered are clearly linked to stand development, how they each relate to changes in ecophysiology for different species is not well understood due to the complex nature of forest ecosystems. Regardless, they are useful proxy measures of combinations of fine-scale processes.

Both spruce and aspen growth models result in favorable fit statistics. When the observed tree size values are plotted against the predicted tree size values (as shown in the top panels of Figures 3.6 and 3.8), the models appear to perform quite well. However, this is somewhat deceptive because relative to the size of domain, trees barely grow at all. A more helpful diagnostic plot may be one where the observed change in tree size is plotted against the predicted change in tree size. Additionally, the slight skewness that results from the longer right tails in the model residuals (see the middle panels of Figures 3.6 and 3.8) suggests that a non-Gaussian alternative, such as a log-normal distribution, may be more appropriate and should be tested in future work.

The relative productivity of mixedwoods compared to monocultures has been a pressing question for mixedwood forest managers and scientists (Alberta Reforestation Standards Science Council, 2001; Lieffers et al., 2008; Lieffers and Beck, 1994; Pretzsch and Schütze, 2009). As a first step towards addressing this question, I used the coupled IPM which includes competitive structure to make stem

density and basal area predictions based on initial data for four cover classes taken from a natural-origin post-fire stand. None of these cover classes is strictly monoculture; the classes range from predominantly deciduous to predominantly conifer, with intermediate mixture classes. Based on the thirty-year IPM predictions, the results indicate that according to both measures, mixtures were more productive than the forests which initially began with a predominantly single species composition. The conifer-dominated stand showed the highest spruce mortality, and the slowest basal area increase causing it to be the least productive forest. Except for the conifer case, the relative ordering of initial conditions determined the relative ordering of the predicted outcomes. In other words, forests that were more productive in terms of density or basal area remained more productive, except in the case of the conifer-dominated stand. This in itself is not surprising given the short-projection time scale, but does agree with other work that highlights the importance of site-specific conditions during the establishment phase (Peters et al., 2005). These results are preliminary in nature – the unrealistically high basal area projections for aspen suggest that the aspen kernel needs to be refined. The inclusion of a non-constant aspen mortality may remedy this problem in part, but I suspect that the aspen growth model is overpredicting diameter increase. This overprediction is a direct result of the data, where aspen samples were purposely taken from dominant trees, thereby excluding aspen with a reduced growth potential.

Although the IPM with competition performs well when used to predict at shorter time-scales, prediction uncertainty increases as I predict further into the future. To improve prediction accuracy at both shorter and longer time scales, the proposed model can be modified to include site specific predictors that are known to influence stand composition and productivity such as edaphic qualities, geographical attributes (latitude, longitude, elevation), as well as time-varying climatic predictors.

Also, I note that predicting the number of individuals using a population model can pose challenges due to the complicated nature of individual mortality events. Although commonly modeled using population-scale models, mortality is the culmination of the interaction of many factors, some of which can be easily described such as size and competition, as well as others that may not be accounted for such as both genotypic and phenotypic variation as well as microsite conditions. In particular, recent growth and local competition have been shown to be indicators of mortality risk, although the inclusion of these factors requires a model that has the ability to track individuals and deal with spatial structure to some extent, both of

which are not possible with the IPM. Given that mortality is a rare event, it may be overly optimistic to assess fit using plots of observed versus predicted numbers of individuals. The number of individuals in a forest is large relative to the number of individuals dying each year, which implies that the population density appears to change very little with time. A more instructive approach may be to assess how the IPM is able to predict the annual change in number of individuals.

Spruce						Aspen					
Growth			Survival			Growth			Survival		
1	$a_0^{sw}$	1.43 (4.03e-2)	1	$b_0^{sw}$	4.78 (1.23e-1)	1	$a_0^{aw}$	3.75 (5.33e-2)	1	$b_0^{aw}$	0.96
$x$	$a_1^{sw}$	1.02 (6.57e-4)	$x$	$b_1^{sw}$	3.42e-2 (2.55e-3)	$x$	$a_1^{aw}$	9.95e-1 (3.10e-4)			
$S_1^*$	$a_2^{sw}$	-3.88e-3 (2.84e-4)	$S_1^*$	$b_2^{sw}$	-7.38e-3 (4.23e-4)	$S_1^*$	$a_2^{aw}$	-1.48e-2 (4.42e-4)			
$N_1^* + N_2^*$	$a_3^{sw}$	-6.66e-2 (1.23e-2)	$A_2^*$	$b_3^{sw}$	-2.99e-2 (5.74e-3)						
$x^2$	$a_4^{sw}$	-5.43e-5 (3.06e-6)									

Table 3.1: Parameter mean and standard error estimates for demographic models with competitive interactions for the significant covariates. Note that 1 refers to the intercept,  $x$  to subject tree diameter measured in millimetres,  $S_1^*$  to the sum of thicker spruce diameters (mm/ha),  $N_1^* + N_2^*$  to the number of thicker spruce and aspen (#/ha),  $A_2^*$  to the basal area of thicker aspen (mm<sup>2</sup>/ha), and  $x^2$  to square diameter of the subject tree (mm<sup>2</sup>). Note that all competition indices are determined based on all tree in the plot (plot-level).

Spruce						Aspen					
Growth			Survival			Growth			Survival		
1	$a_0^{sw}$	5.99e-1 (2.47e-2)	1	$b_0^{sw}$	3.55 (7.96e-2)	1	$a_0^{aw}$	2.35 (8.30e-2)	1	$b_0^{aw}$	0.96
$x$	$a_1^{sw}$	1.03 (6.14e-4)	$x$	$b_1^{sw}$	3.15e-2 (2.03e-3)	$x$	$a_1^{aw}$	1.00 (1.05e-3)			
$x^2$	$a_2^{sw}$	-6.55e-5 (3.09e-6)				$x^2$	$a_2^{aw}$	-1.34e-5 (3.08e-6)			

Table 3.2: Parameter mean and standard error estimates for demographic models without competitive interactions for the significant covariates. Note that 1 refers to the intercept,  $x$  to diameter measured in millimetres, and  $x^2$  to square diameter (with units of mm<sup>2</sup>).

Overstory cover group	Spruce					Aspen				
	Density per 10m <sup>2</sup>	Diameter at breast height (mm)				Density per 10m <sup>2</sup>	Diameter at breast height (mm)			
		Mean	SD	Min	Max		Mean	SD	Min	Max
C	8.846	25.7	17.1	3.8	53.5	3.308	30.5	22.9	9.4	76.1
CD	3.778	25.7	17.1	3.8	53.5	7.278	63.8	28.5	23.7	109.2
D	0.036	25.7	17.1	3.8	53.5	6.964	52.5	27.3	11.1	112.5
DC	2.529	25.7	17.1	3.8	53.5	9.118	29.3	19.4	3.3	68.6

Table 3.3: Data used to formulate the initial conditions for the IPM with competition structure for the four overstory cover classes. Cover classes are based on tree density and are defined as follows: 80% deciduous is classified as D; 50-80% deciduous is classified as DC; 20-50% deciduous is classified as CD; and <20% deciduous is classified as C. For each cover class, density/10m<sup>2</sup> determines the number of individuals, while the diameter at breast height mean, standard deviation (SD), minimum (min), and maximum (max) define the truncated normal distribution from which the tree diameters were drawn. Note that the spruce diameter data was pooled across cover classes due to small sample sizes.

	Spruce (with comp)		Spruce without comp		Aspen (with and without comp)	
	statistic	p-value	statistic	p-value	statistic	p-value
<i>F</i>	73.4	0.0135	74.1	0.0134	100	0.00992
<i>t</i>	1.66	0.0976	1.67	0.0966	1.06	0.289
Theil	0.0929	–	0.0933	–	0.0919	–
<i>U</i>	1.07e+04	0.0641	1.07e+04	0.0637	1.08e+04	0.079
Pearson <i>r</i>	0.964	4.99e-89	0.963	7.13e-89	0.979	3.63e-107
MSEP	9.59e+03	–	9.68e+03	–	6.48e+03	–
MC	0.293	–	0.293	–	0.183	–
SC	0.198	–	0.201	–	0.386	–
RC	0.509	–	0.506	–	0.431	–

Table 3.4: Statistics obtained from the comparison of predicted and observed population numbers. Statistics are shown for the IPMs with and without competitive structure. For aspen, the resulting statistics for the two cases are equivalent as a result of constant mortality. The F statistic tests if the best-fit regression line of the data against the model predictions is different from the null hypothesis line with slope 0 and intercept 1. All p-values associated with this statistic are somewhat inconclusive so the null cannot be rejected with confidence - they all fall between 0.009 and 0.015. The t statistic p-values also do not allow the null (which specifies that the model and data means are equal) to be rejected. Theil's inequality coefficients are all small (over the [0,1] interval), which indicates accurate models with the aspen model performing best by this measure. Mann-Whitney test results (U) agree with the paired t-test results, where the large p-values indicate that we cannot reject the null that the difference in distributions between groups are equal. Pearson's correlation coefficient (Pearson r) show that in all cases the predictions are highly correlated with the data. The final four rows show the mean square error of predictions (MSEP) as a sum of three components that indicate the proportional error resulting from the bias error (MC), the slope-not-unity error (SC), and finally the random error (RC), where  $MC + SC + RC = 1$ . In all cases the, RC component is much larger than than the other error components, indicating that random error is the dominant error source.

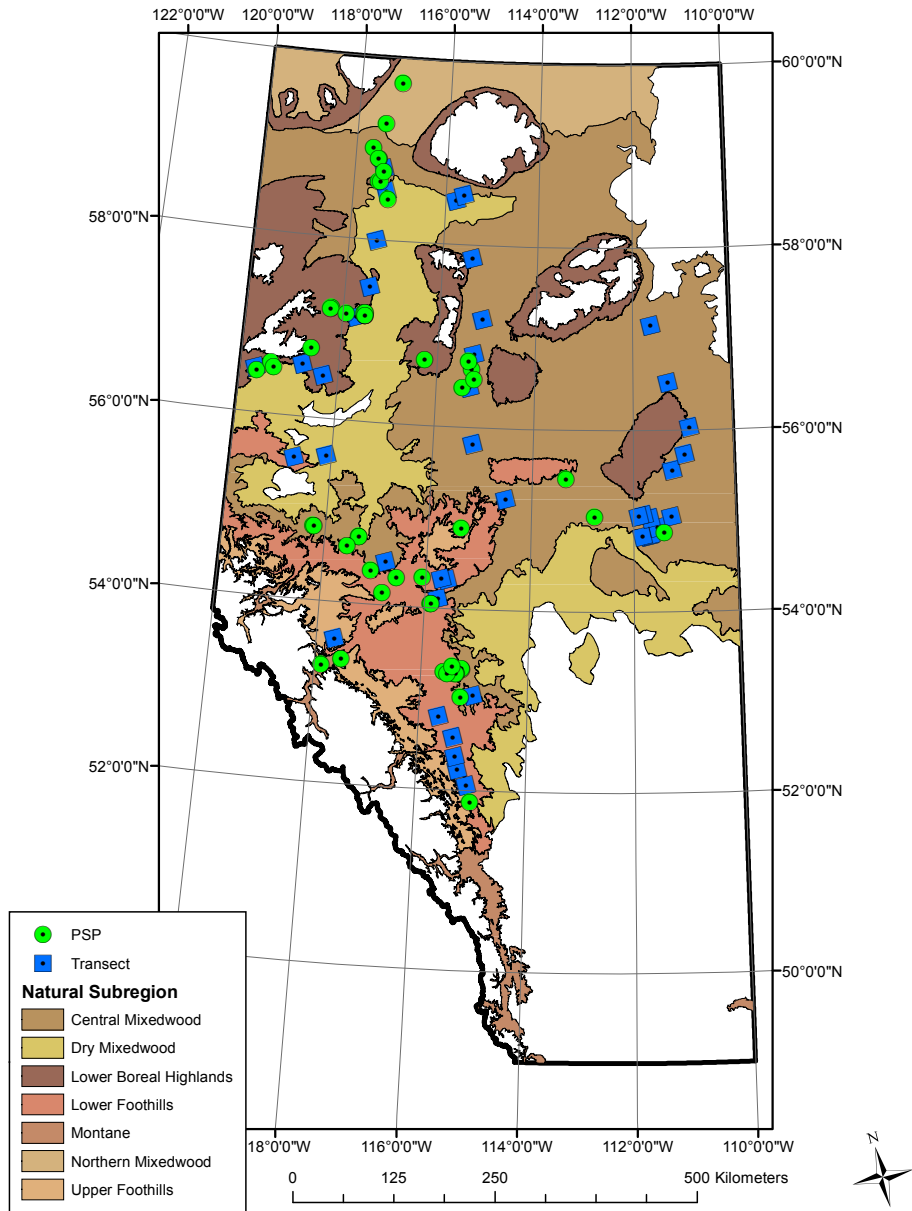


Figure 3.1: Provincial map of Alberta indicating the locations of retrospective sample plots and PSP location, with pertinent natural subregions indicated.

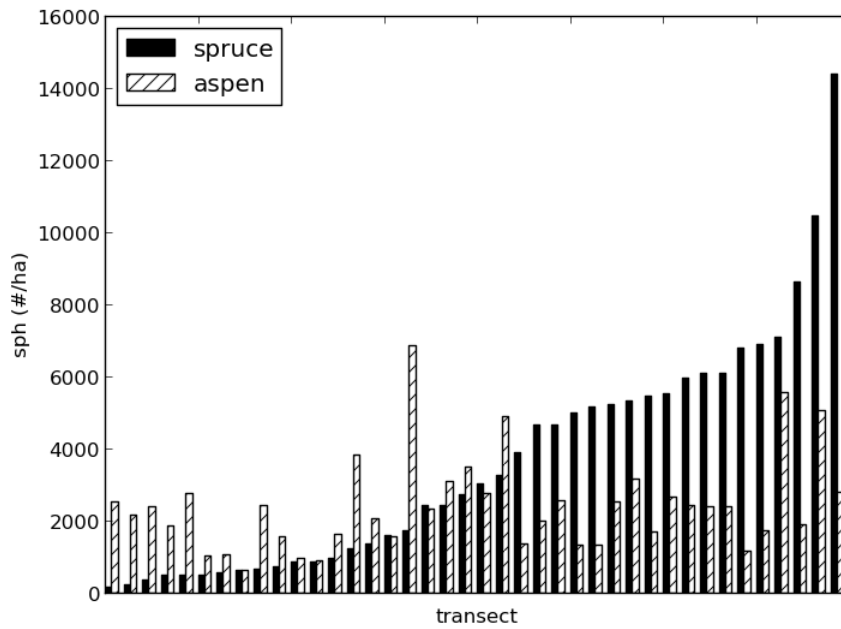


Figure 3.2: Spruce and aspen sample plot densities in stems per hectare for the retrospective data set, as measured at year of sampling.

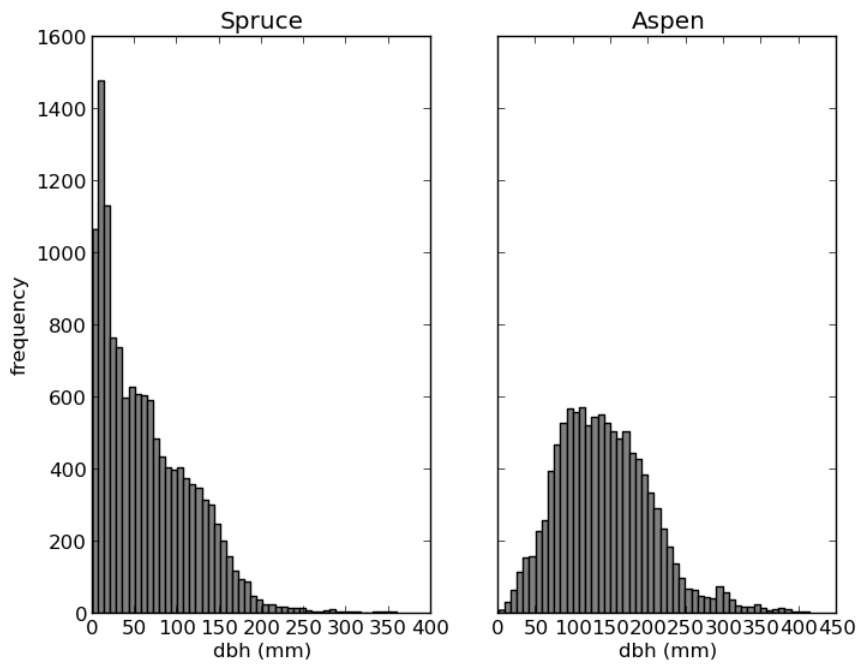


Figure 3.3: Diameter distributions for spruce (left panel) and aspen (right panel) for the entire retrospective data set.

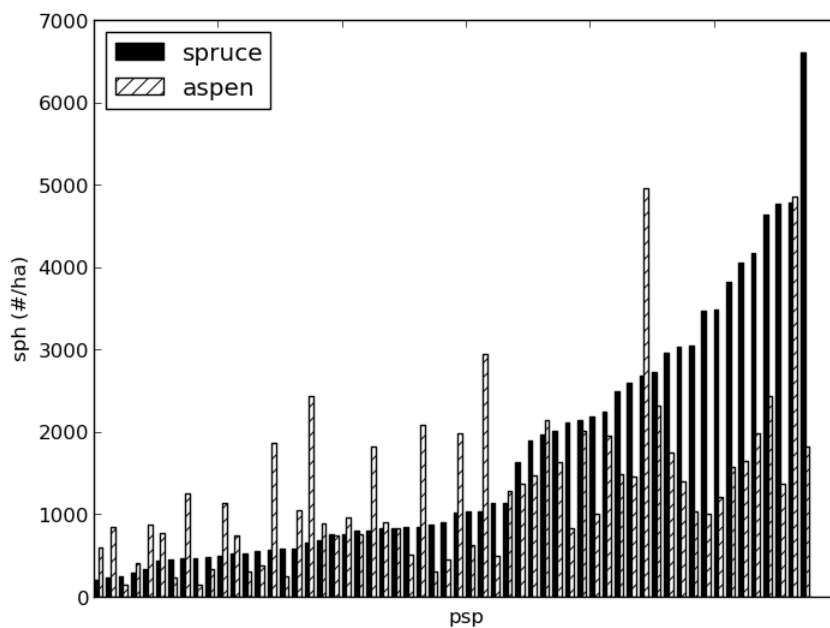


Figure 3.4: Spruce and aspen sample plot densities in stems per hectare for the PSP data set, as measured at initial year of sampling. Note that spruce densities are in general not as high as those in the retrospective data set, which is largely a reflection of the older stand ages of the PSP stands.

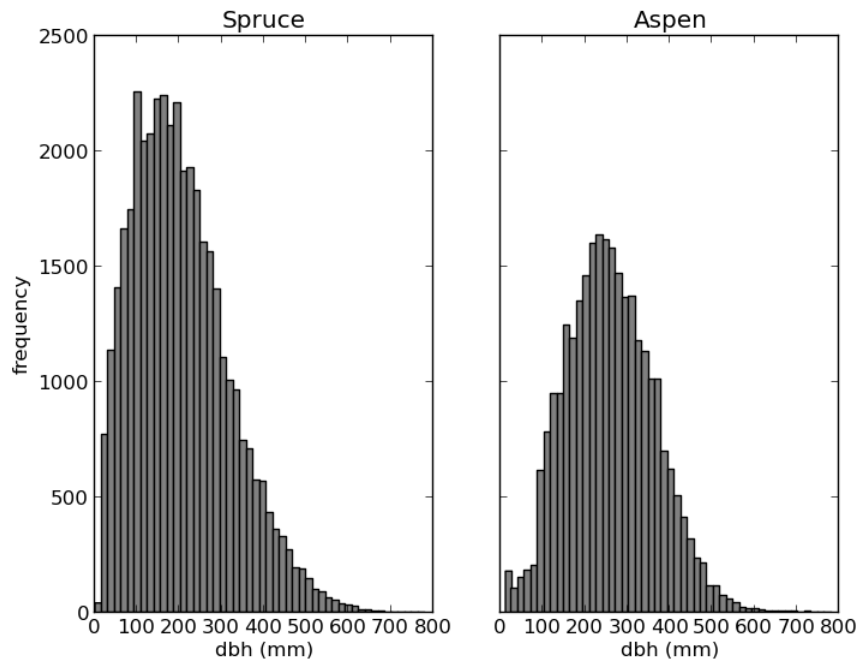


Figure 3.5: Diameter distributions for spruce (left panel) and aspen (right panel) for the entire PSP data set. The range of diameters is larger than those seen in the retrospective data set, and on average both spruce and aspen diameters are larger. This is again likely a result of the older stand ages of the PSP stands.

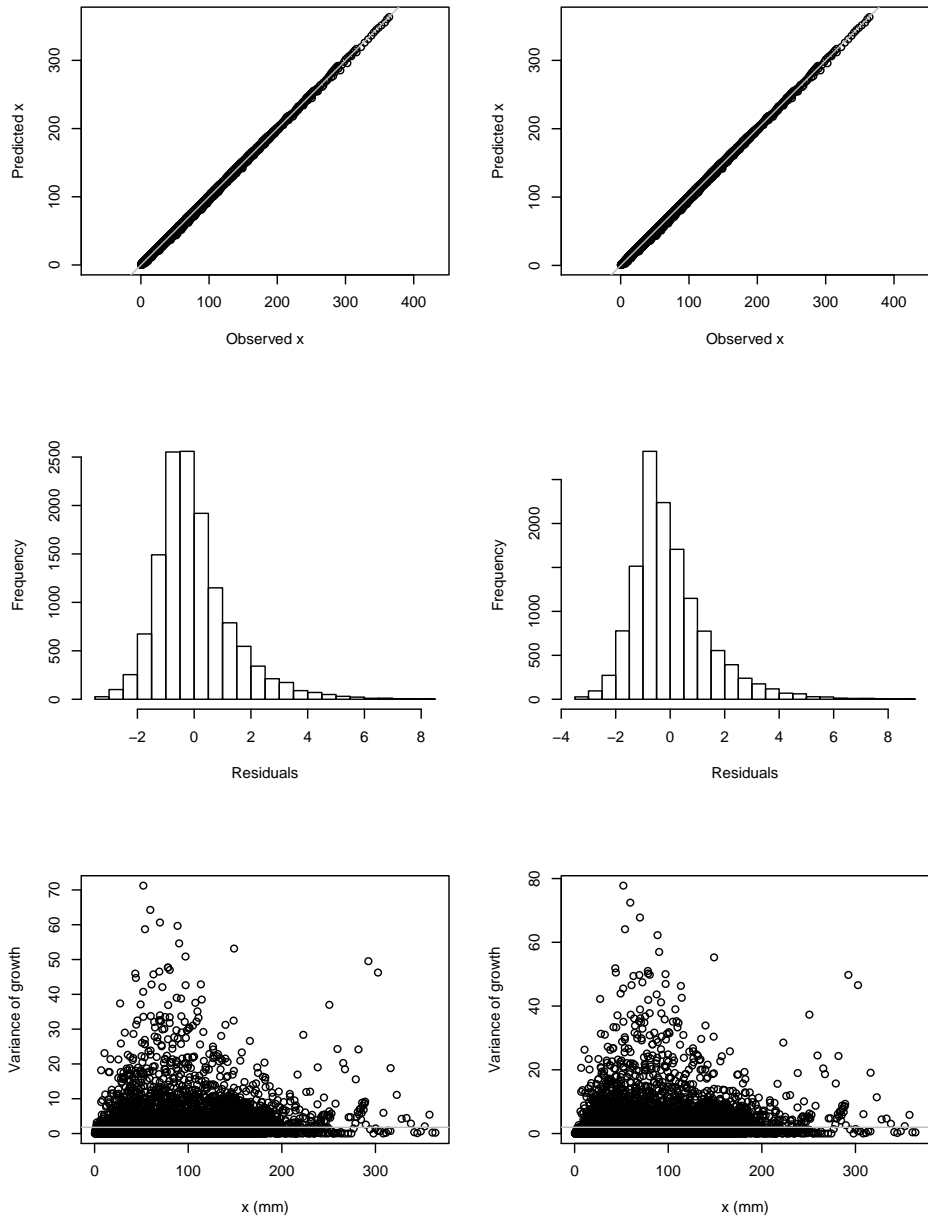


Figure 3.6: Spruce growth model summary plots for the model with (left panels) and without (right panels) competitive structure. Top panels show spruce size (DBH) as predicted by the best-fit linear growth model plotted against observed spruce size (points), as well as the reference line  $y = x$  (grey line). Middle figures show histograms of the frequency of growth model residuals. Bottom panels show the growth variance  $\sigma^2$  against size (points). The best-fit line is indicated (grey line), indicating that in both cases variance does not show significant size-dependence.

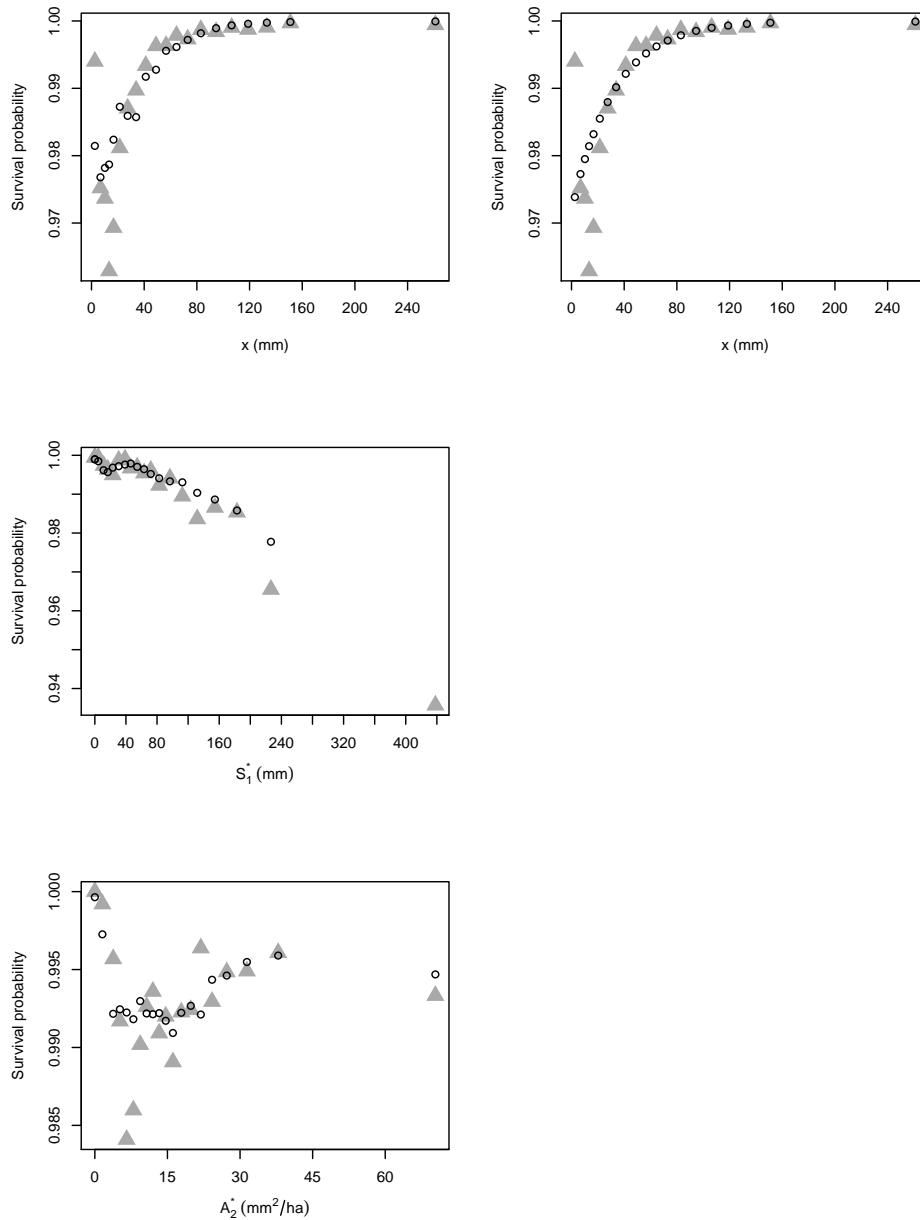


Figure 3.7: Average survival probabilities from the data (grey triangles) and best-fit model (open circles) plotted against survival model covariates for each of the twenty covariate data quantiles. Left panel shows the survival model with competitive interactions, while the right panel shows the survival model without. Average survival probability is plotted against: diameter at breast height ( $x$ ) in upper panel; sum of diameters of thicker spruce ( $S_1^*$ ) in middle panel; and basal area of thicker aspen ( $A_2^*$ ).

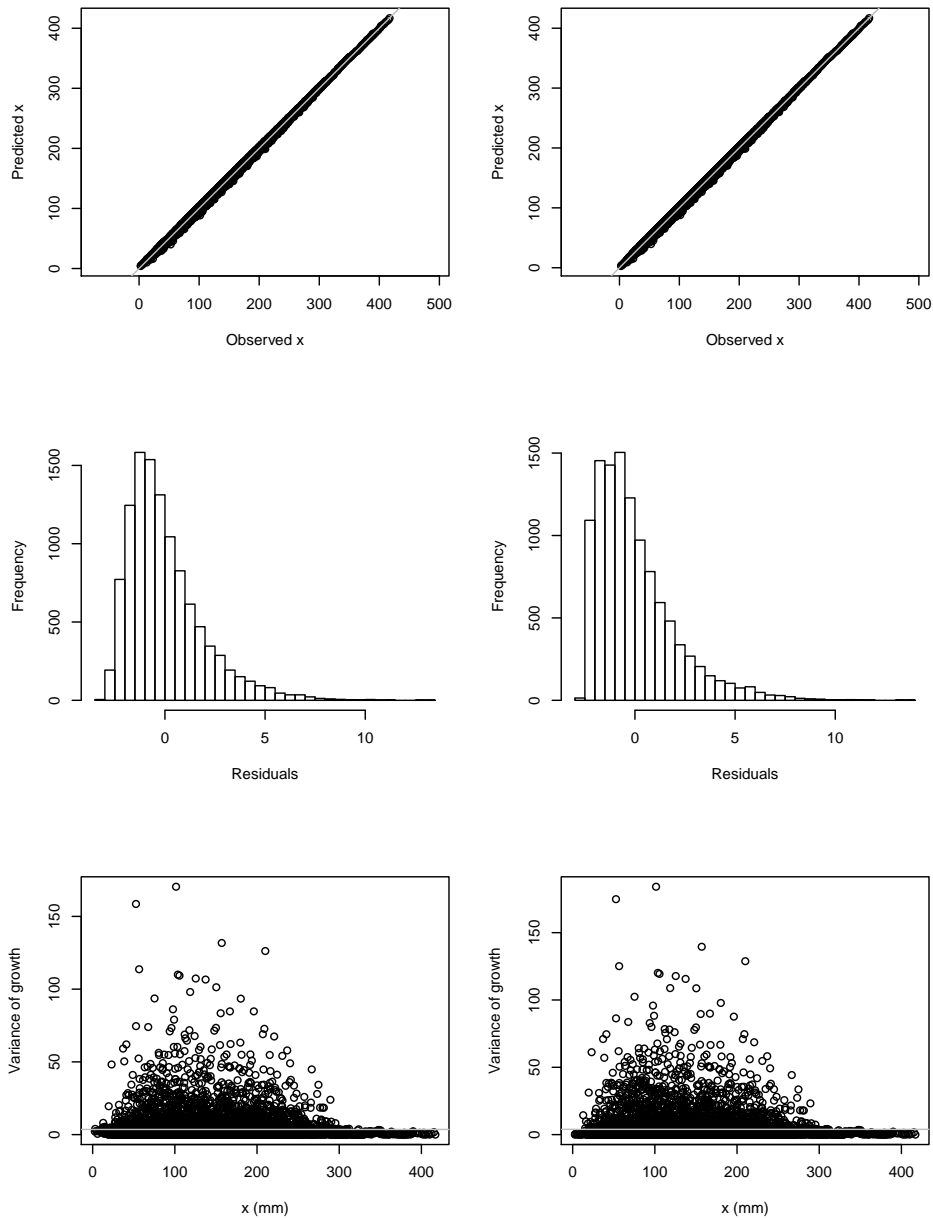


Figure 3.8: Aspen growth model summary plots for the model with (left panels) and without (right panels) competitive structure. Top panels show aspen size (DBH) as predicted by the best-fit linear growth model plotted against observed size (points), as well as the reference line  $y = x$  (grey line). Middle figures show histograms of the frequency of growth model residuals. Bottom panels show the growth variance  $\sigma^2$  against size (points). The best-fit line is indicated (grey line), indicating that in both cases variance does not show significant size-dependence.

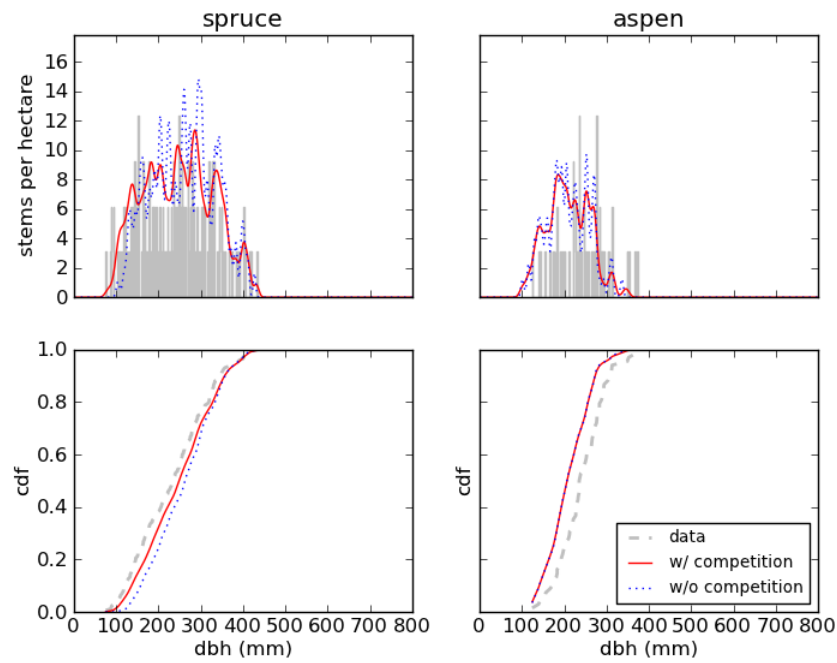


Figure 3.9: Empirical and predicted size distributions (top panels) and cumulative density functions (bottom panels) for the IPMs with and without competitive structure for PSP 237 for the year 2000 based on model initialization using the 1988 empirical distribution. Note that visually there is little difference between the projection from the IPMs with and without competitive structure. In the case of aspen, constant mortality was assumed and therefore we do not expect a large difference between the two models – the only change between the two IPMs occurs in the kernel growth function.

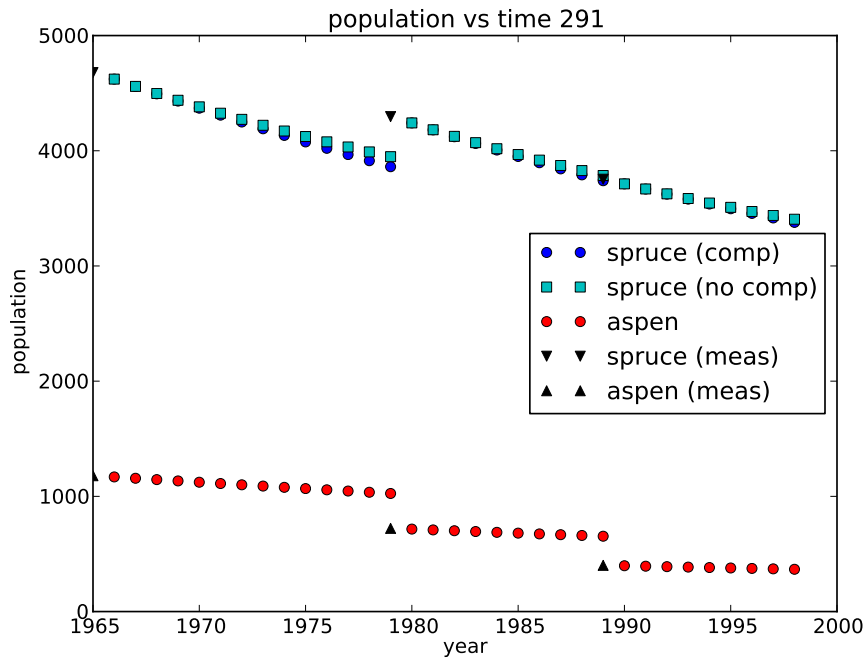


Figure 3.10: Predicted and observed numbers of spruce and aspen for PSP 291. Model is reinitialized at each year for which there is data available. As expected, the IPM with competitive structure predicts higher spruce mortality than the IPM without competition. Aspen mortality is constant in both models, which is why aspen population numbers remain the same regardless of the model.

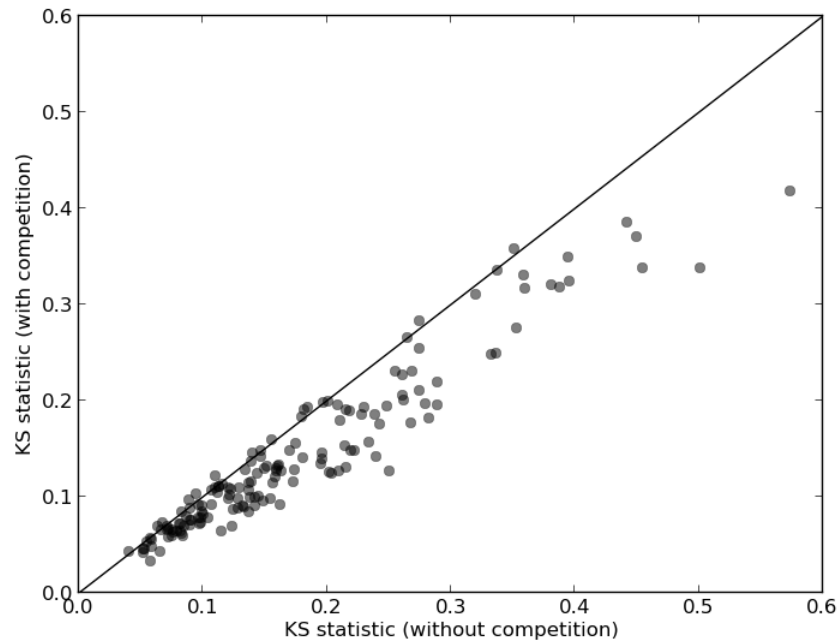


Figure 3.11: White spruce Kolmogorov-Smirnov (KS) statistic values for the IPM with competition plotted against those from the IPM without competition (grey points). Darker regions indicate dense regions of points. Reference line  $y = x$  also shown. In 138 out of 154 cases, the KS statistic for the IPM with competition was smaller than for the IPM without competition, indicating that the IPM with competition performs better according to this metric.

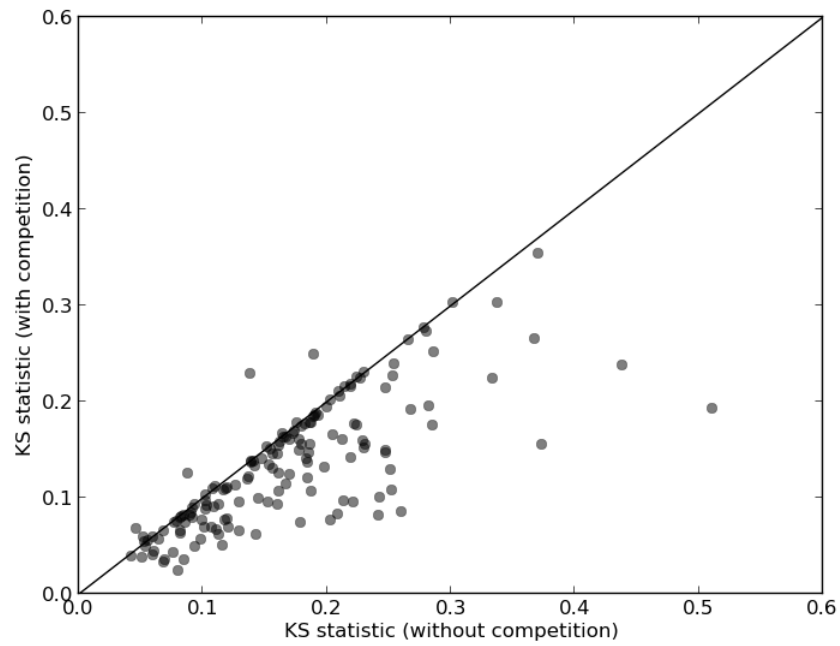


Figure 3.12: Aspen Kolmogorov-Smirnov (KS) statistic values for the IPM with competition plotted against those from the IPM without competition (grey points). Darker regions indicate dense regions of points. Reference line  $y = x$  also shown. In 142 out of 154 cases, the KS statistic for the IPM with competition was smaller than for the IPM without competition, indicating that the IPM with competition performs better according to this metric.

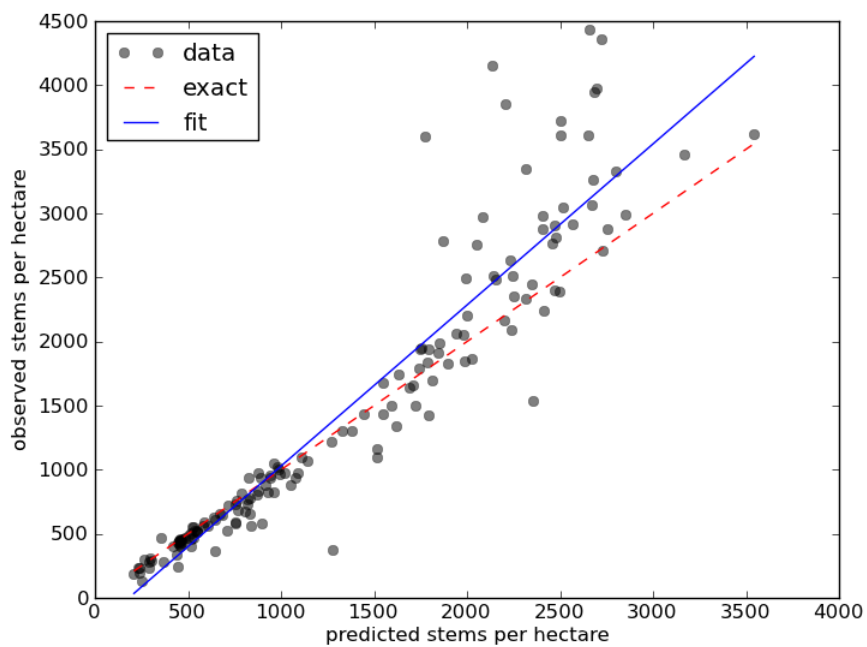


Figure 3.13: Observed versus number of spruce predicted by the model with competition, measured in stems per hectare. Solid blue line shows the line  $y = x$ , and dashed red line shows the best-fit regression line. For a perfect model, all the points would fall along the dashed red line.

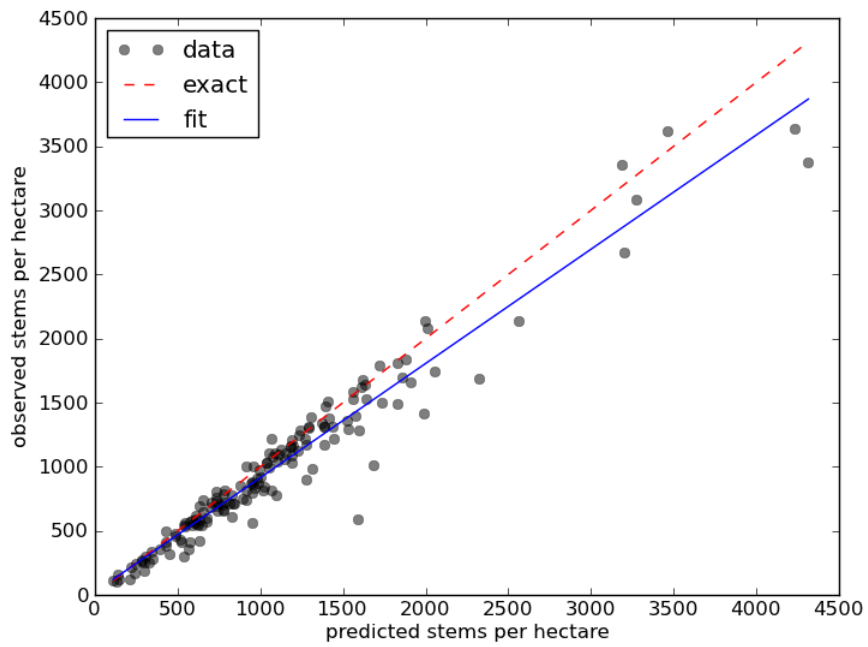


Figure 3.14: Observed versus number of aspen predicted by the model with competition, measured in stems per hectare. Solid blue line shows the line  $y = x$ , and dashed red line shows the best-fit regression line.

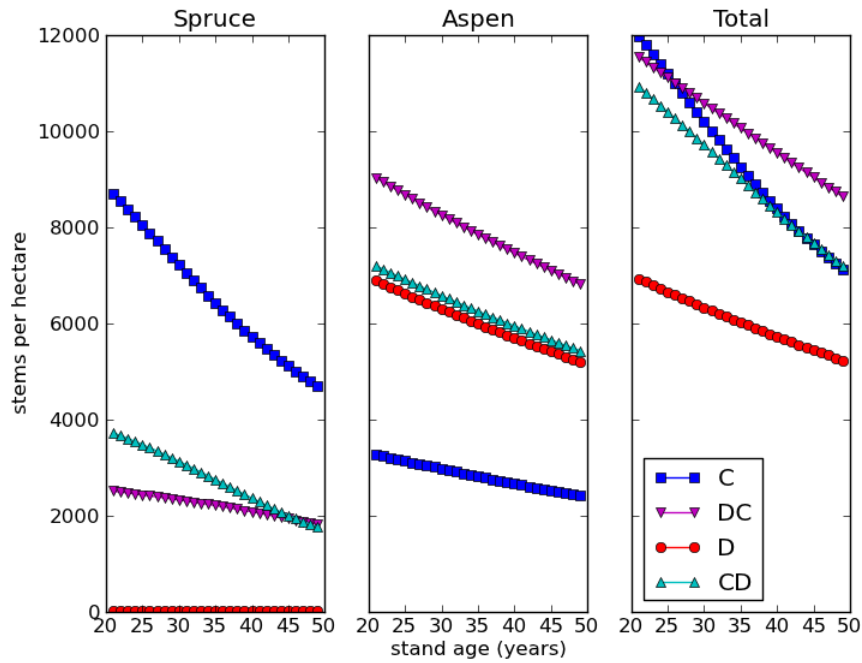


Figure 3.15: Predicted stems per hectare shown for 30 years post-initialization year based on the IPM model with competitive structure. Predictions are made for each of the four cover classes: conifer (C), deciduous-conifer (DC), deciduous (D), and conifer-deciduous (CD). Note that the C and CD scenarios experience the highest spruce mortality. As indicated by the total population, after 30 years the DC stand has the highest density, followed by the CD and C which have approximately equal densities.

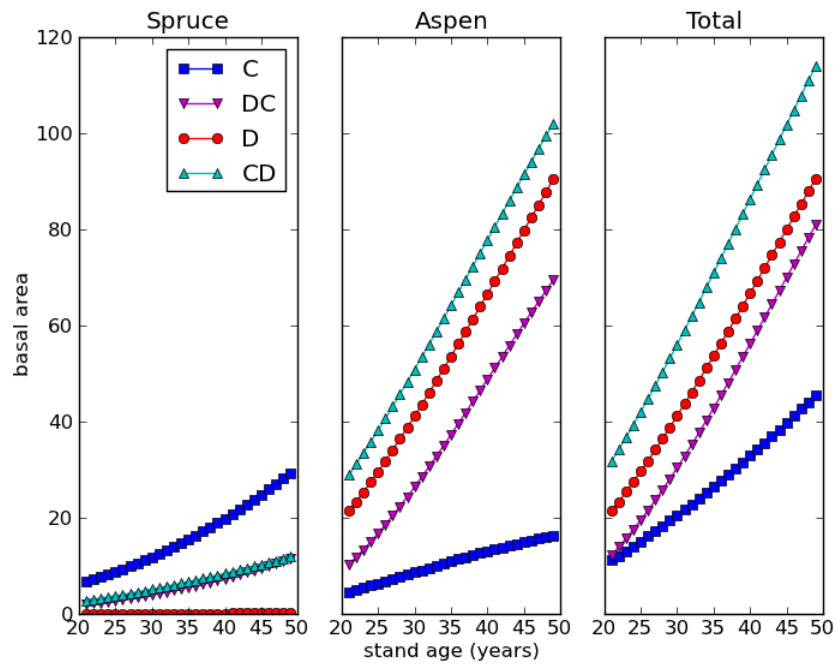


Figure 3.16: Predicted basal area in  $m^2/ha$  shown for 30 years post-initialization year based on the IPM model with competitive structure. Predictions are made for each of the four cover classes: conifer (C), deciduous-conifer (DC), deciduous (D), and conifer-deciduous (CD). Here we see that although the C stand experiences the largest increase in spruce basal area over 30 years, it still has the smallest total basal area. The CD and D stands have the largest total basal area after 30 years as a result of the larger sizes of the aspen relative to the spruce.

# Bibliography

- Adler, P., Dalgleish, H., and Ellner, S. Forecasting plant community impacts of climate variability and change: when do competitive interactions matter? *Journal of Ecology*, 2012.
- Adler, P., Ellner, S., and Levine, J. Coexistence of perennial plants: an embarrassment of niches. *Ecology Letters*, 13(8):1019–1029, 2010.
- Alberta Environment and Sustainable Resource Development. *Reforestation Standard of Alberta*, 2012. <http://srd.alberta.ca/LandsForests/ForestManagement/ForestManagementManualsGuidelines.aspx>.
- Alberta Reforestation Standards Science Council. Linking Regeneration Standards to Growth and Yield and Forest Management Objectives. Tech. rep., Alberta's Minister of Sustainable Resource Development, 2001.
- Alberta Sustainable Resource Development. 2005 Natural regions and subregions of Alberta. 2005.
- Bokalo, M., Comeau, P., and Titus, S. Early development of tended mixtures of aspen and spruce in western Canadian boreal forests. *Forest Ecology and Management*, 242(2):175–184, 2007.
- Briggs, J., Dabbs, K., Holm, M., Lubben, J., Rebarber, R., et al. Structured population dynamics. *Mathematics Magazine*, 83(4):243–257, 2010.
- Chen, H. and Popadiouk, R. Dynamics of North American boreal mixedwoods. *Environmental Reviews*, 10(3):137–166, 2002.
- Childs, D., Rees, M., Rose, K., Grubb, P., and Ellner, S. Evolution of size-dependent flowering in a variable environment: construction and analysis of a stochastic integral projection model. *Proceedings of the Royal Society of London. Series B: Biological Sciences*, 271(1537):425–434, 2004.
- Clark, J. Individuals and the variation needed for high species diversity in forest trees. *Science*, 327(5969):1129–1132, 2010.
- Clark, J., Bell, D., Chu, C., Courbaud, B., Dietze, M., et al. High-dimensional coexistence based on individual variation: a synthesis of evidence. *Ecological Monographs*, 80(4):569–608, 2010.

- Dawson, A., Stadt, K., and Huang, J. Predicting white spruce mortality from retrospective data: competition versus recent growth. *In preparation*, 2013.
- Easterling, M., Ellner, S., and Dixon, P. Size-specific sensitivity: applying a new structured population model. *Ecology*, 81(3):694–708, 2000.
- Ellner, S. and Rees, M. Integral projection models for species with complex demography. *The American Naturalist*, 167(3):410–428, 2006.
- Feng, Z., Stadt, K., and Lieffers, V. Linking juvenile white spruce density, dispersion, stocking, and mortality to future yield. *Canadian Journal of Forest Research*, 36(12):3173–3182, 2006.
- Filipescu, C.N. and Comeau, P.G. Competitive interactions between aspen and white spruce vary with stand age in boreal mixedwoods. *Forest Ecology and Management*, 247(1):175–184, 2007.
- Freckleton, R., Matos, D., Bovi, M., and Watkinson, A. Predicting the impacts of harvesting using structured population models: the importance of density-dependence and timing of harvest for a tropical palm tree. *Journal of Applied Ecology*, 40(5):846–858, 2003.
- Gärtner, S., Bokalo, M., Stadt, K., and Macdonald, E. Benchmarking Natural Origin Stand Development. Tech. rep., Department of Renewable Resources, University of Alberta, 2009.
- Haefner, J. *Modeling Biological Systems: Principles and Applications*. Springer, 2005.
- Hosmer, D.W. and Lemeshow, S. *Applied logistic regression*, vol. 354. Wiley-Interscience, 2004.
- Huang, J.G., Stadt, K.J., Dawson, A., and Comeau, P. Modelling growth-competition relationships in trembling aspen and white spruce mixed boreal forests of western Canada. *Submitted to PLoS One*, 2013.
- Kneeshaw, D., Leduc, A., Messier, C., Drapeau, P., Gauthier, S., et al. Development of integrated ecological standards of sustainable forest management at an operational scale. *The Forestry Chronicle*, 76(3):481–493, 2000.
- Kobe, R. and Coates, K. Models of sapling mortality as a function of growth to characterize interspecific variation in shade tolerance of eight tree species of northwestern British Columbia. *Canadian Journal of Forest Research*, 27(2):227–236, 1997.
- Kohyama, T. Simulating stationary size distribution of trees in rain forests. *Annals of Botany*, 68(2):173–180, 1991.
- Kozak, A. and Kozak, R. Does cross validation provide additional information in the evaluation of regression models? *Canadian Journal of Forest Research*, 33(6):976–987, 2003.

- Leslie, P.H. On the use of matrices in certain population mathematics. *Biometrika*, 33(3):183–212, 1945.
- Lieffers, V., Armstrong, G., Stadt, K., and Marenholtz, E. Forest regeneration standards: are they limiting management options for Alberta’s boreal mixed-woods? *The Forestry Chronicle*, 84(1):76–82, 2008.
- Lieffers, V. and Beck, Jr, J. A semi-natural approach to mixedwood management in the prairie provinces. *The Forestry Chronicle*, 70(3):260–264, 1994.
- Lieffers, V., Pinno, B., and Stadt, K. Light dynamics and free-to-grow standards in aspen-dominated mixedwood forests. *The Forestry Chronicle*, 78(1):137–145, 2002.
- Luo, Y. and Chen, H. Competition, species interaction and ageing control tree mortality in boreal forests. *Journal of Ecology*, 99(6):1470–1480, 2011.
- Lytle, D. and Merritt, D. Hydrologic regimes and riparian forests: a structured population model for cottonwood. *Ecology*, 85(9):2493–2503, 2004.
- MacPherson, D.M., Lieffers, V.J., and Blenis, P.V. Productivity of aspen stands with and without a spruce understory in alberta’s boreal mixedwood forests. *The Forestry Chronicle*, 77(2):351–356, 2001.
- Man, R. and Lieffers, V. Are mixtures of aspen and white spruce more productive than single species stands? *The Forestry Chronicle*, 75(3):505–513, 1999.
- Murphy, P., Rousseau, A., and Stewart, D. Sustainable forests: a Canadian commitment national forest strategy and canada forest accord process and results. *The Forestry Chronicle*, 69(3):278–284, 1993.
- Natural Resources Canada. The Atlas of Canada; Boreal Forest. 2009. [http://atlas.nrcan.gc.ca/site/english/learningresources/theme\\_modules/borealforest/index.html](http://atlas.nrcan.gc.ca/site/english/learningresources/theme_modules/borealforest/index.html), Accessed 02/02/2013.
- Peters, V., Macdonald, S., and Dale, M. The interaction between masting and fire is key to white spruce regeneration. *Ecology*, 86(7):1744–1750, 2005.
- Plaut, J. *Carbon accumulation and distribution in a boreal mixedwood logged chronosequence near Wabowden, Manitoba*. Ph.D. thesis, Brown University, 2002.
- Popper, K. The logic of scientific discovery. *London: Hutchinson*, 16, 1959.
- Pretzsch, H. and Schütze, G. Transgressive overyielding in mixed compared with pure stands of Norway spruce and European beech in Central Europe: evidence on stand level and explanation on individual tree level. *European journal of forest research*, 128(2):183–204, 2009.
- Public Lands and Forests Division , Forest Management Branch. *Permanent sample plot (PSP) field procedures manual*. Alberta Sustainable Resource Development, 2005.

- Rebarber, R., Tenhumberg, B., and Townley, S. Global asymptotic stability of density dependent integral population projection models. *Theoretical Population Biology*, 2011.
- Rees, M. and Ellner, S. Integral projection models for populations in temporally varying environments. *Ecological Monographs*, 79(4):575–594, 2009.
- Reich, P., Tjoelker, M., Walters, M., Vanderklein, D., and Buschena, C. Close association of rgr, leaf and root morphology, seed mass and shade tolerance in seedlings of nine boreal tree species grown in high and low light. *Functional Ecology*, 12(3):327–338, 2002.
- Silvertown, J., Franco, M., Pisanty, I., and Mendoza, A. Comparative plant demography—relative importance of life-cycle components to the finite rate of increase in woody and herbaceous perennials. *Journal of Ecology*, pp. 465–476, 1993.
- Stadt, K., Huston, C., Coates, K., Feng, Z., Dale, M., et al. Evaluation of competition and light estimation indices for predicting diameter growth in mature boreal mixed forests. *Annals of Forest Science*, 64(5):477–490, 2007.
- Thorpe, H., Astrup, R., Trowbridge, A., and Coates, K. Competition and tree crowns: A neighborhood analysis of three boreal tree species. *Forest Ecology and Management*, 259(8):1586–1596, 2010.
- Usher, M.B. A matrix approach to the management of renewable resources, with special reference to selection forests. *Journal of Applied Ecology*, pp. 355–367, 1966.
- Van Mantgem, P. and Stephenson, N. The accuracy of matrix population model projections for coniferous trees in the sierra nevada, california. *Journal of Ecology*, 93(4):737–747, 2005.
- Waring, R., Schroeder, P., and Oren, R. Application of the pipe model theory to predict canopy leaf area. *Canadian Journal of Forest Research*, 12(3):556–560, 1982.
- Yang, Y. *Mortality models for major boreal mixedwood species in Alberta*. Ph.D. thesis, University of Alberta, 2002.
- Zuidema, P., Jongejans, E., Chien, P., During, H., and Schieving, F. Integral projection models for trees: a new parameterization method and a validation of model output. *Journal of Ecology*, 98(2):345–355, 2010.

## Chapter 4

# A guide to efficient integration schemes for integral projection models (IPMs)<sup>1</sup>

### 4.1 Introduction

Introduced by Easterling (1998), and more prominently in Easterling et al. (2000), the integral projection model (IPM) is an increasingly popular method for modelling population dynamics (Dalglish et al., 2011; Rebarber et al., 2011; Rees and Ellner, 2009; Zuidema et al., 2010). The IPM is an attractive alternative to the traditional matrix model approach, which requires that a population be divided into discrete classes based on a potentially continuous attribute. Class size and cutoff determination is somewhat subjective, but the real difficulty arises with the assumption that all individuals within a class are treated equally with respect to the continuous attribute. Intuitively, to solve this issue of homogeneity within classes, one could choose arbitrarily small class sizes. However, the number of classes may affect transient behavior when the total number of individuals is considered (Tenhumberg et al., 2009). Even though the approach of choosing small class sizes may approximate dependence on a continuous attribute, it leads to another difficulty - transitions between all classes must be parameterized (more classes implies more parameters). The IPM is a natural extension of the matrix projection model that allows both of these issues to be dealt with simultaneously

---

<sup>1</sup>A modified version of the chapter titled “A guide to efficient integration schemes for integral projection models (IPMs)” has been submitted to *Methods in Ecology and Evolution*.

by modeling the population as a function of a continuous attribute. The IPM allows ecologists to use demographic data to parameterize growth, survival, and fecundity models as a function of this continuous variable, and then use these models to construct a redistribution kernel. This kernel determines how the population distribution changes with (discrete) time through iteration of the IPM. As with a matrix model, long-term growth rates, sensitivity, and elasticity values can also be computed (Easterling, 1998). Conditions that guarantee the existence and uniqueness of an asymptotic growth rate (dominant eigenvalue) and a stable population distribution (eigenvector associated with dominant eigenvalue) are given in Ellner and Rees (2006). Much of the standard IPM theory is summarized nicely by Briggs et al. (2010).

The IPM has also been used to address other questions in population ecology. For example, in Rees and Rose (2002) the IPM is used to determine the evolutionarily stable strategy for a monocarpic perennial. Rose et al. (2005) used the IPM to study the effects of native and non-native insect herbivory on a flowering plant by developing kernels for four different herbivory scenarios and comparing the evolutionarily stable flowering size under these four scenarios. An extension of the IPM which allowed flowering probability to depend on both size and age was developed in Childs et al. (2003), and further extended to include stochasticity through a time-varying kernel dependent on the environment (Childs et al., 2004). Further theoretical results are developed in Lubben et al. (2009) where a growth-decline boundary can be identified for a group of projection models (matrix and integral) which allows one to determine how model parameterization affects the leading eigenvalue.

I consider the following IPM

$$n(y, t + 1) = \int_L^U k(x, y)n(x, t) dx \quad (4.1)$$

where  $n(x, t)dx$  is the number of individuals in the interval  $[x, x + dx]$  at time  $t$  for  $x \in [L, U]$  and  $k(x, y)$  is the kernel. The kernel represents the transition of an individual of size  $x$  to a size  $y$  individual between time  $t$  and  $t + 1$ . IPM kernels are often of the form

$$k(x, y) = s(x)g(x, y) + r(x)f(y) \quad (4.2)$$

where  $s(x)$  is the survival probability,  $g(x, y) = \phi(y; \mu(x), \sigma^2(x))$ , where  $\phi$  is the normal probability distribution function that defines how an individual of size  $x$  grows to size  $y$ , and  $r(x)f(y)$  is the fecundity (number of recruits  $r(x)$  and

distribution of new recruits  $f(y)$ ).

The implementation of this model requires that a numerical quadrature scheme be employed. The IPM literature has recognized that: (i) results may be sensitive to the chosen scheme (Zuidema et al., 2010), and (ii) computational time varies widely between schemes and their implementations (Easterling et al., 2000; Rees and Ellner, 2009).

Despite the increasing prevalence of the use of the IPM in ecological studies, few studies have considered the challenges that arise from the need to perform numerical integration. Discretizing and implementing IPMs accurately and efficiently is important for several reasons, including: (i) recovering numerically accurate population projections over long time periods, (ii) recovering numerically accurate estimates for quantities such as growth rates and elasticities, and (iii) employing IPMs in ensemble runs for Markov Chain Monte-Carlo (MCMC) simulations or Bayesian inference. After the mathematical construction of an IPM, it is typical for ecologists to rely on software packages for model implementation and analysis. At this stage, it is important to have some confidence that the implementation is performing the integration of the associated IPM correctly: for very long simulations the hope is that the implementation is accurate enough so that small numerical errors do not accumulate substantially so as to give false estimates of, eg, population distributions and growth rates. Furthermore, in situations for which there is a need to perform thousands of iterations of a time dependent IPM, the efficiency of the implementation becomes important: if one iteration takes 0.1s of computer time vs 10s (a factor of 100 is not unreasonable as will be shown), a thousand iterations would take less than 2 minutes vs more than 2 hours. I note that a new IPM package “IPMpack” has been developed in the R programming language (Metcalf et al., 2012) and encourage ecologists to consider using this package for their studies.

Several integration schemes for IPMs are presented in Section 4.2. The methods discussed include: the (ubiquitous) midpoint method and related “bin-to-bin” variants; and the classical Gaussian quadrature methods and related sub-grid variants. The midpoint method (which is cell-based) is the fastest scheme with acceptable accuracy, while its bin-to-bin variants are more robust but often expensive in terms of computational time. The classic Gaussian methods do not handle non-trivial kernels well, but their sub-grid variants are extremely accurate and reasonably fast. Most of the methods presented have been used in previous IPM studies, with the exception of the sub-grid variants of the Gaussian methods. To examine the accuracy and efficiency of these schemes, each scheme is tested against three IPM

kernels, which are presented in Section 4.3. The kernels used include a synthetic kernel (the “virtual” kernel) that yields an exact analytical solution (which is useful for testing numerical schemes), a kernel used by Easterling, Ellner, and Dixon (2000) (the “shrub” kernel), and a kernel used by Zuidema, Jongejans, Chien, During, and Schieving (2010) (the “tree” kernel). Numerical results are presented in Section 4.4, and I conclude with a discussion of the results and recommendations for those wishing to implement a numerical scheme for an IPM in Section 4.5.

## 4.2 Integration schemes

Integration schemes for IPMs are ultimately numerical discretizations of (4.1), and can be categorized into two broad classes: (i) point based discretizations in which the value of the population density is stored at discrete points and the kernel is sampled at the same discrete points; and (ii) cell based discretizations in which the average value (and perhaps higher order moments) of the population density is stored in cells (bins) and the kernel is sampled according to the particular discretization scheme (eg, the midpoint rule).

Note that once the discretization has been chosen, IPMs do *not* necessarily reduce to matrix models. Discretizing (4.1) allows us to approximate the  $dx$  integral in (4.1), but we are free to sample the right-hand-side of the IPM at any  $y$  – which is a continuous variable – that we choose. This is not possible with matrix models. In practice, however, to project the population through time we typically sample the IPM at the same set of discrete points  $y$  as were used to perform the original discretization ( $x$ ). In this case (linear) integration schemes ultimately simplify to a projection of the form

$$\mathbf{n}^{t+1} = A\mathbf{n}^t \tag{4.3}$$

where  $\mathbf{n}^t$  is a vector with  $N$  entries that represents the discrete population at time  $t$ , and  $A$  is an  $N \times N$  matrix. The number  $N$  of mesh points (or cells) used to discretize the continuous population  $n(x, t)$  determines both the numerical accuracy and computational cost of the integration scheme. However, for a fixed mesh size  $N$ , some schemes are more accurate, efficient, and/or robust than others. I note again that the projection matrix  $A$  obtained by discretizing an IPM depends on the discretization method used and is fundamentally different from a projection matrix obtain from a matrix model – the entries of a projection matrix associated with a matrix model represent transition probabilities between population classes, while the entries of an IPM projection matrix represent a particular discretization of a continuous population model.

Once the projection matrix  $A$  is determined, standard matrix techniques can be used to compute stable population distributions (eigenvectors), growth rates (eigenvalues), and elasticities. However, we will not concern ourselves here with issues related to computing eigenvalues and eigenvectors, but instead recommend that users investigate the ARPACK (Lehoucq et al., 1998) routines (which are available in R and Python) to compute *only* the dominant eigenvalue and its associated eigenvector instead of computing the entire eigensystem, especially for large  $N$ .

Before proceeding I note that while cell based methods (such as the midpoint rule) are commonly used since they fit naturally with “binned” data and allow for straightforward comparisons to matrix models, binning is *not* necessary even when working with raw measurements. Regardless of the choice of discretization, the first projection can be performed using the empirical distribution

$$n(x, 0) = \sum_i n_i^0 \delta(x - x_i) \quad (4.4)$$

where  $(x_i, n_i^0)$  represents the raw measurements, and  $\delta$  is the Dirac delta function. With this initial distribution, the first projection becomes

$$n(y, 1) = \int_L^U k(x, y) \left[ \sum_i n_i^0 \delta(x - x_i) \right] dx = \sum_i n_i^0 k(x_i, y). \quad (4.5)$$

Subsequently, (4.5) can be used by particular integration schemes to compute discrete point-based or cell-based population distributions.

Hereafter I will denote continuous population distributions by  $n(x, t)$  and discrete population distributions by  $n_i^t$ , which represents the discrete population at the  $i^{\text{th}}$  mesh point/cell at time  $t$ .

### 4.2.1 Point based discretizations

Point-based methods, such as Gaussian quadrature (GQ) methods, discretize the continuous population density  $n(x, t)$  by storing its value at a discrete set of mesh points  $x_i \in [L, U]$  for  $i = 1 \dots N$ . In these methods, mesh points are not uniformly spaced along the domain, but are instead chosen according to Gaussian quadrature rules, which result in more accurate quadratures than an equivalent number of

uniformly spaced nodes. The discrete IPM is therefore

$$n_j^{t+1} \approx \sum_{i=1}^N w_i k(x_i, y) n_i^t \quad (4.6)$$

so that (4.3) holds with

$$A_{ji}^{\text{GQ}} = w_i k(x_i, x_j) \quad (4.7)$$

where  $w_i$  is the quadrature weight associated with the mesh/quadrature point  $x_i$ . The choice of quadrature points  $x_i$  and weights  $w_i$  determine the type, accuracy, and cost of the scheme.

### Classical Gaussian quadrature methods

Classical Gaussian quadrature methods were designed to integrate polynomials of degree  $2N$  exactly, but unfortunately suffer two important flaws for our purposes: (i) they do not handle discontinuities well, and (ii) their quadrature points tend to pile up near the end points  $L$  and  $U$  for large  $N$  (and hence the mesh is relatively sparse in the middle of the domain). As will be noted in Section 4.5, slow-growing species require a dense mesh, and abrupt changes in species survival and/or fecundity result in discontinuities. As such, these methods are not appropriate for most IPMs and hence I have excluded them from the remainder of this study.

### Sub-interval based Gaussian quadrature methods

To obtain more robust schemes using the classical Gaussian quadrature methods one can divide the domain of interest  $[L, U]$  into several sub-intervals and apply lower-order Gaussian quadrature rules to each sub-interval. If the sub-intervals are chosen correctly the resulting quadrature rule can handle kernels with discontinuities quite well, and the quadrature points are distributed more evenly throughout the domain so that a dense mesh is attained. These methods are extremely accurate and easily vectorized, but may result in large projection matrices.

I consider three types of sub-interval based Gaussian quadrature:

- Gauss-Legendre over sub-intervals, hereafter denoted  $\text{GL}(k)$  where  $k$  denotes the number of standard Gaussian quadrature points per sub-interval. The interval  $[L, U]$  is uniformly divided into  $N$  sub-intervals, each of which contains  $k$  quadrature points (so that the total number of mesh points is  $kN$ ).

Note that the  $GL(k)$  quadrature points *do not* include the endpoints of the sub-intervals.

- Clenshaw-Curtis over sub-intervals, hereafter denoted  $CC(k)$ . Again, this is the same as  $GL(k)$  except the Clenshaw-Curtis quadrature rule is used in each sub-interval. Note, however, that the  $CC(k)$  quadrature points *do* include the endpoints of the sub-intervals. This has important consequences for kernels with discontinuous terms.
- Adjusted Gauss-Legendre over sub-intervals, hereafter denoted  $AGL(k)$ . This is the same as the  $GL(k)$  method except that the sub-intervals are adjusted so that their edges align with any discontinuities present in the kernel. For example, with  $N = 10$  cells on the domain  $[L, U] = [0, 10]$  with discontinuities at  $x = 0.15$  and  $0.25$ , the uniform cell edges would be

$$[0.0, 1.0, 2.0, 3.0, 4.0, 5.0, 6.0, 7.0, 8.0, 9.0, 10.0]$$

whereas the adjusted cell edges would be

$$[0.0, 0.15, 0.25, 1.46875, 2.6875, 3.90625, 5.125, 6.34375, 7.5625, 8.78125, 10.0].$$

In this adjusted sub-interval case, the second and third cell edges have been moved so that they correspond exactly with the kernel discontinuities (so that the  $AGL(k)$  method does not sample the kernel where it is discontinuous), and the remaining cell edges are shifted so that they uniformly divide the remainder  $[0.25, 10.0]$  of the domain. Sub-interval adjustment for the Clenshaw-Curtis rule would not offer any improvement because the kernel discontinuities would still be sampled.

In each case, the kernel is sampled  $k^2 N^2$  times, so that the computational cost is proportional to  $k^2 N^2$ . Figure 4.2 depicts the  $GL(3)$  sub-interval based quadrature rule (see caption for details). All of the other sub-interval based Gaussian quadrature rules are similar to the depicted  $GL(k)$  method, however: the  $CC(k)$  rules have quadrature points at each of the sub-interval edges, and the widths of the  $AGL(k)$  sub-intervals are not necessarily uniform.

## 4.2.2 Cell based discretizations

Cell based methods, such as the ubiquitous midpoint method, discretize the continuous population  $n(x, t)$  by storing its value at the centers of each of a finite set

of cells (bins)  $C_i$ . The cells  $C_i$  are obtained by dividing the interval  $[L, U]$  into  $N$  uniform bins.

### Midpoint method

The midpoint method is obtained by approximating  $n(x, t)$  by  $n_i(t)$  and  $k(x, y)$  by  $k(x_i, y_j)$  where  $x_i$  and  $y_j$  are the cell centers of  $C_i$  and  $C_j$ , respectively. The corresponding discrete IPM is therefore

$$n_j^{t+1} \approx \sum_{i=1}^N k(x_i, y_j) n_i^t \quad (4.8)$$

so that (4.3) holds with

$$A_{ji}^{\text{MP}} = k(x_i, y_j). \quad (4.9)$$

As such, the midpoint method samples the kernel exactly  $N^2$  times to construct the projection matrix, and therefore its computational cost is proportional to  $N^2$ . This midpoint method is easy to implement and vectorized, but is not nearly as accurate as the sub-interval based Gaussian quadrature methods.

### Bin-to-bin methods

Several authors have also used “bin to bin” methods (Zuidema et al., 2010), where the population  $n(x, t)$  is approximated by  $n_i^t$  in bin  $C_i$  while the kernel is treated more precisely. More specifically, for cell based methods the discrete population  $n_i^t$  formally represents the average value of the population density over the cell  $C_i$  (ie,  $n_i^t = \frac{1}{\Delta x_i} \int_{C_i} n(x, t) dx$ ) and hence the associated discrete IPM is

$$n_j^{t+1} = \frac{1}{\Delta x_j} \int_{C_j} n(y', t + 1) dy' \approx \sum_{i=1}^N \frac{1}{\Delta x_j} \int_{C_j} \int_{C_i} k(x', y') n_i^t dx' dy' \quad (4.10)$$

so that (4.3) holds with

$$A_{ji}^{\text{B2B}} = \frac{1}{\Delta x_j} \int_{C_j} \int_{C_i} k(x', y') dx' dy'. \quad (4.11)$$

This technique essentially breaks the integrand  $k(x, y) n(x, t)$  into two pieces: the  $n(x, t)$  piece is held constant over each cell while the  $k(x, y)$  piece is integrated more accurately (exactly or numerically). The order of accuracy is formally the same as the midpoint method (due to the treatment of the  $n(x, t)$  piece), except that the

kernel is integrated from “bin to bin” which results in a more robust method. The computational cost of these methods depends on how the integrations in (4.11) are performed. Figure 4.3 depicts the general idea behind bin-to-bin quadrature methods (see caption for details).

In many cases the integral with respect to  $dy'$  in (4.11) can be evaluated exactly (after swapping the order of integration since  $C_i \times C_j$  is a rectangle in  $\mathbb{R}^2$ ). For example, for a simple kernel of the form (4.2) we obtain

$$\begin{aligned}
\int_{C_j} \int_{C_i} k(x', y') dx' dy' &= \int_{C_i} \int_{C_j} k(x', y') dy' dx' \\
&= \int_{C_i} \left[ s(x') \int_{C_j} N(y'; \mu(x'), \sigma^2(x')) dy' + r(x') \int_{C_j} f(y') dy' \right] dx' \\
&= \int_{C_i} \left[ s(x') \left( \Phi(y_{j+1}; \mu(x'), \sigma^2(x')) - \Phi(y_j; \mu(x'), \sigma^2(x')) \right) \right] dx' \\
&\quad + (F(y_{j+1}) - F(y_j)) \int_{C_i} r(x') dx',
\end{aligned} \tag{4.12}$$

where  $\Phi(x; \mu, \sigma^2)$  is the normal cumulative density function for the random variable  $x$  with mean  $\mu$  and standard deviation  $\sigma$ , and  $F(x)$  is the antiderivative of  $f(x)$ .

For more general kernels adaptive quadrature (i.e. R’s integrate function, which ultimately calls QUADPACK) or fixed-order quadrature (i.e. Gaussian quadrature) can be used to compute the projection matrix. During the course of this study I noted that bin-to-bin methods using adaptive quadrature were computationally expensive, and as such I have omitted them from the remainder of our discussion. The remaining bin-to-bin variants are hereafter denoted by

- INTB2BGL( $k$ ) - the  $dy'$  integral is evaluated exactly, as in (4.12), and the  $dx'$  integral is evaluated numerically using Gaussian quadrature with  $k$  quadrature points.
- GENB2BGL( $k$ ) - both the  $dx'$  and  $dy'$  integrals are evaluated numerically using Gaussian quadrature with  $k$  quadrature points in each dimension.

These methods are much more accurate than the midpoint method for small meshes, and the resulting projection matrices are smaller relative to those obtained using the midpoint method. Unfortunately they are not easily vectorized.

## Zuidema method

The Zuidema (ZB2B) method (Zuidema et al., 2010) is a variant of the bin-to-bin methods introduced above (Sec. 4.2.2). It uses a quasi-midpoint method with  $M$  sub-intervals to compute the bin-to-bin integrals in (4.11). That is,

$$A_{ji}^{\text{ZB2B}} = \frac{\Delta x}{M} \sum_{m=1}^M k(x_{i,m}, x_{j,m}) \quad (4.13)$$

where  $x_{i,m} = L + i\Delta x + m\Delta x/M$  and  $\Delta x = (U - L)/N$ . Note that the sum in (4.13) does not formally approximate the double integral in (4.11), but in practice performs fairly well. The kernel is sampled  $MN^2$  times and therefore the computational cost is proportional to  $MN^2$ .

## 4.3 Sample IPM kernels

### 4.3.1 Virtual kernel

Consider the kernel

$$k(x, y) = \lambda e^{-\lambda x} N(y; x + \mu, \sigma^2) \quad (4.14)$$

together with the initial condition

$$n_0(x) = N(x; \mu_0, \sigma_0^2) \quad (4.15)$$

on the domain  $(-\infty, \infty)$ , where  $\lambda e^{-\lambda x}$  describes the size-dependent survival probability (larger individuals experience greater mortality). Then, the projected population at time  $t = 1$  is

$$\begin{aligned} n_1(y) &= \int_{-\infty}^{\infty} k(x, y) n_0(x) dx = \frac{\lambda}{2\pi\sigma\sigma_0} \int_{-\infty}^{\infty} \exp\left(-\lambda x - \frac{(y-x-\mu)^2}{2\sigma^2} - \frac{(x-\mu_0)^2}{2\sigma_0^2}\right) dx \\ &= \lambda e^{-\lambda/2(\lambda\sigma_0^2 - \mu_0)} N(x; \mu, \sigma^2) * N(x; \mu_0 - \lambda\sigma_0^2, \sigma_0^2)(y). \end{aligned} \quad (4.16)$$

where  $*$  denotes convolution. Applying the convolution theorem for Gaussian distributions, we obtain

$$n_1(y) = \lambda e^{-\lambda/2(\lambda\sigma_0^2 - \mu_0)} N(y; \mu_0 + \mu - \lambda\sigma_0^2, \sigma_0^2 + \sigma^2). \quad (4.17)$$

That is, projection shifts the mean by  $\mu - \lambda\sigma_0^2$ , expands the variance by  $\sigma^2$ , and increases/decreases the total population by a factor of  $\lambda e^{-\lambda(\lambda/2 - \mu_0)}$ . The population at time  $t$  can therefore be computed exactly by repeatedly applying (4.17).

In the numerical results that follow, this kernel will be denoted VIRTUAL. It affords us the opportunity to compare numerical methods to a known solution. The parameter values used for the VIRTUAL kernel in the remainder of this study are:  $[L, U] = [0, 20]$ ,  $\sigma^2 = 2.0$ ,  $\mu = 1.0$ ,  $\lambda = 0.02$ ,  $\mu_0 = 5.0$ , and  $\sigma_0^2 = 1.0$ .

### 4.3.2 Shrub kernel

The IPM presented by Easterling, Ellner, and Dixon (2000) models the dynamics of Northern Monkshood as a continuous function of size. The kernel takes the standard form (4.2) with

$$\begin{aligned} s(x) &= \text{logit}^{-1}(1.34 + 0.92x) \\ g(x, y) &= N(y; \mu = 0.37 + 0.73x, \sigma^2 = 0.127 + 0.23x) \\ r(x) &= 0.034 + 0.038x \\ f(y) &= \begin{cases} 10 & \text{if } 0.15 \leq y \leq 0.25 \\ 0 & \text{otherwise.} \end{cases} \end{aligned} \tag{4.18}$$

This kernel is hereafter denoted by SHRUB. The SHRUB kernel is fairly well behaved except near the points  $y = 0.15$  and  $y = 0.25$  where the fecundity term is discontinuous.

This discontinuity in the kernel causes difficulty for many integration schemes unless the mesh is sufficiently refined. Although the fecundity model can be altered to smooth out these discontinuities, having an integration scheme that is able to handle discontinuities well is advantageous regardless: it will handle a larger class of IPMs. As such, I will implement the shrub IPM with the fecundity model as presented.

### 4.3.3 Tree kernel

The IPMs presented by Zuidema, Jongejans, Chien, During, and Schieving (2010) model the dynamics of several threatened Vietnamese tree species. For species which are long-lived and slow-growing, as are most tree species, discretization of the IPM using the traditional midpoint method requires that the domain be

divided into a large number of cells to appropriately deal with the slow growth of individuals. In Zuidema et al., a new integration scheme is presented as a viable scheme to be used in such cases. Here I use one of the six fitted kernels as an example of a kernel that may arise from a population of tree-like individuals. In the subsequent text I give a brief overview of the kernel construction - for those interested, further details are given in Zuidema et al. (2010). Of the six tree species models presented, I consider the IPM for *Parashorea chinensis* which consists of two classes: (i) a seedling class for individuals less than 1 cm in diameter at breast height which consists of four discrete sub-classes; and (ii) a mature (reproductive) class that models demographic dynamics as a continuous function of size using survival, growth, and fecundity functions that were fitted to individual-level data.

The seedling class is itself partitioned into four classes based on seedling height, as done in Chien et al. (2008), where the transition probabilities between classes are defined as in a standard matrix model approach.

The continuous portion of the kernel which models the growth and survival of larger individuals takes the standard form (4.2) with

$$\begin{aligned} s(x) &= 0.98 \\ g(x, y) &= N(y; \mu = \mu(x), \sigma^2 = 0.1054) \end{aligned} \tag{4.19}$$

where

$$\mu(x) = x + \frac{2.258 \cdot 144.0x^{2.258-1.0}}{144.0 + x^{2.258/42.1}}, \tag{4.20}$$

where the size  $x$  is the tree diameter at breast height (DBH).

After Discretizing the continuous portion to obtain the projection matrix  $A$ , the overall projection matrix  $P$  can be written as

$$P = \begin{bmatrix} K_{ss} & K_{ts} \\ K_{st} & A \end{bmatrix} \tag{4.21}$$

where  $K_{ss}$  is a  $4 \times 4$  matrix describing the seedling transitions, and  $A$  is an  $N \times N$  matrix (where  $N$  is the number of cells). The sub-matrix  $K_{ts}$  describes the fecundity, or addition of new individuals into the smallest seedling class (therefore only the first row contains non-zero entries). The number of new individuals is given by the product of: the probability of survival, the size-dependent reproduction probability, and the number of new seedlings per reproductive tree. The sub-matrix  $K_{st}$  describes the transition of seedlings in the largest seedling class to the tree class (therefore only the fourth column contains non-zero entries). These

transition values are taken to be as described in Zuidema et al. (2010), where it is assumed that the next year DBH of those trees in the largest seedling class can be modeled as a truncated normal distribution, and the value of the corresponding probability density for a given DBH is multiplied with the probability of moving to another class as determined in Chien et al. (2008).

This kernel is hereafter denoted by TREE. In practice, the TREE kernel is fairly well behaved except in the case where the standard deviation of the size (DBH) increment is very small.

## 4.4 Numerical results

When discussing efficiency I report both the number of times the particular integration scheme sampled the kernel as well as the run times of the numerical tests. By reporting sampling counts I expose the algorithmic complexity associated with the discretization method instead of issues relating to the choice of implementation or language (e.g. R, Python, Fortran etc). I do so with an eye toward performing ensemble runs of projections for kernels that depend on time (e.g. through climate so that  $A$  must be reconstructed before each projection). In this case we may be required to perform thousands of projections of a particular IPM (and hence thousands of constructions of  $A$ ) and hence computational efficiency is important. In contrast, reporting run times will highlight that some integration schemes are more easily vectorized than others, which becomes particularly important when using dynamic languages such as R or Python.

All of the numerical experiments presented here were implemented in the Python programming language using the NumPy package for vectorization and matrix products, and were performed on a UNIX workstation with a 2.2GHz processor.

When comparing the accuracy and efficiency of the various integration methods described in Section 4.2 I present two types of plots: (i) error vs. the number of computational complexity (ie, number of times the kernel is sampled), and (ii) error vs. run time. The errors reported are  $E_{\text{pop}}$  and  $E_{\text{growth}}$  where

$$\begin{aligned} E_{\text{pop}} &= | \text{exact total population} - \text{approximate total population} |, \\ E_{\text{growth}} &= | \text{exact growth rate} - \text{approximate growth rate} | \end{aligned} \quad (4.22)$$

where the growth rates are computed by finding the dominant eigenvalue of the projection matrix. Total population is computed after projecting an initial population through five years. Figure 4.1 shows how these three types of graphs should

be interpreted: accurate methods appear at the bottom of the plots while inaccurate methods appear at the top; and, fast/efficient methods appear at the left of these plots while slow/inefficient methods appear at the right.

For the SHRUB and TREE kernels, an exact (reference) population is computed with the GL(13) method using  $N = 800$  sub-intervals. The error plots presented throughout use logarithmic scales. As a general rule of thumb, a method that obtains an error of  $10^{-4}$  has obtained the solution correct to 4 digits.

Although only the absolute errors are reported hereafter, the direction (over- vs. under-estimate) of the population and growth rate errors was computed. Whether a method over- or under-estimates the population or growth rate is perhaps only interesting when the absolute error is relatively large, which typically occurs for small mesh sizes. Unless otherwise noted, it was observed that when the absolute error was greater than  $10^{-4}$ , all quadrature methods over-estimated both the total population and growth rate.

The code to perform all of the numerical experiments (and generate the corresponding plots) presented here is available online at <https://github.com/memmett/PyIPM>.

#### 4.4.1 Virtual kernel

Figure 4.4 shows the error of the total population and growth rate vs. the computational cost for the Virtual kernel. All of the cell-based methods exhibit first order convergence regardless of how the kernel is sampled because they approximate  $n(x, t)$  by  $n_i^t$  within each cell. However, the cell-based methods are distinguished by their complexity, with the midpoint rule being the least expensive. In contrast to the cell-based methods, the sub-interval point-based methods are extremely accurate and relatively efficient.

#### 4.4.2 Shrub kernel

Figure 4.5 shows the error of the total population and growth rate vs. computational cost for the SHRUB kernel. The cell based (MidPoint and B2B) methods exhibit decent accuracy and behave quite predictably. However, the B2B methods are more accurate for small  $N$  compared to the MidPoint rule since they are able to successfully sub-sample the kernel within each cell. For slow-growing species the MidPoint rule may not properly resolve growth if the bins are too large relative to

the annual size increment of the species. This is because the MidPoint rule only samples the kernel (and hence growth) at the center of each bin. In contrast, the B2B methods sample the kernel throughout each bin.

The sub-interval based  $GL(k)$  methods do not perform well until at least  $N = 200$ , at which point they achieve very high accuracy regardless of  $k$ . This is because the edges of the sub-intervals associated with the  $GL(k)$  discretizations do not align well with the discontinuities in the kernel associated with the fecundity term until  $N = 200$ . Once the sub-interval edges match the kernel discontinuities, the  $GL(k)$  methods obtain their formal order of accuracy and obtain a very high degree of accuracy (many orders of magnitude better than other methods).

The sub-interval based  $CC(k)$  methods do not exhibit the same behavior as the  $GL(k)$  methods where accuracy is increased for large  $N$  because the quadrature points of Clenshaw-Curtis rules contain the edges of the sub-intervals (the  $GL(k)$  rules do not). This means that even after the sub-interval edges match the discontinuities in the kernel associated with the fecundity term, the discontinuities are still sampled by the  $CC(k)$  methods whereas they weren't sampled by the  $GL(k)$  methods. The  $CC(9)$  method both under- and over-estimated the total population and growth rate, depending on the value of  $N$ .

In contrast, the adjusted  $AGL(k)$  method performs very well for mesh sizes less than  $N = 200$  precisely because they avoid sampling the kernel where it is discontinuous by adjusting their mesh.

Figure 4.6 shows the error of the total population and growth rate vs. total run time for the SHRUB kernel. The point-based quadrature methods and midpoint methods are easily vectorized and are therefore very fast (several orders of magnitude faster than the B2B methods). Furthermore, the  $AGL(k)$  method clearly outperforms all of the other methods: it achieves extremely high accuracy even on relatively small meshes.

Figure 4.7 shows the error of the total population and growth rate vs. total run time for the SHRUB kernel with different growth parameters:  $g(x, y) = \phi(y; \mu = 1.01x, \sigma^2 = 0.005 + 0.001x)$ , where  $\phi$  is the normal probability density function. These parameter choices result in a kernel with slow-growth and small variance, and retains the discontinuities in the fecundity term. The errors shown here are similar to those in the regular SHRUB kernel, indicating that once discontinuities are resolved then difficulties relating to slow-growth and small variance are also resolved. Again, the  $AGL(k)$  method performed extremely well even for small

mesh sizes. A wider range of growth parameter values were tested, and the overall behavior of all quadrature methods was similar (not shown).

### 4.4.3 Tree kernel

Figure 4.8 shows the error of the total population and growth rate versus computational cost for the TREE kernel.

The sub-interval based Gaussian quadrature methods perform significantly better than the other methods. The GL(9) and CC(9) methods have the highest accuracy because they sample the kernel many times within each sub-interval and hence resolve the kernel well. The bin-to-bin methods are more accurate than both the MidPoint and ZB2B methods since they formally approximate the integrals in (4.11) to higher order.

The MidPoint and ZB2B methods under-estimated both the total population and growth rates for the TREE kernel for small mesh sizes.

## 4.5 Discussion

I have applied several cell-based and point-based integration schemes to three IPMs and have presented their computational cost in terms of both complexity (the number of times the kernel must be sampled) and run time. The kernels used to expose the computational cost of the discretization methods contain two important features: (i) the SHRUB kernel contained discontinuities in its fecundity term, and (ii) the TREE kernel's growth distribution was relatively "tall and skinny" due to the slow-growing long-lived nature of the species (leading to a small growth variance). A robust numerical method that is suitable for a broad set of IPMs should be able to handle both of these difficulties efficiently.

Regarding cell-based methods, although the bin-to-bin variants (the B2B methods) appear to be more robust (in the sense that for a small mesh they obtain decent accuracy), for a given level of accuracy the midpoint method is more efficient in terms of both computational complexity and run time. In other words, although the midpoint method requires a larger mesh to obtain the same level of accuracy as its bin-to-bin variants, it can operate on this larger mesh much faster than the bin-to-bin variants operate on their smaller mesh. Furthermore, the implementation of the midpoint method is extremely simple: it takes less time to develop and is easier

to maintain than the bin-to-bin variants. Finally, I note again that one perceived benefit of the bin-to-bin variants is that, unlike the midpoint method, they result in smaller projection matrices  $A$ . To address this shortcoming of the midpoint method, I strongly recommend using the ARPACK (Lehoucq et al., 1998) routines to compute the dominant eigenvalues and eigenvectors of  $A$ , and note that the ARPACK routines are callable from R and Python. For example, Fig. 4.9 shows Python and R code snippets to compute only the dominant eigenvalue of a matrix  $A$  using ARPACK. For an  $800 \times 800$  random matrix  $A$ , using R's `eigen` command took approximately 4.7 seconds (on the same workstation used to perform the numerical experiments presented here) to compute all of the eigenvalues of  $A$ , whereas calling `arpack` took approximately 0.052 seconds to compute the dominant eigenvalue and its associated eigenvector.

Regarding point-based methods, although most of these methods do not handle discontinuities well, if the discontinuities are known in advance (as was the case for the SHRUB kernel), then the automatically adjusting AGL( $k$ ) method performs extremely well. If accuracy is important or long time periods are being considered, I strongly recommend using the sub-interval based adjusted Gauss-Legendre method, i.e. AGL( $k$ ) with  $k = 9$  or higher. In particular, for all of the kernels tested here the AGL(9) method was more accurate than all of cell based methods for a given mesh size. AGL(9) was also faster than the other cell based methods except for the midpoint rule.

Overall, I recommend that authors use either the midpoint method or a high-order, self adjusting, sub-interval based Gauss-Legendre rule such as the AGL(9) method. Both of these are straight forward to implement and are easy to vectorize (which is important for dynamic languages such as R and Python). When using the midpoint method authors are encouraged to use large meshes. If accuracy is important, the self adjusting sub-interval based Gauss-Legendre method is very powerful even for discontinuous and/or “tall and skinny” distributions (i.e. for slow-growing species).

Table 4.1 summarizes various relationships between biological attributes typically found in IPMs, their mathematical manifestation in IPM kernels, and numerical aspects for implementers of IPMs to consider. Table 4.2 summarizes our recommendations.

Biological	Mathematical	Numerical
Species are slow growing relative to the domain.	Growth function has a small $\sigma^2$ relative to the domain size.	Dense mesh required.
Attributes ( $x$ values) of new individuals fall within a closed interval.	Discontinuities in the fecundity term.	Method must be robust with respect to discontinuities at a few mesh points.
Abrupt changes in the survival probability.	Discontinuities (or near discontinuities) in the survival term.	Method must be robust with respect to discontinuities at a few mesh points.
Species do not shrink.	Growth function is truncated and hence the kernel is discontinuous with respect to $y$ (for each $x$ , the kernel will be discontinuous at $y = x$ ).	Method must be robust with respect to discontinuities at each mesh point.

Table 4.1: Biological attributes and their mathematical manifestations and numerical considerations.

	Slow-growing	Sharp fecundity	Abrupt surv. prob.	Non shrinking
Speed	MP, GL( $k$ ), AGL( $k$ )	MP, AGL( $k$ )	MP, AGL( $k$ )	MP (large $N$ )
Accuracy	GL( $k$ ), AGL( $k$ )	AGL( $k$ )	AGL( $k$ )	MP (large $N$ )
Small matrix	INT/GENB2BGL( $k$ )	INT/GENB2BGL( $k$ )	INT/GENB2BGL( $k$ )	–

Table 4.2: Quadrature method recommendation given biological attribute and desired numerical property.

Finally, to determine a suitable mesh size  $N$  and number of quadrature points  $k$  before beginning a large MCMC simulation, I recommend computing a reference solution with a large mesh for a few representative sets of parameters. Subsequently, one could then generate plots similar to those presented here to inform their choice of numerical discretization.

## 4.6 Acknowledgements

This work was supported by NSERC, the MixedWood Management Association, MITACS, and through the Queen Elizabeth II Scholarship from the University of Alberta. The authors would like to thank Stephen Ellner of Cornell University for his insightful comments and suggestions which helped guide this work. I also thank Mark Lewis, Ken Stadt, and Phil Comeau from the University of Alberta for their support. Finally, I thank Jim Clark and the entire Clark Lab at Duke University for thought-provoking discussions related to this work. In particular, Jim Clark was gracious enough to share his techniques for integrating kernels of the form (4.2).

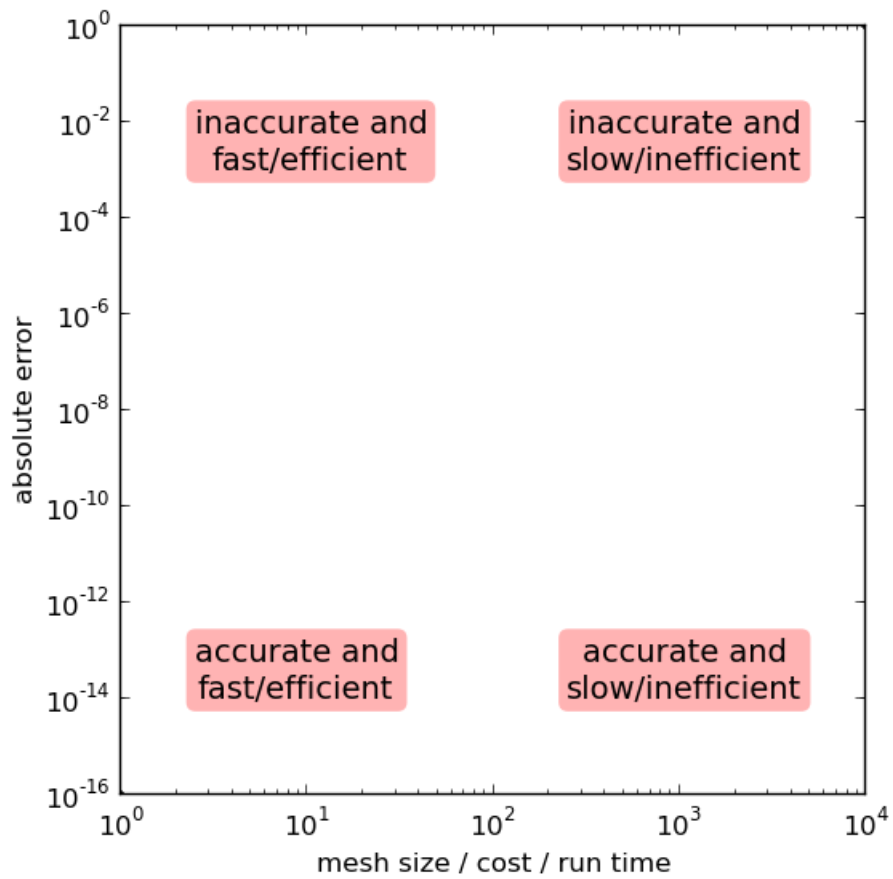


Figure 4.1: Typical error vs mesh size / computational cost / runtime plot and how to interpret them.

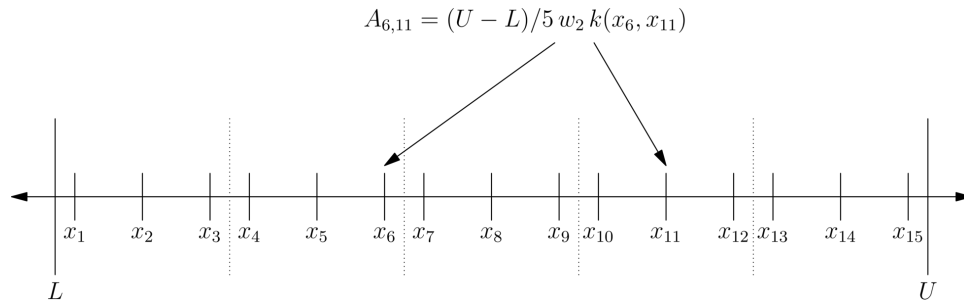


Figure 4.2: Diagram of the  $GL(k = 3)$  discretization method with  $N = 5$  sub-intervals on the interval  $[L, U]$ . The dotted vertical lines depict the edges of the  $N$  sub-intervals. The solid vertical ticks depict the locations of the quadrature points within each sub-interval (which in this case are the Gaussian quadrature points for  $k = 3$ ). Increasing  $k$  would result in more quadrature points within each sub-interval, while increasing  $N$  would result in more sub-intervals across the domain. The entries of the projection matrix  $A$  are determined by evaluating the kernel at the quadrature points and weighting them appropriately (eg, here  $w_2$  is the second quadrature weight of the standard three-point Gaussian quadrature scheme).

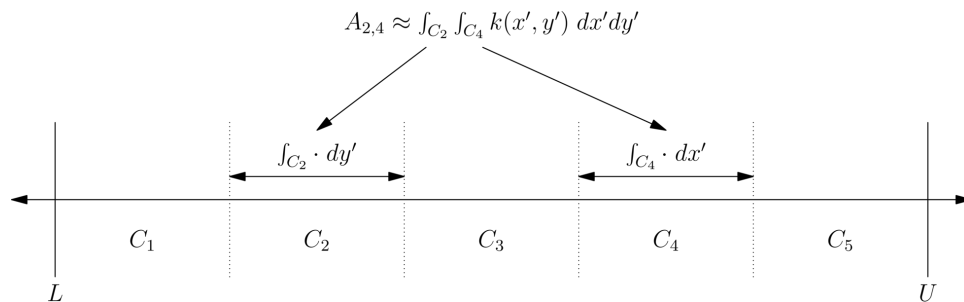


Figure 4.3: Diagram of bin-to-bin discretization methods with  $N = 5$  cells on the interval  $[L, U]$ . The dotted vertical lines depict the edges of the  $N$  bins/cells. Each particular bin-to-bin method (MP, INTB2B, GENB2B, Zuidema) has a particular way of approximating the double-integral to obtain the entries of the projection matrix  $A$ .

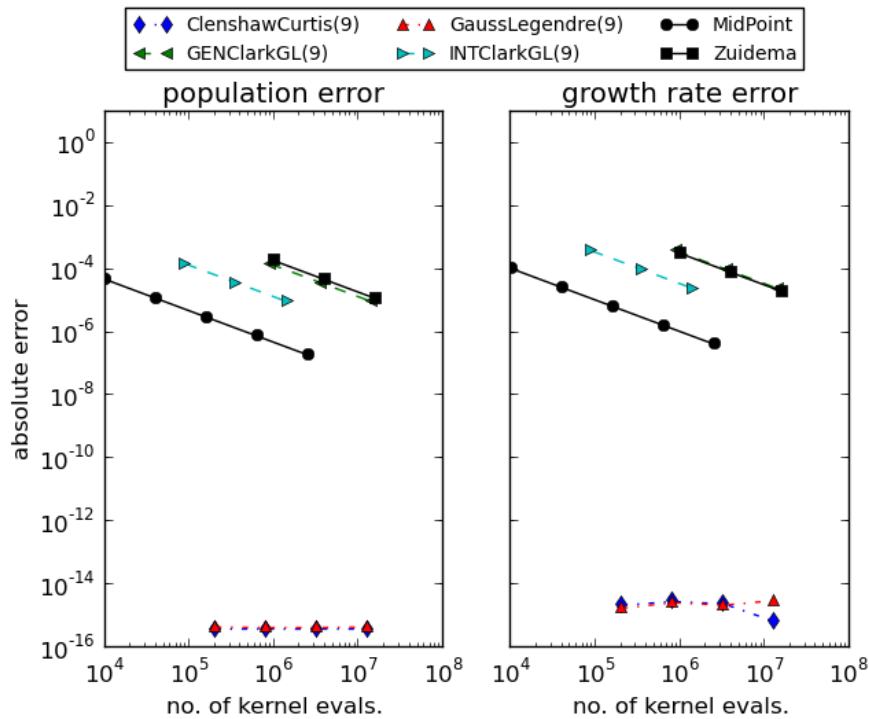


Figure 4.4: Error of the total population and growth rate after 5 years vs computational cost for various integration methods and the Exact kernel. Note that the cell based methods (GENB2BGL(9), INTB2BGL(9), MidPoint and Zuidema) exhibit first order convergence and are much less accurate than the point-based methods, which are exceptionally accurate here. For a given level of accuracy, the MidPoint method is the fastest cell-based method (even if a larger mesh is required).

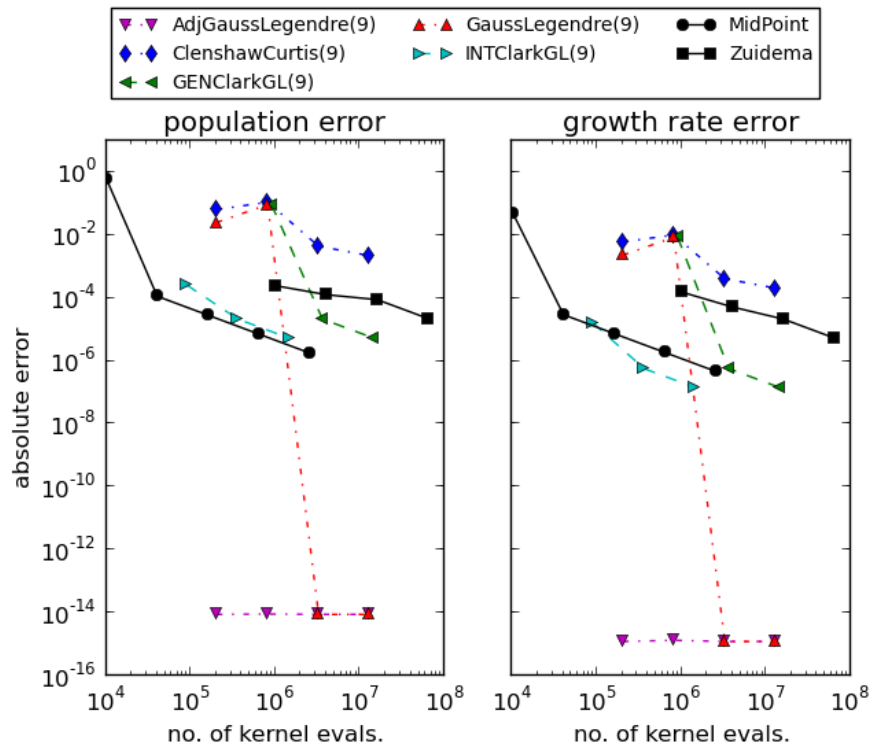


Figure 4.5: Error of the total population and growth rate after 5 years vs computational cost for various integration methods and the SHRUB kernel. Note that in all cases, except for the Adjusted Gauss Legendre method, each method performs poorly until a sufficiently large mesh is used due to the discontinuity in the fecundity term.

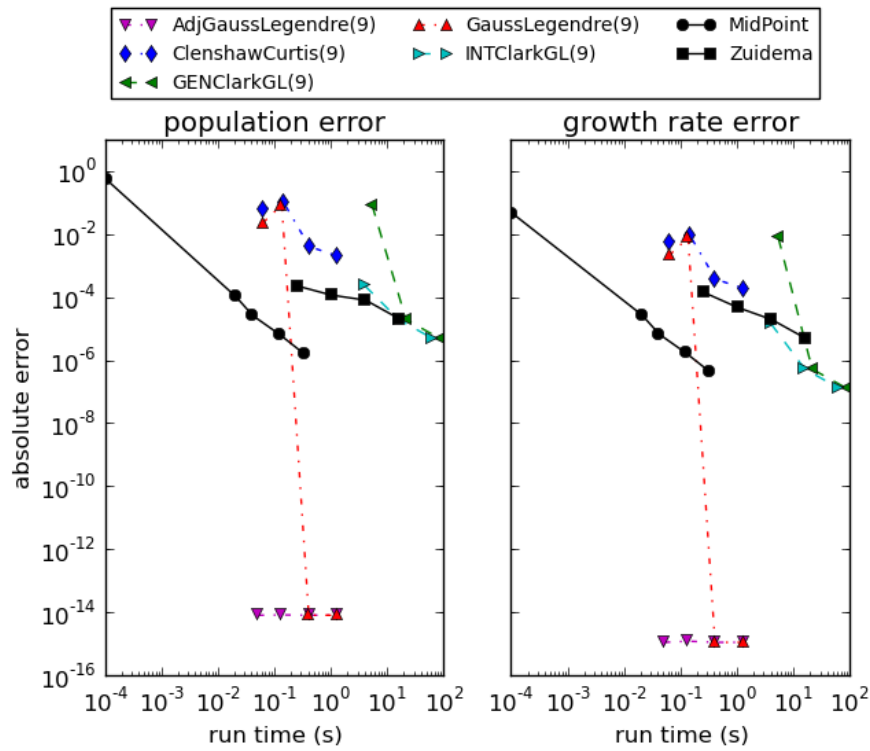


Figure 4.6: Error of the total population and growth rate after 5 years vs run time for various integration methods and the SHRUB kernel. Note that although the point based methods are easily vectorized and often exhibit faster run times than most of the cell based methods even though their computational complexity is similar.

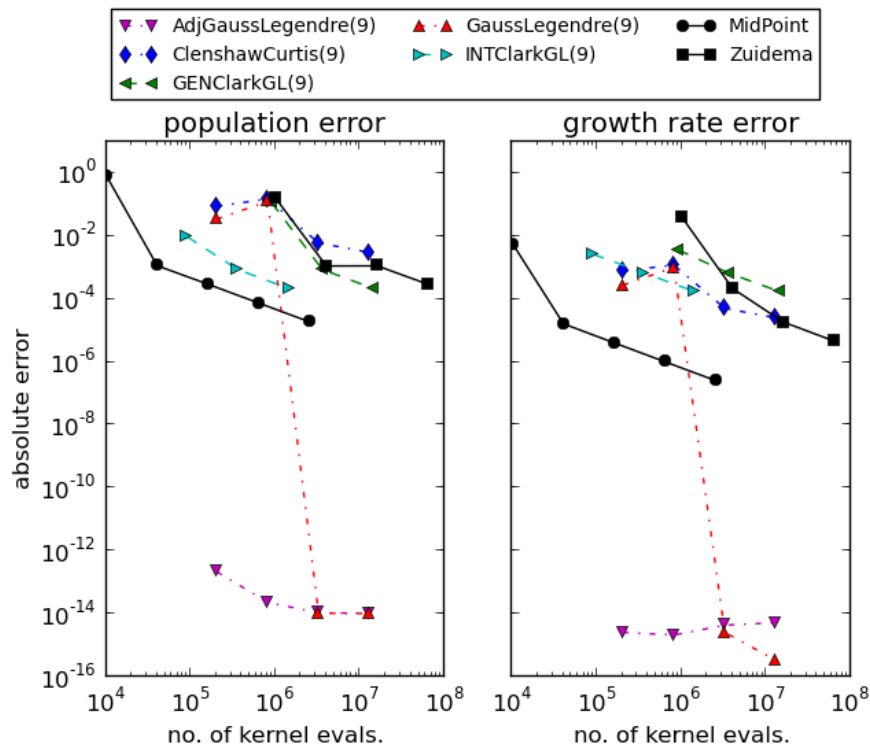


Figure 4.7: Error of the total population and growth rate after 5 years vs computational cost for various integration methods and the SHRUB kernel with modified growth parameters. Note that even after modifying the growth parameters to simulate a slow-growing species, the midpoint method still performs quite well once the discontinuity is resolved, and that the Adjust Gauss Legendre method is still extremely accurate.

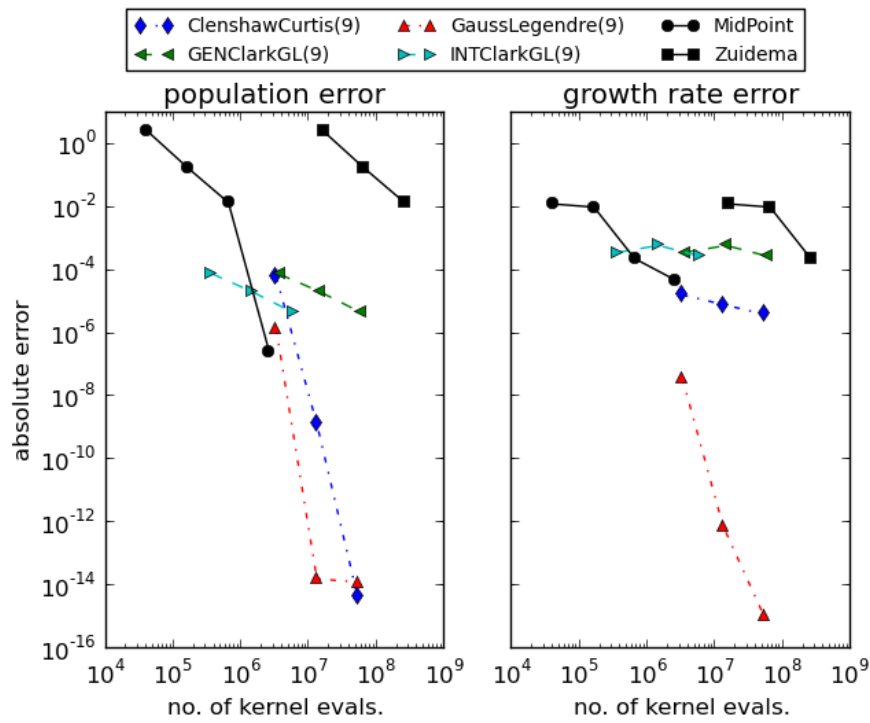


Figure 4.8: Error of the total population and growth rate after 5 years vs computational cost for various integration methods and the TREE kernel. Note that the bin-to-bin methods (except the Zuidema method) perform well for small mesh sizes as they are able to resolve slow growth more effectively than the MidPoint method.

```
# Python code
from scipy.sparse.linalg.eigen import eigs
evals = eigs(A, k=1, return_eigenvectors=False)
growth_rate = evals[0]

# R code
library(igraph)
matmul <- function(x, A) { A %*% x }
result = arpack(matmul, extra=A, options=c(n=nrow(A), nev=1))
growth.rate = result$values[1]
```

Figure 4.9: Code snippets for computing only the dominant eigen-value of a matrix  $A$  using ARPACK.

# Bibliography

- Briggs, J., Dabbs, K., Holm, M., Lubben, J., Rebarber, R., et al. Structured population dynamics. *Mathematics Magazine*, 83(4):243–257, 2010.
- Chien, P., Zuidema, P., and Nghia, N. Conservation prospects for threatened vietnamese tree species: results from a demographic study. *Population Ecology*, 50(2):227–237, 2008.
- Childs, D., Rees, M., Rose, K., Grubb, P., and Ellner, S. Evolution of complex flowering strategies: an age- and size-structured integral projection model. *Proceedings of the Royal Society of London. Series B: Biological Sciences*, 270(1526):1829–1838, 2003.
- Childs, D., Rees, M., Rose, K., Grubb, P., and Ellner, S. Evolution of size-dependent flowering in a variable environment: construction and analysis of a stochastic integral projection model. *Proceedings of the Royal Society of London. Series B: Biological Sciences*, 271(1537):425–434, 2004.
- Dalgleish, H., Moffet, C., Koons, D., Hooten, M., and Alder, P. The influence of historical climate on the population dynamics of three dominant sagebrush steppe plants. *Ecology*, 92(1):75–85, 2011.
- Easterling, M. *The integral projection model: theory, analysis and application*. Ph.D. thesis, North Carolina State University., 1998.
- Easterling, M., Ellner, S., and Dixon, P. Size-specific sensitivity: applying a new structured population model. *Ecology*, 81(3):694–708, 2000.
- Ellner, S. and Rees, M. Integral projection models for species with complex demography. *The American Naturalist*, 167(3):410–428, 2006.
- Lehoucq, R., Sorensen, D., and Yang, C. *ARPACK users' guide: solution of large-scale eigenvalue problems with implicitly restarted Arnoldi methods*, vol. 6. SIAM, 1998.
- Lubben, J., Boeckner, D., Rebarber, R., Townley, S., and Tenhumberg, B. Parameterizing the growth-decline boundary for uncertain population projection models. *Theoretical population biology*, 75(2):85–97, 2009.
- Metcalf, C., McMahon, S., Salguero-Gómez, R., and Jongejans, E. IPMpack: an R package for Integral Projection Models. *Methods in Ecology and Evolution*, p. in press, 2012.

- Rebarber, R., Tenhumberg, B., and Townley, S. Global asymptotic stability of density dependent integral population projection models. *Theoretical Population Biology*, 2011.
- Rees, M. and Ellner, S. Integral projection models for populations in temporally varying environments. *Ecological Monographs*, 79(4):575–594, 2009.
- Rees, M. and Rose, K. Evolution of flowering strategies in *Oenothera glazioviana*: an integral projection model approach. *Proceedings of the Royal Society of London. Series B: Biological Sciences*, 269(1499):1509–1515, 2002.
- Rose, K., Louda, S., and Rees, M. Demographic and evolutionary impacts of native and invasive insect herbivores on *Cirsium canescens*. *Ecology*, 86(2):453–465, 2005.
- Tenhumberg, B., Tyre, A., and Rebarber, R. Model complexity affects transient population dynamics following a dispersal event: a case study with pea aphids. *Ecology*, 90(7):1878–1890, 2009.
- Zuidema, P., Jongejans, E., Chien, P., During, H., and Schieving, F. Integral projection models for trees: a new parameterization method and a validation of model output. *Journal of Ecology*, 98(2):345–355, 2010.

## Chapter 5

# A tree-ring based reconstruction of early summer precipitation in southwestern Virginia (1750-1981)<sup>1</sup>

### 5.1 Introduction

One of the most important centers of forest diversity in North America is the Southern Appalachian region. This region has supported continuous forest communities longer than any other area on the continent and hosts many rare, endemic species (North Carolina Natural Heritage Program (NCNHP), 1999). Additionally, it harbors many disjunct species populations, all of which make it one of the most important centers of forest diversity on the continent. The southern Appalachians also provide ecosystem services such as carbon storage, watershed and water quality protection, and serve as a timber source (Zipper et al., 2011). In order to protect these valuable resources, it is crucial that we thoroughly understand the past climate of this area and how it has influenced the many ecosystems within the region. A sound understanding of the past relationship between climate and southern Appalachian ecosystems will enable scientists and landowners to better manage the natural resources in the future.

---

<sup>1</sup>A modified version of the chapter titled “A tree-ring based reconstruction of early summer precipitation in southwestern Virginia (1750-1981)” is in preparation for submission to *Climate Research*.

Global circulation models project an increase in average global surface temperatures of  $1.0 - 3.5^\circ$  by the end of this century due to continued increases in greenhouse-gas emissions (Pachauri and Reisinger, 2007; Kattenberg et al., 1996). However the influence of increased radiative forcing on precipitation regimes is not well understood, and this is particularly the case for the southeastern United States (US). The 24 models used to make predictions about climate change in the Intergovernmental Panel on Climate Change Fourth Assessment Report were not in consensus with respect to drought frequency (Pachauri and Reisinger, 2007; Seager et al., 2009). Uncertainty in climate projections makes it difficult to predict water and power usage. The ability to do so is crucial because the southeastern US has experienced substantial increases in population and energy consumption, over the last decade (Seager et al., 2009; Sobolowski and Pavelsky, 2012). It is important that the public and planners in the Southeast have access to information regarding climate change projections and mitigation. Through the use of tree-ring based climate reconstructions, scientists may better understand past precipitation regimes at decadal- to centennial time-scales in order to better project future precipitation patterns in a changing climate.

In order to reduce uncertainty in climate model projections and to extend meteorological records further back in time, tree-ring data are commonly used as regional proxies, particularly in regions where drought (e.g. the American Southwest, (Cook et al., 2004)) or summer temperature (e.g. the European Alps, (Büntgen et al., 2007)) is the limiting tree growth factor. However, tree-ring data have also successfully been used for climate reconstructions in the eastern US (LeBlanc, 1993; Stahle and Cleveland, 1993; Cook et al., 1999). Traditionally it has been understood that trees in a closed-canopy forest are not limited by climate to the same extent as trees growing on the forest border (Fritts, 1976). Within a dense forest, stand dynamics play an important role in shaping the forest structure through their influence on radial tree growth and tree survival. As these interactions between individuals increase in strength, the climatic influence on tree growth becomes less dominant.

Trees growing in temperate regions characterized by high humidity such as those in the Southeast US are typically thought to be less sensitive to climate than trees in semiarid regions (Phipps, 1982). This belief supports the idea that the degree to which an environmental factor is limiting affects the amount of variability in that factor that is seen in tree-ring time series. Although water access may not be limiting in southeastern US sites, a large sample size may compensate to help identify the common climate signals despite site and individual variability. In

regions that are subject to site heterogeneity, where significant climatic variance cannot be identified for a standard sample size, principal component analysis can be an effective means to overcome the lack of strength of climate signal (Peters et al., 1981; Anchukaitis et al., 2006; Jacoby and D'Arrigo, 1989). Through the application of principal component analysis (PCA), tree-ring data collected from a network of regional sites can be combined to reduce-site level noise through the identification of a common climate signal across sites.

Despite the challenges of finding a climate signal in tree-ring time series in southeastern US forests, numerous studies have identified climate-growth correlations (Pan et al., 1997; Speer et al., 2009; Rubino and McCarthy, 2000). For example, Pan et al. Pan et al. (1997) showed that after tree-ring standardization, both annual ring-width and basal area increments of four deciduous species in Virginia were positively correlated with precipitation from both the prior summer, autumn, and current summer. They also report negative correlations with air temperature of the current growing season. Speer et al. Speer et al. (2009) found similar correlations between precipitation and temperature and annual tree growth for oak chronologies from closed canopy forest in the Southern Appalachian Mountains.

In this study, we determined the presence of a significant relationship between chestnut oak growth-series in the eastern US and early summer precipitation and ascertained the viability of a climatic reconstruction based on the chestnut oak growth series as proxy data. The annual growth proxy data was subsequently used to reconstruct early summer precipitation using Bayesian methods. Finally, I evaluated the reliability of the reconstruction by comparing it to other verified regional reconstructions.

## 5.2 Materials and Methods

### 5.2.1 Tree ring data

The study site was an Upland Oak-Pine forest located on the North facing slope of Brush Mountain in South-West Virginia (37° 22.2' N, 80° 14.8' W), with a site elevation of 558 m (Figure 5.1). This region is classified as either humid continental or mountain temperate, and characterized by warm, humid summers and winters that are predominantly cool with intermittent warm spells. The mean annual precipitation 1901-2010 at Blacksburg weather station was 1073 mm and the mean annual temperature was 10.9°C.

The study site supported older chestnut oak trees amongst a canopy of many species, including scarlet oak (*Quercus coccinea*), northern red oak (*Quercus rubra*), red maple (*Acer rubrum*), Virginia pine (*Pinus virginiana*), pitch pine (*Pinus pungens*), and eastern white pine (*Pinus strobus*). Site access was adjacent to the Appalachian trail, but the site was selected to minimize human interference. The steepness of this slope suggested that climate may be a limiting growth factor, although the closed canopy and stand density suggested that stand dynamics may also play a significant role in shaping the forest structure.

Two cores were collected from each of the 56 chestnut oak trees sampled. Samples were dried, mounted, and sanded according to standard guidelines (Stokes and Smiley, 1996). Crossdating was performed using reflected light microscopy and the list method, which facilitates the identification of marker years that signify relatively favorable or unfavorable growth years in a stand (Yamaguchi, 1991). All samples were measured using a LINTAB measurement stage with 0.01mm precision, and visual crossdating was checked using COFECHA (Holmes, 1983). COFECHA uses segmented time series correlation techniques that make use of common variability present in samples from a given site to identify potential crossdating errors (Grissino-Mayer, 2001). COFECHA also computes inter-series correlation, which is a measure of stand-level signal, and mean sensitivity, which measures the year-to-year variability in a time series. Based on inter-series correlation coefficients, a total of 76 tree-ring series from 53 trees contained enough common growth signal to be used for further analysis.

Non-climatic age-dependent and stand-dynamics related trends were removed from the individual tree-ring series using smoothing splines with a 50 % cutoff at 50 years (ARSTAN software, (Cook and Peters, 1997)). This method allowed us the flexibility to remove the episodic-like interaction effects from the time series, while retaining the high-frequency climatic variability. Note that as with any filtering technique, inevitably some portion of the climatic signal will be lost through the removal of these non-climatic trends (Cook and Peters, 1981). I here assume that the loss of climatic signal was negligible, and comparison of the detrended time series with climatic data ultimately determined if the strength of the remaining signal was sufficient to perform further analyses. Furthermore, serial correlation is common in tree-ring time series, typically due to the availability of stored water or photosynthates. This autocorrelation effectively reduces the number of independent observations, and therefore must be taken into account through either reduction of the effective sample size to ensure that observation independence, or through autoregressive and/or moving average (ARMA) modeling (Monserud,

1986; Cook, 1987). All series were checked for autocorrelation to determine if prewhitening via ARMA modeling was necessary, and applied when deemed necessary. The Brush Mountain site chronology was then developed based on the individually detrended tree-ring width time series, and will hereafter be referred to as BM.

I also computed the expressed population signal (EPS) to measure the common variability in the chronology at an annual resolution. EPS depends on both signal coherence and annual sample-depth. When EPS values which fall below a predetermined cutoff (0.85), the chronology is no longer dominated by a coherent signal, and is therefore deemed less than ideal for climatic reconstructions.

### 5.2.2 Principal component analysis

It is often the case that data from a single closed-canopy site does not show a strong relationship with climate. In this case, data from additional sites may provide some insight into the regional climate signal through the use of principal component analysis (PCA). PCA can help identify common patterns in climate-modulated tree growth between sites and reduce the dimensionality of the data. A total of 8 *Quercus prinus* chronologies from the eastern US obtained from the International Tree-Ring Database (ITRDB) were considered for inclusion in a PCA analysis. Chronology reliability for each of the 8 chronologies was assessed based on the mean sensitivity, inter-series correlation, the EPS, and the first-order autocorrelation. For each considered site, raw ring-width time series were detrended using a smoothing spline with 50% cutoff at 50 years, and subsequently used to build chronologies for each of the respective sites. These chronologies were then considered for use in our PCA with the goal of developing a stronger climatic signal. Only chronologies which extended back to at least 1845 and which were significantly correlated with precipitation anomalies were retained for further analysis. A set of 4 nearby tree-ring chronologies (3 *Quercus prinus* and 1 *Quercus alba*) met these conditions (Table 5.1, Fig. 5.2), and were combined with the BM chronology in a nested singular value decomposition PCA (Wold et al., 1987). The first PCA (5 contributing chronologies) was performed on the 1845-1981 time interval, and the second PCA (4 contributing chronologies) on the 1750-1981 interval. The PCA components with eigenvalues larger than one were retained for further analysis and the components explaining the largest amount of common variance in the tree-ring chronologies were included in a climate correlation analysis.

### 5.2.3 Climate data

Monthly precipitation, mean temperature, as well as mean Palmer Drought Severity Index (PDSI, Palmer 1965) were computed from daily measurements at the Blacksburg climate station (37° 12' N, 80° 24' W; elevation 634 m; 1901-2006). PDSI is an index of drought severity that is based on a simplified water balance equation (Wells et al., 2004). This method requires that for each month of the year, soil moisture and water potential values are computed and then used to compute an excess or shortage of precipitation when compared to the precipitation the is deemed climatically appropriate for existing conditions. When this result is multiplied with something called a climatic characteristic which allows the measure to be standardized across space, the result is the moisture index.

Precipitation, temperature and PDSI were all used in a correlation function analysis with the PCA time series. Pearson's correlation coefficients were calculated for all months starting in April of the year previous to the growing season through current December, as well as for the seasons (Apr-June, July-Sep, Oct-Dec, Jan-Mar) and annual means.

The Blacksburg station monthly/seasonal climate variable with the strongest correlation with the BM chronology was then used as guidance for a spatial correlation analysis using a gridded ( $0.5^\circ \times 0.5^\circ$ ) monthly climate data set for the period 1901-2006 (Mitchell and Jones, 2005). The grid point with the strongest correlation coefficient was then used as a target reconstruction.

### 5.2.4 Reconstruction methods

To perform the reconstruction of computed climate variable anomalies, I use Bayesian linear regression with the selected principal components as proxies. I assume that the precipitation anomalies ( $y$ ) satisfy  $y_t \sim Normal(\mu_t, \sigma^2)$ , where  $\mu_t = \beta_0 + \beta_1 x_t$  where  $x_t$  is the first principal component value at year  $t$ . In a Bayesian regression formulation I make the assumption that the true parameter values  $\beta_0$ ,  $\beta_1$ , and  $\sigma^2$  are distributed according to a probability distribution function (PDF), and that these distributions express the degree of belief about where the true values lies. In a Bayesian framework, the PDFs are approximated by the posterior distribution, which is proportional to the likelihood multiplied by a prior. Posterior distributions can either be sampled directly if a closed-form solution exists, or can be indirectly sampled using a Markov Chain Monte Carlo (MCMC) algorithm. Due to the absence of prior information, parameters

are assigned uninformative priors which take the form  $\beta_i \sim \text{Normal}(\vec{0}, 1000)$  and  $\sigma^2 \sim \text{Uniform}(0, 100)$ . These uninformative priors indicate that I assign approximately equal weight to all possible parameters values because there was no reason to assume that any specific value is more likely than another. Model parameter distributions were determined using an MCMC algorithm with a Metropolis step method, and was run for 100,000 iterations with a burn-in of 50,000 which I found was more than sufficient to ensure convergence. For the sense of practicality, parameter estimates were thinned so that only every tenth estimate was saved to memory. The output from the MCMC algorithm generates a chain of parameter values sampled from the posterior distribution, and computing the 0.025, 0.5 and 0.975 quantiles of these chains allows us to define an upper and lower bound for a 95% credible interval as well as the median for that parameter (which allows us to say that the true parameter has a 0.95 probability of falling within that credible interval). For each set of sampled parameters, I generate predicted precipitation values for the years 1745 though 1981 according our model using our growth proxy principal component values ( $x_t$ ), and similarly define a 95% predictive interval using quantiles. This method allows us to estimate the uncertainty associated with our predictions based on our model.

### 5.2.5 Model calibration and verification

To assess the accuracy of the modeled precipitation anomalies, I split the data into two periods: 1901-1940, and 1941-1981. Both the 1901-1940 and 1941-1981 periods of data were used in turn as the calibration period, to determine if the accuracy of the reconstruction was sufficient to warrant further analysis. Data from the period not used for calibration served as verification data, and for both calibration/verification pairs I computed the mean squared error (MSE), reduction of error (RE) (Fritts, 1976), coefficient of efficiency (CE) (Cook et al., 1994), and the squared correlation ( $r^2$ ) (See the National Research Council report Surface Temperature Reconstructions for the Last 2,000 Years (Committee on Surface Temperature Reconstructions for the Last 2, 2006) for further details on assessing reconstruction skill). Lastly, I computed the sign test or Gleichläufigkeit (GLK) score which measures the similarity of the relative annual change in value between two time series (Speer, 2010; Schweingruber et al., 1988).

### 5.2.6 Reconstruction assessment

To identify any dominant cyclical behavior in the reconstruction, I use a periodogram to calculate the significance of different frequencies in our time series. In the periodogram, peaks in the estimated spectrum are tested to determine if they are different from the underlying white-noise spectrum. Spectrum values are averaged with 2 frequencies per bin to simplify interpretation.

The precipitation reconstruction was compared to other regional precipitation and drought reconstructions as external validation. For the southeastern US I identified a total of six published reconstructions that were used for comparison (Table 5.6). Out of these six, two were drought reconstructions. The first was obtained from the North American Drought Atlas (Cook et al., 1999) which is a gridded reconstruction of PDSI values for June through August (NADA), while the second is a July PDSI reconstruction (JT) for Virginia and North Carolinian coastal regions developed by Stahle and Cleaveland (Stahle et al., 1998). The remaining four reconstructions identified for comparison were precipitation reconstructions. The first set were developed by Stahle and Cleaveland for the North Carolina (NC), South Carolina (SC), and Georgia (GA) regions for the months of April through June for NC and March through June for SC and GA (Stahle and Cleaveland, 1992). The second precipitation reconstruction for early summer anomalies (MP) was developed by Druckenbrod (Druckenbrod et al., 2003).

## 5.3 Results

The BM chronology covered the years 1764-2010, had an interseries correlation of 0.556 and a mean sensitivity of 0.208 (Table 5.1). The EPS was greater than the 0.85 cutoff for the years 1845-1981. The highest correlation between the BM chronology and the meteorological weather data was with average May-June precipitation (mjPR) or average June-July PDSI (jjPDSI). To increase the signal to noise ratio in our tree-ring record and better identify the regional precipitation effects, I included four oak chronologies from nearby locations in our analysis. These four chronologies met the requirements for inclusion in the proceeding analysis: they were significantly correlated with mjPR or jjPDSI and covered at least the same time period as the BM chronology (1845 - 1981) as shown in table 5.1). The locations and time series of the suitable chronologies, hereafter referred to by abbreviations of their locations as LH, WD, CC, and OC, are shown in figures 5.1

and 5.2. A nested PCA was performed using these identified chronologies in addition to BM.

The first PCA was performed on all five chronologies for the overlapping time period 1845-1981 determined by the BM EPS values, resulting in a first principal component which explained 57.0% of the common variance, and a second component which explained 15.2%. The scores plot (Fig. 5.3) illustrates the relationship between the five chronologies with respect to the first two principal components: all chronologies have a positive score along PC1 while only BM, WD, and LH have a positive score along PC2. The second PCA was performed on the subset of four chronologies which extended back to the year 1750 (LH, WD, CC, OC), and in this case the first principal component explained 48.6%, while the second component explained 29.1%. The relationship between these four chronologies is shown in (Fig. 5.3). All chronologies have a positive score along PC1 and a negative score along PC2. Overlapping portions of the first principal components that resulted from both decompositions were compared via correlation to confirm that both of these were in fact accounting for the same independent axis ( $r = 0.93$ ,  $p < 0.01$ ). First principal components were merged at the year 1845 (PCA2: 1750-1844, PCA1: 1845-1981) to form a single proxy record extending from 1750 to 1981. The sample depth for each year for the resulting principal component growth proxy is shown in Figure 5.4.

The BM chronology had multiple significant correlations with monthly precipitation and PDSI values, from May of the previous year to December of the current year (Fig. 5.5). I found significant positive correlations between BM and precipitation of previous year June and current year May and June. The strongest correlation was found with average precipitation of the months May and June ( $r = 0.50$ ,  $p < 0.01$ ). Correlations with PDSI were significantly positive, particularly during the May through August growing season, with the strongest correlation being with average June and July PDSI ( $r = 0.55$ ,  $p < 0.01$ ). In general, BM correlations with temperature were not significant, except for the previous July, which was negative ( $r = -0.19$ ,  $p < 0.05$ ). Both average May-June precipitation (mjPR) and average June-July PDSI (jjPDSI) were considered as candidate climatic targets for reconstruction. The BM chronology was strongly correlated with both mjPR and jjPDSI, but an assessment of the reconstruction verification statistics (results not shown) suggested that the accuracy of a reconstruction based on this proxy data may not be sufficient.

When comparing the merged PCA time-series with monthly climate variables, I generally find stronger correlations than for BM (Table 5.4, Fig. 5.5). This is

particularly true for average precipitation for the months May and June ( $r = 0.61$ ,  $p < 0.01$ ) and average PDSI for the months June and July ( $r = 0.63$ ,  $p < 0.01$ ).

In the next step, I tested mjPR and jjPDSI as potential reconstruction targets in a split calibration/verification scheme ((Fritts et al., 1990); Table 5.3). Overall calibration and verification  $R^2$  statistics (0.56 - 0.64) and GLK values (0.55-0.79) were strong. However, when the earlier period (1901-1941) was used as the calibration period, the RE and CE statistics for mjPR were low but greater than 0; these statistics were higher for jjPDSI for the same period. RE and CE were also higher for mjPR using the later period (1942-1981), whereas values for jjPDSI were negative indicating a poor fit of the reconstruction model. RE and CE are key statistics to determine the skill of a reconstruction, and our decision to reconstruct early summer (May-June) precipitation rather than summer PDSI was based on these values. Our final mjPR reconstruction was calibrated against the entire 1901-1981 interval.

Posterior parameter distributions for the Bayesian linear regression model were determined via the adaptive Markov chain Monte Carlo (MCMC) algorithm. Parameter means and credible intervals are shown in Table 5.4. The adaptive MCMC algorithm updated proposal distributions accordingly when acceptance rates fell outside ideal range of 0.2-0.5, which ensured that there was good mixing. Each iteration of the algorithm generated a set of parameters from the posterior, and predicted precipitation values were computed for each set from the resulting parameter chains for all years. Predicted precipitation quantiles were used to obtain a 95% credible interval for average May-June precipitation for each year. Annual predicted precipitation means were also computed. The resulting precipitation reconstruction covers the years from 1750 through 1981, which allows us to extend the instrumental mjPR record back 150 years. Figure 5.8 shows a plot of the reconstruction and the associated uncertainty as described by the 95 % quantiles for the 1750-1981 period as well as the available averaged May-June precipitation data. Despite our encouraging reconstruction statistics and high correlation between the proxy and climate variable, our model fit generated wide credible intervals which showed the uncertainty associated with the reconstruction.

The periodogram shows peaks with significant power at approximately 11, 17, and 24 years, as shown in Figure 5.9. These peaks indicate that the reconstruction contains strong sinusoidal components with periods corresponding to the observed peaks.

The mjPR reconstruction correlated significantly positively with four other reconstructions, namely JT (July PDSI reconstruction), NADA (average summer

PDSI), NC (early summer precipitation), and MP (early summer precipitation) (Table 5.6). Reconstructions were compared for the overlapping period 1750-1981, except in the case of MP which only covered the period 1784-1966. The strongest correlation was found between our mjPR reconstruction and the NADA drought reconstruction ( $r = 0.59$ ,  $p < 0.01$ ), followed by the MP early summer precipitation anomalies reconstruction ( $r = 0.38$ ,  $p < 0.01$ ), and the NC averaged April-May-June precipitation reconstruction ( $r = 0.23$ ,  $p < 0.01$ ). Figure 5.10 shows the annual and decadal variability in the mjPR and six compared moisture reconstructions for the entire period covered by the longest reconstruction, while Figure 5.11 shows the same variability but only for the years which overlap with 1750-1981 time period covered by the mjPR reconstruction.

## 5.4 Discussion

In this study, I investigated the relationship between climate and annual radial growth of *Quercus prinus* growing at a closed canopy site in the southeastern US. After removing the portion of the signal attributed to stand dynamics and intrinsic age trends, I found that the BM chronology was most strongly positively influenced by early summer (May through July) moisture from the year of ring formation. Similar climate-growth relationships have been identified by previous oak studies in the southeastern US (Speer et al., 2009; Li, 2011) and can be explained by ecophysiological mechanisms. Radial growth of oak species typically starts in April or May after leaf-out, and even in wetter years is 90% complete by the end of July (Robertson, 1992). In earlier months of the growing season, carbon is allocated predominantly to radial thickening, while later in the season the focus of this allocation is shifted to carbohydrate storage (Zweifel et al., 2006). Under severe moisture stress, oak carbon allocation is shifted from shoot to root, thereby increasing the root/shoot ratio (Dickson and Tomlinson, 1996). *Quercus prinus* is considered to be more tolerant to drought stress than other oak species and exhibits several morphological adaptations in order to better cope with moisture stress events (Dickson and Tomlinson, 1996), but I found that its radial growth was strongly influenced by moisture availability. This suggests that in years with inadequate moisture, radial growth is not a priority, and carbon allocation is likely focused on maintenance or root development. The identifiable moisture-response in the detrended BM chronology demonstrates that oaks in a closed-canopy forest can indeed be used to generate paleoclimatic data, although care must be taken when removing the non-climatic portion of the signal. The assumption that the low frequency component of a tree-ring time series is solely attributed to age and

stand dynamics trends may not be valid over long-time, and some climatic signal will inevitably be lost during detrending. Without the ability to measure age and stand dynamic effects independently of climatic effects, the effects of filtering via various detrending methods are difficult to evaluate. The development of a biologically motivated trend removal algorithm may improve current practices in dendroclimatology. In addition, care must be taken in closed canopy forests when attempting to use growth series as proxy records as younger stands in the stem-exclusion phase may be dominated by the effects of competition (Oliver, 1980).

To isolate and strengthen the moisture-growth relationship of the BM chronology I performed a nested principal component analysis on regional *Quercus* chronologies that also showed significant correlations with early summer moisture. Five chronologies were included in the principal component analysis which increased the strength of the BM climate signal. The strong relationship of the first principal component (PC1) with early summer moisture is depicted in Figure 5.6. The spatial pattern of this relationship indicates that the tree-growth proxy PC1 is most influenced by moisture in the Great Appalachian Valley. Mountains play an important role in the hydrological cycle for several reasons, one of which being that they are the points of origin of most rivers (Beniston et al., 1997). Increases in precipitation in mountainous regions leads to increased stream flow volumes and surface runoff, which in turn increases soil moisture in the Appalachian watershed.

The average May-June precipitation reconstruction (mjPR) showed anomalies consistent with the instrumental precipitation record for 1901-1981, as shown in Figures 5.13 and 5.14. In particular, the reconstruction correctly identifies the severe nation-wide dust bowl-era drought in the 1930s, the 1954 drought, as well as the dry spell in the 1970s. Other notable years of low early summer precipitation seen in both the instrumental record as well as the reconstruction are 1911, 1914, and 1925. I also note the agreement of extreme precipitation in the years 1928, 1942, and 1950, where documented flooding occurred in the southeastern US. All of the late-spring/early-summer anomalies have been observed across the southeastern US in instrumental records, except for the dry spell in the 1970s (Edwards, 1997). In years prior to the instrumental record, the mjPR reconstruction identifies several dry periods, as shown in Table 5.7, most of which have been observed in other moisture reconstructions for the US. I also note that as I extend the reconstruction further back in time, reliability inevitably decreases as a result of the decrease in sample size.

Our reconstruction shows similar variability when compared to other reconstructions of moisture variability in the southeastern US (Table 5.5). The strongest

similarity was found with the NADA PDSI Cook reconstruction. A comparison of the relationship between these two moisture reconstructions identified two time periods in which reconstruction values were not consistent, as shown in figure 5.12 where the reconstructions are standardized prior to plotting to highlight similarities and discrepancies.

The first anomaly occurred in 1774, which our reconstruction identified as an early summer drought. Although this year showed low moisture relative to other years in several other regional reconstructions, the suggestion of drought was not as defined. A closer examination of the chronologies on which the principal component analysis was performed revealed that this drastic departure from the mean MJ precipitation signal was propagated through the PCA by the Craig Creek chronology. Since this year was not identified as a local minimum growth year in other chronologies I assume that this drastic reduction in growth at the Craig Creek site is site-specific, and is attributed to local disturbance with a localized effect on growth.

The second anomaly manifested itself during the 1853 through 1866 period, where the correlation between both the NADA reconstruction and the mjPR reconstruction becomes no longer significant as shown by a 31 year windowed correlation (see figure 5.15). With the goal of better understanding this anomaly, I return to the five chronologies. A plot of a 31 year windowed correlation between each of the regional oak chronologies and the NADA PDSI reconstruction shows that all five chronologies show this same pattern of reduced correlation with the NADA PDSI reconstruction during these years, as shown in figure 5.16. These years correspond with the persistent drought near 1860, which also coincides with a La Nina event which occurred from 1855 - 1863. Although La Nina effects are typically seen on the West Coast, these events have effects on weather patterns throughout North America, and have even been shown to effect the Atlantic hurricane season (Pielke Jr and Landsea, 1999). As opposed to being driver by moisture availability, tree growth during these years was likely driven by the combination of high temperatures and low moisture availability brought on by the large-scale ocean-atmosphere phenomenon.

Spectral analysis of the precipitation reconstruction identified a dominant 11-year cycle, a periodicity that has been observed in both instrumental and paleo-reconstructed temperature and moisture indices (Hancock and Yarger, 1979; Lassen and Friis-Christensen, 1995). In particular, this cyclic pattern has been identified in June precipitation in the south-eastern US (Hancock and Yarger, 1979), but was not apparent in western US PDSI tree-ring based reconstructions (Cook et al., 1997). This observed 11-year periodicity is a hallmark characteristic of the solar

cycle, which has been shown to be associated with terrestrial climate, identified as one of the contributing factors that determine global temperature (Reid, 2002; Board on Global Change, 1994; Lassen and Friis-Christensen, 1995). Solar periods of high and low activity can be measured by the number of sunspots or the solar cycle length. A larger number of sunspots indicates greater solar activity, and the magnetic fields in these sunspots have the ability to release large amount of stored energy as solar flares or coronal mass ejections, and these changes in released energy in turn affect the realized weather patterns. Studies have shown that these changes in released energy may also influence hydroclimate (Nichols and Huang, 2012; Hancock and Yarger, 1979). However, despite the presence of strong correlations between terrestrial climate records and solar cycles, physical mechanisms which explain the effects of external solar forcing on global circulation patterns have yet to be fully understood (Franks, 2002).

Chron	Lat (N), Long (W)	SIC	MS	# Series	MSL	Period	Citation
BM	37.37, 80.24	0.556	0.208	76	128.3	1764 - 2010	
LH	35.62, 85.43	0.609	0.171	19	181.4	1750 - 1997	Stahle, D.W. & Therrell, M.D. 2005
WD	38.50, 78.35	0.523	0.163	26	250.8	1642 - 1981	Cook, E.R. 1994
CC	37.35, 80.37	0.592	0.218	20	194.1	1722 - 2001	Copenheaver, C.A. 2010
OC	39.88, 76.40	0.575	0.169	18	260.2	1631 - 1981	Cook, E.R. 1994

Table 5.1: Site-specific details for the Brush Mountain (BM), Lynn Hollow, Watchdog Mountain (WD), Craig Creek (CC), and Otter Creek (CC) sites, including location, series intercorrelation (SIC), mean sensitivity (MS), number of series (# Series), mean series length (MSL), and the data citation.

Proxy	Climate covariate	
	mjPR	jjPDSI
BM	0.50	0.55
LH	0.55	0.48
WD	0.43	0.59
CC	0.38	0.50
OC	0.24*	0.19**
PC1	0.61	0.63

Table 5.2: Correlations between the growth proxies (site chronologies and first principal component PC1) with both the averaged May-June precipitation (mjPR) and averaged June-July PDSI (jjPDSI). All correlation statistics were significant at the  $p < 0.01$  level except the correlations indicated by \*, which was significant at the  $p < 0.05$  level, and \*\*, which was not significant ( $p = 0.09$ ).

	Calibration			
	mjPR		jjPDSI	
	1901-1941	1942-1981	1901-1941	1942-1981
RE	0.10	0.30	0.44	-0.41
CE	0.10	0.30	0.39	-0.60
Calibration $R^2$	0.64	0.56	0.58	0.74
Verification $R^2$	0.56	0.64	0.74	0.59
GLK	0.55	0.79	0.68	0.64

Table 5.3: Reconstruction accuracy statistics for mjPR and jjPDSI. Statistics include the reduction of error (RE), coefficient of efficiency (CE), calibration and verification period  $R^2$ , and the Gleichläufigkeit (GLK).

Parameter	Mean	Median	95% Credible Interval
$\beta_0$	102.73	102.72	(98.51, 107.21)
$\beta_1$	67.73	68.02	(51.65, 83.66)
$\sigma$	23.19	23.07	(20.28, 26.40)

Table 5.4: Posterior parameter mean, median, and 95% credible interval for the intercept ( $\beta_0$ ), slope ( $\beta_1$ ) and standard deviation ( $\sigma$ ) in the linear model which describes average May-June precipitation as a function of the first principal component growth proxy.

	<b>Recon</b>	<b>PDSI</b>		<b>Precip</b>			
	mjPR	JT	NADA	NC	SC	GA	MP <sup>A</sup>
mjPR	1						
JT	0.215	1					
NADA	0.593	0.502	1				
NC	0.227	0.396	0.424	1			
SC	0.118*	0.178	0.352	0.581	1		
GA	0.079*	0.196	0.345	0.474	0.766	1	
MP	0.378	0.288	0.499	0.132*	0.090*	0.109*	1

<sup>A</sup> Reconstruction covers only the period 1764 - 1966.

Table 5.5: Correlation between the mjPR reconstruction and other reconstructions including the NADA and JT drought reconstructions; and the NC, SC, GA and MP precipitation reconstructions. All values shown were significantly correlated at the  $p < 0.01$  level, except for those indicated by \* which were not significant.

Site	Location	Variable	Range (years)	Data type	Variance explained ( $R^2$ ) <sup>A</sup>
NADA (Cook et al., 1999)	37°30' N, 80°0' W VA	Jun-Aug PDSI	1185-2006	Tree-rings	0.55*
JC (Stahle et al., 1998)	Coastal NC and VA	July PHDI	1700-1984	Tree-rings	0.44
NC (Stahle and Cleaveland, 1992)	Statewide NC	Apr-Jun precip	933-1985	Tree-rings	0.54
SC (Stahle and Cleaveland, 1992)	Statewide SC	Mar-Jun precip	1005-1985	Tree-rings	0.58
GA (Stahle and Cleaveland, 1992)	Statewide GA	Mar-Jun precip	933-1985	Tree-rings	0.68
MP (Druckenbrod et al., 2003)	38°13' N, 78°10' W; VA	Early summer precip	1784-1966	Tree-rings; Meteorological diary	0.39

<sup>A</sup>  $R^2$  values as reported in cited references; may or may not be adjusted.

\* Median value of  $R^2$  for all gridpoints.

Table 5.6: Details for the six southeastern US moisture reconstructions compared to the mjPR reconstruction.

Years	Moisture	Consistent with
1894-1902	Low	(Warrick et al., 1980; Ruffner and Abrams, 1998; of California, 1990)
1867-1874	Low	(of California, 1990)
1839	Low	
1819	Low	(Lawson and Stockton, 2005)
1772-1777	Low	

Table 5.7: Periods of low moisture availability identified by the mjPR reconstruction and documented sources that corroborate this moisture deficit.

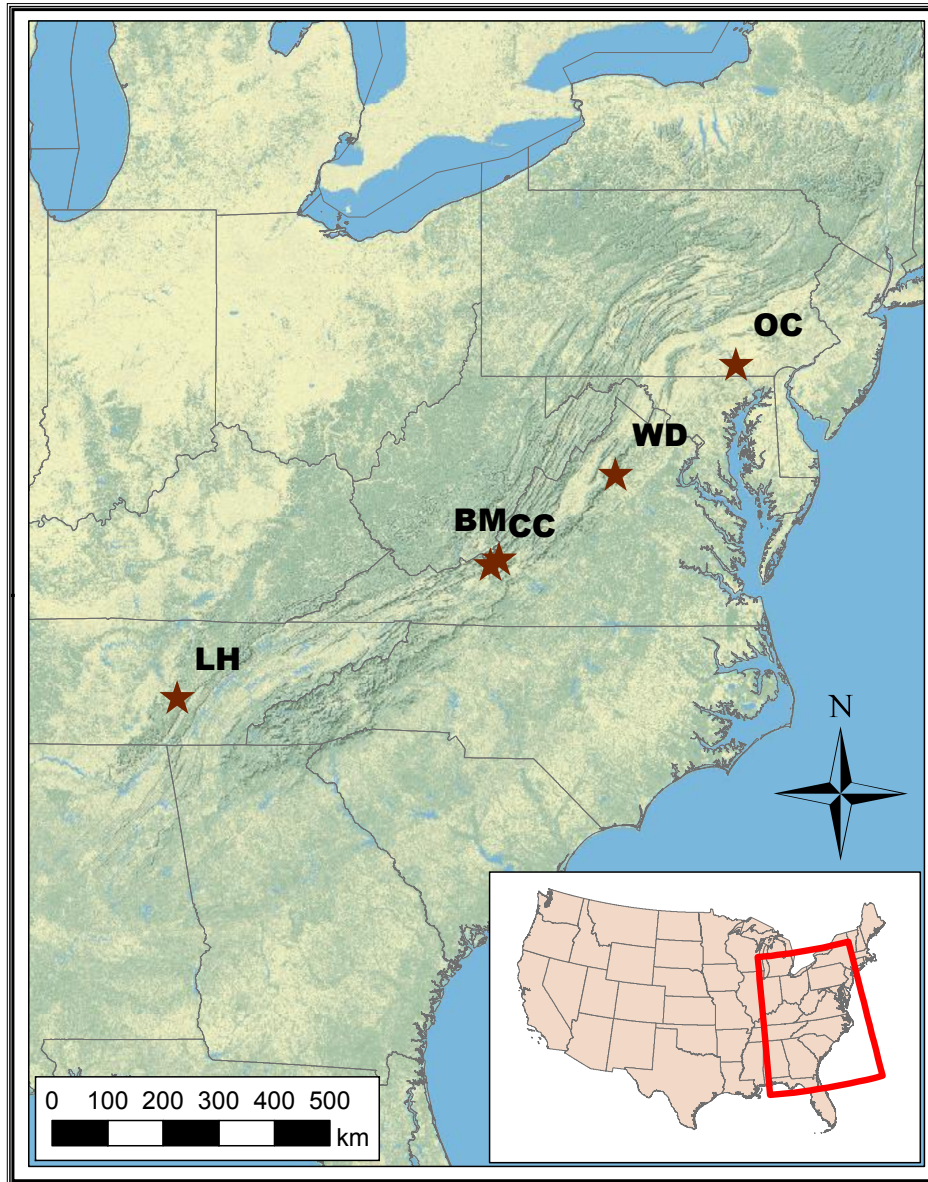


Figure 5.1: Regional chronology sample locations.

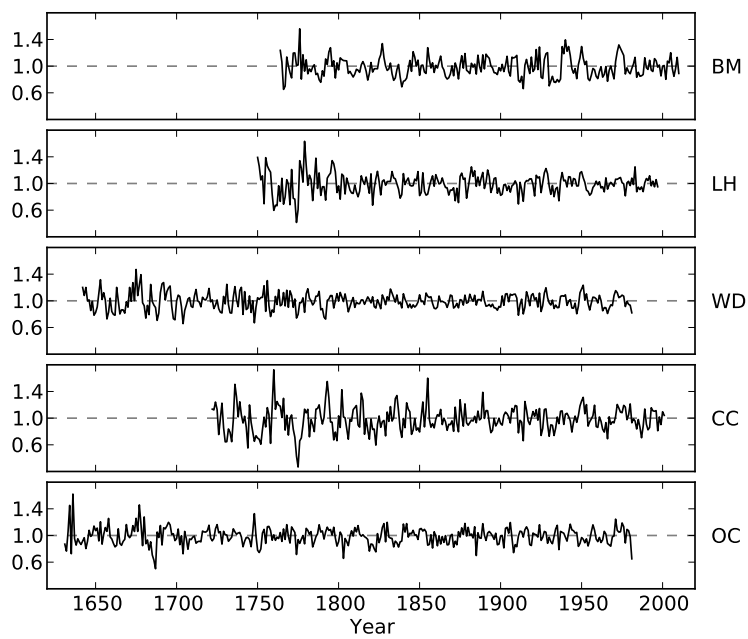


Figure 5.2: Plots of the five chronologies used in the principal component analysis. The top panel shows the chronology built from the sample data at Brush Mountain (BM), while the others are the regional chronologies from Lynn Hollow (LH), watchdog Mountain (WD), Craig Creek (CC), and Otter Creek (OC).

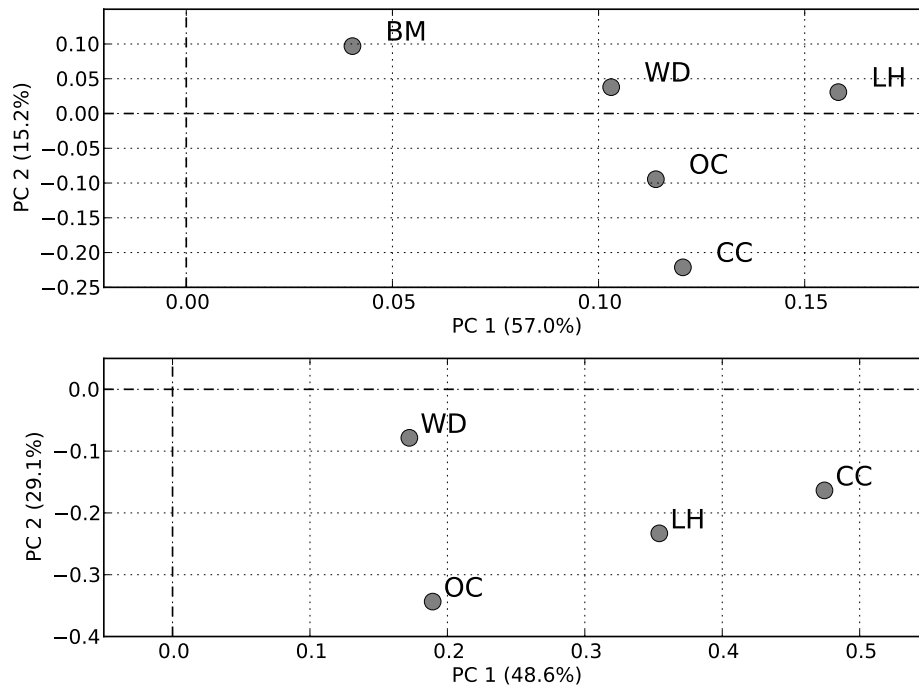


Figure 5.3: Top: Scatter plot of the loadings for the five chronologies analyzed in the first PCA which covered the period 1845-1981. Bottom: Scatter plot of the loadings for the five chronologies analyzed in the second PCA which covered the period 1750-1981.

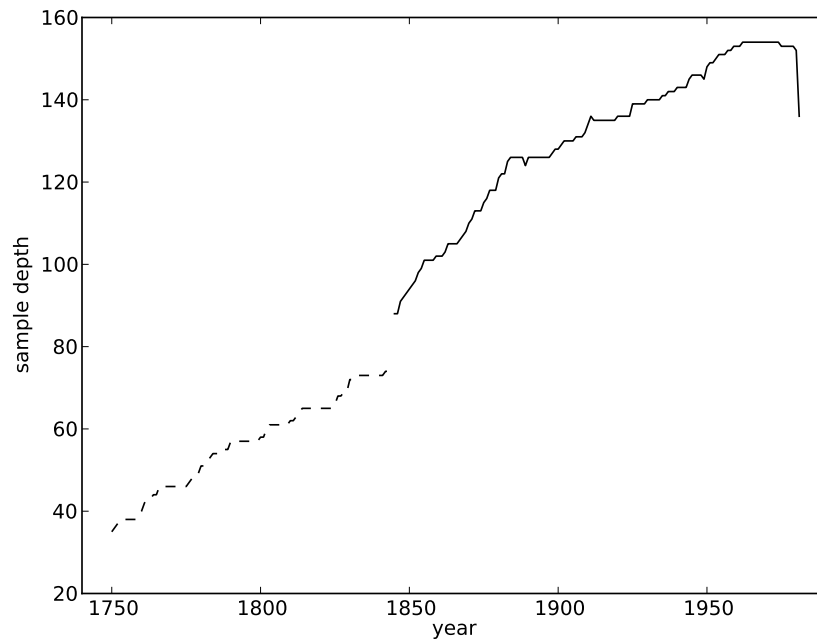


Figure 5.4: Sample depth by each year for the growth proxy obtained from the nested principal component analysis. The dashed line indicates the principal component which contained the years 1750-1844 with only four chronologies (WD, LH, CC, and OC), while the solid line indicates the principal component resulting from the analysis which used all five chronologies (BM, WD, LH, CC, and OC) and covered the years 1845-1981.

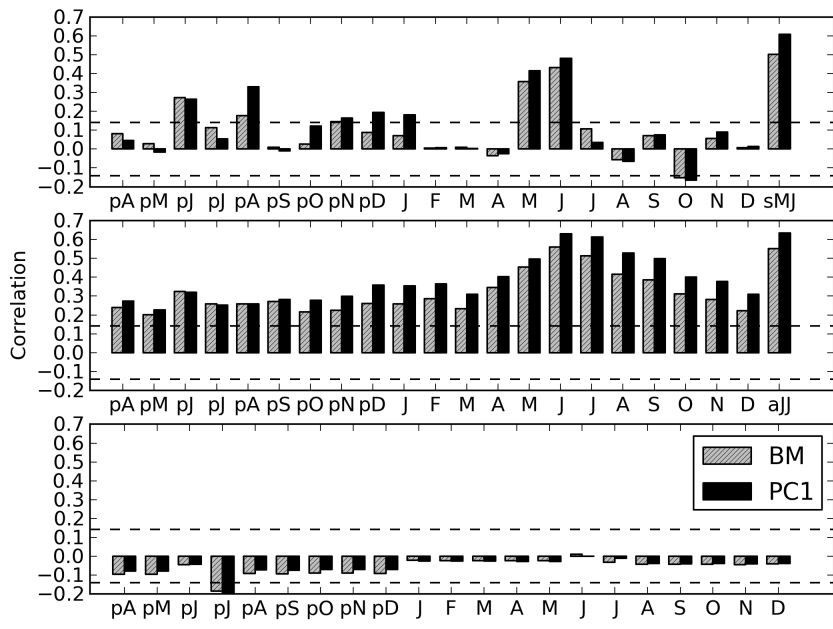


Figure 5.5: Top: Correlation between the growth proxies (BM or PC1) and the monthly precipitation from previous April (pA) through December (D) as well as for average May and June (aMJ). Middle: Correlation between the growth proxies (BM or PC1) and average PDSI from previous April (pA) through December (D) as well as for average June and July (aJJ). Bottom: Correlation between the growth proxies (BM or PC1) and average monthly temperature from previous April (pA) through December (D).

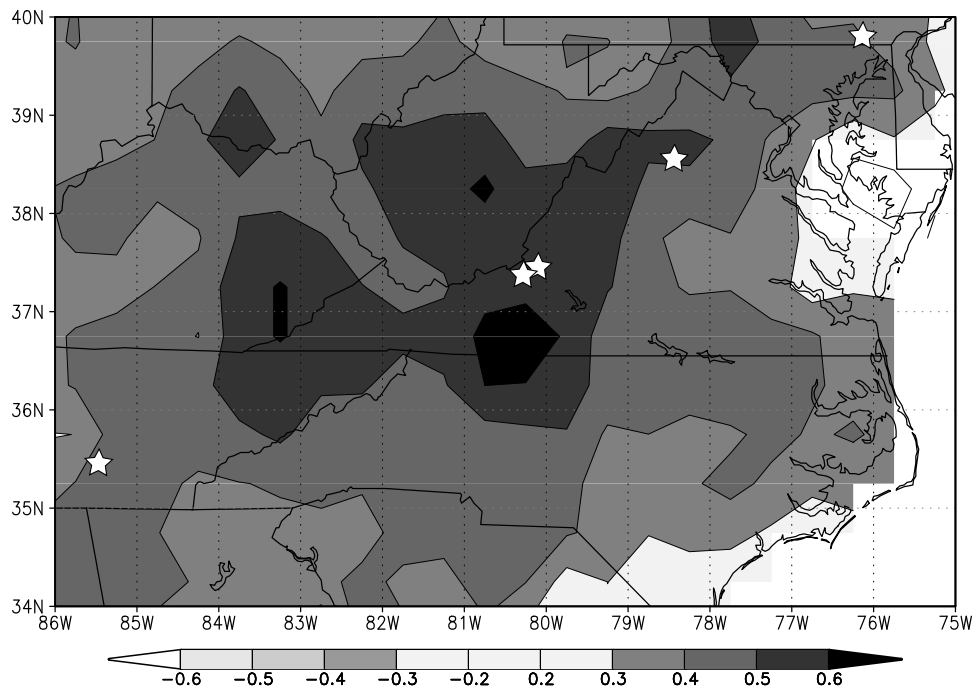


Figure 5.6: Correlation map showing the correlation between the first principal component and averaged May-June precipitation. Stars indicate the locations of the sites where the tree-rings used to develop the contributing chronologies were sampled.

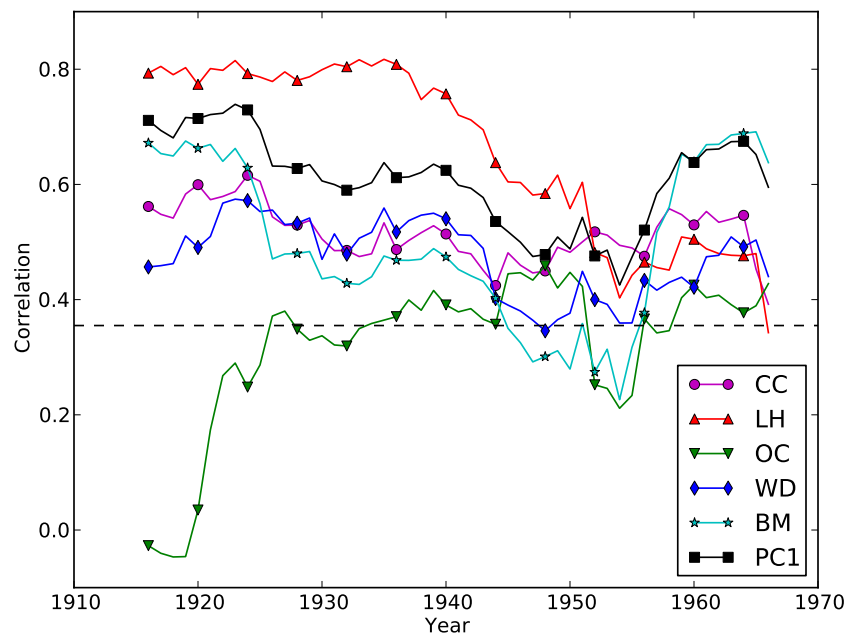


Figure 5.7: A 31-year windowed correlation plot showing the correlations between each growth proxy (chronologies and first principal component) and mjPR. Correlation points are plotted above the window centers. The dashed line indicates the 95% significance level of 0.355.

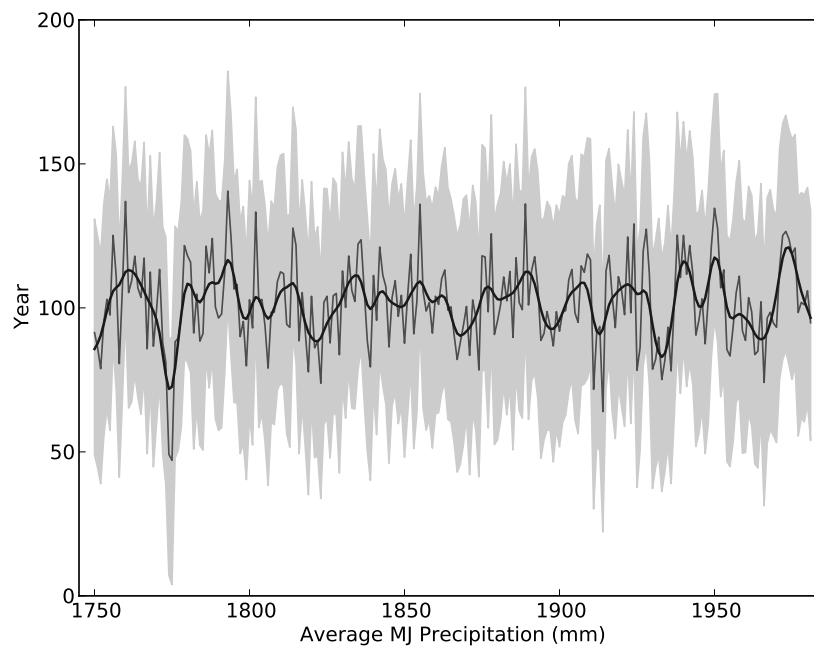


Figure 5.8: Average May-June precipitation (mjPR) reconstruction (grey curve), smoothed estimate showing decadal-scale variable (black curve), and the reconstruction 95% credible interval (shaded grey region).

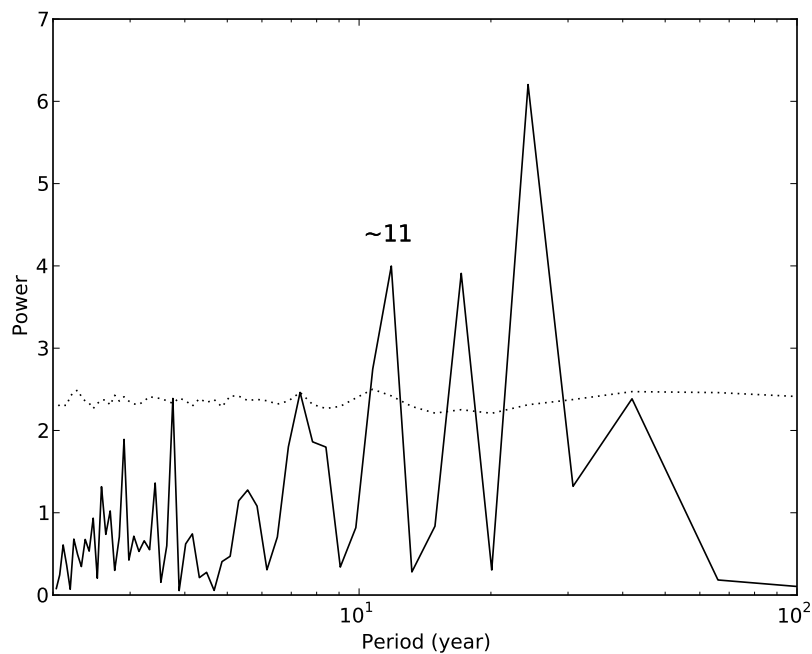


Figure 5.9: Periodogram showing periodicity of high amplitude at approximately 11, 17, and 24 years.

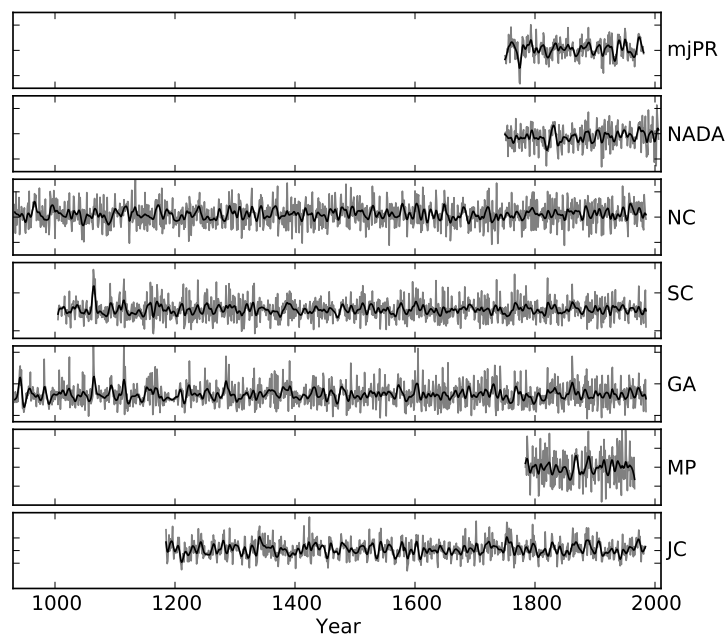


Figure 5.10: Time series plots showing annual- and decadal-scale variability for the mjPR and six compared moisture reconstructions for the period 933-2008.

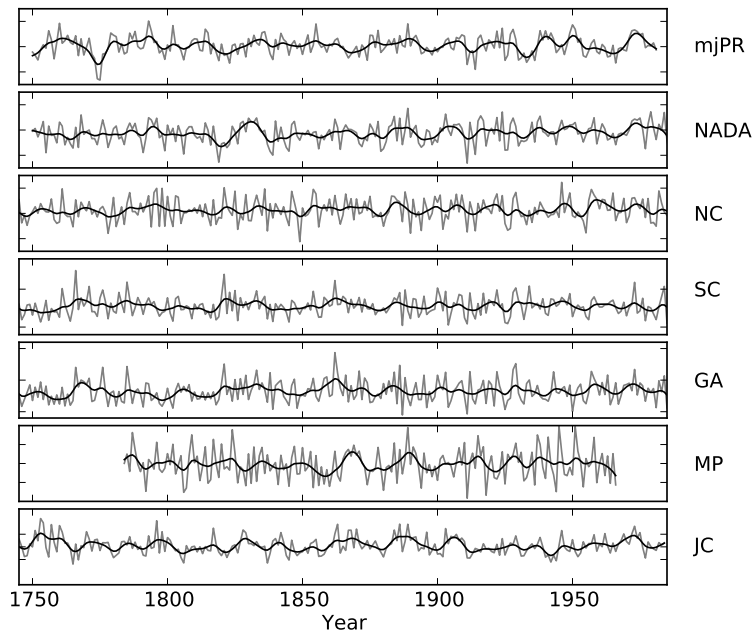


Figure 5.11: Time series plots showing annual- and decadal-scale variability for the mjPR and six compared moisture reconstructions for the period 1745-1985.

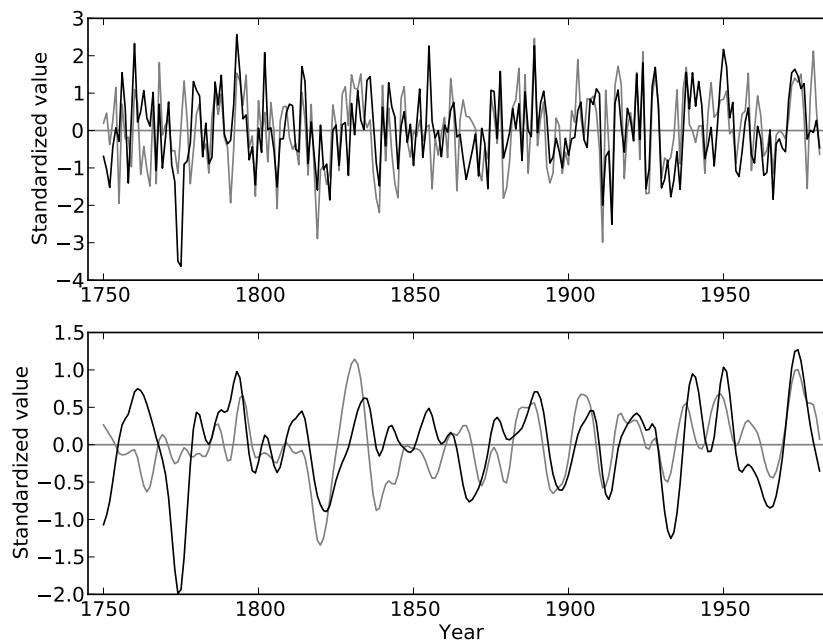


Figure 5.12: The standardized mjPR (black lines) and Cook PDSI (grey lines) reconstructions are plotted against time to highlight both the similarities and the differences. The top panel shows the standardized reconstructions at an annual scale, while the bottom panel shows 5-year smoothed time series to better highlight the decadal-scale variability. Particularly notable differences include the year 1774, and the interval 1855-1863.

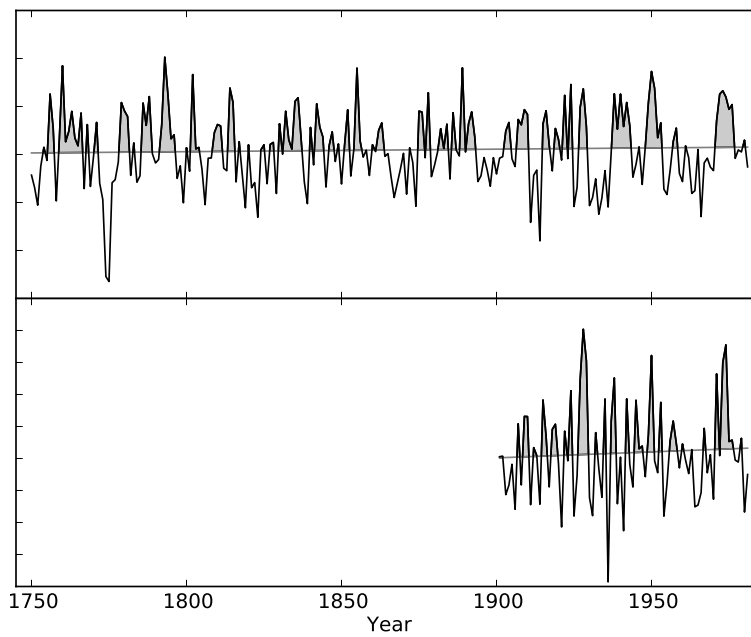


Figure 5.13: The mjPR reconstruction (top panel) and the mjPR instrumental record (bottom panel). Lines show the best-fit regression line through the time series data to indicate any dominant trends. Areas falling above the best-fit lines and the time series data are shaded grey to indicate periods of higher precipitation. Note the correspondence of wetter and drier years between the top and bottom panels.

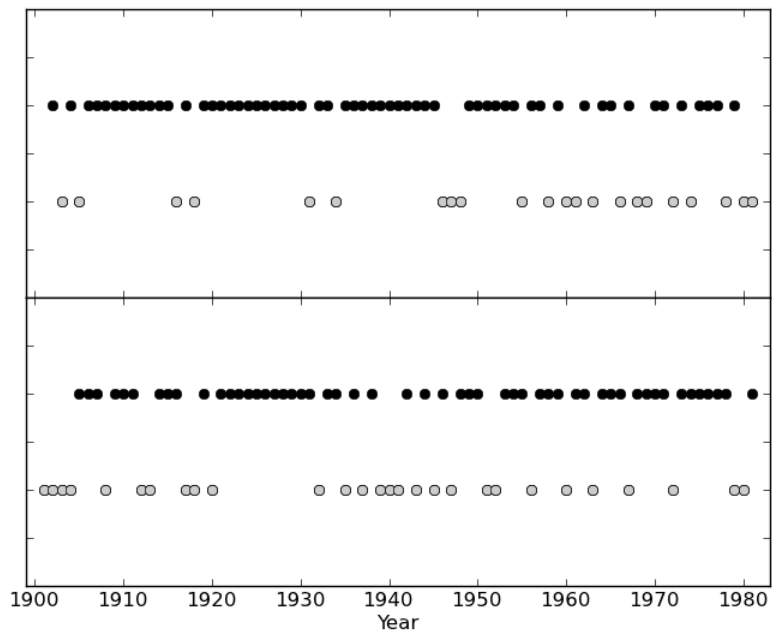


Figure 5.14: A representation of how the mjPR reconstruction and the mjPR instrumental record are changing with respect to each other. Top panels show a black dot if both time series were increasing or decreasing from the previous year to the year indicated, while the grey dots indicate that the time series changes are not synchronous. Time series show synchronous behavior with respect to this measure in 72% of the years. Bottom panel shows a black dot if both time series are either above or below their respective best-fit trend lines, while the grey dots indicate asynchronous behavior. Time series show synchronous behavior with respect to this measure in 65% of the years.

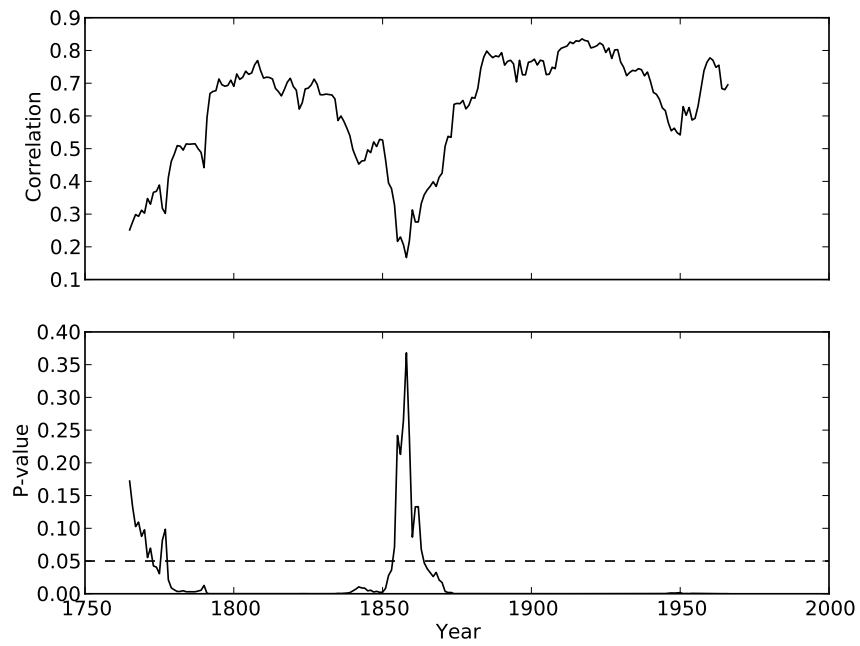


Figure 5.15: A 31 year windowed correlation plot between the mjPR and Cook PDSI reconstructions shows the discrepancy during the 1855-1863 interval. In the top panel correlation values are plotted about window centers, while the bottom panel shows the corresponding p-value (black) as well as the line of significance (dashed).

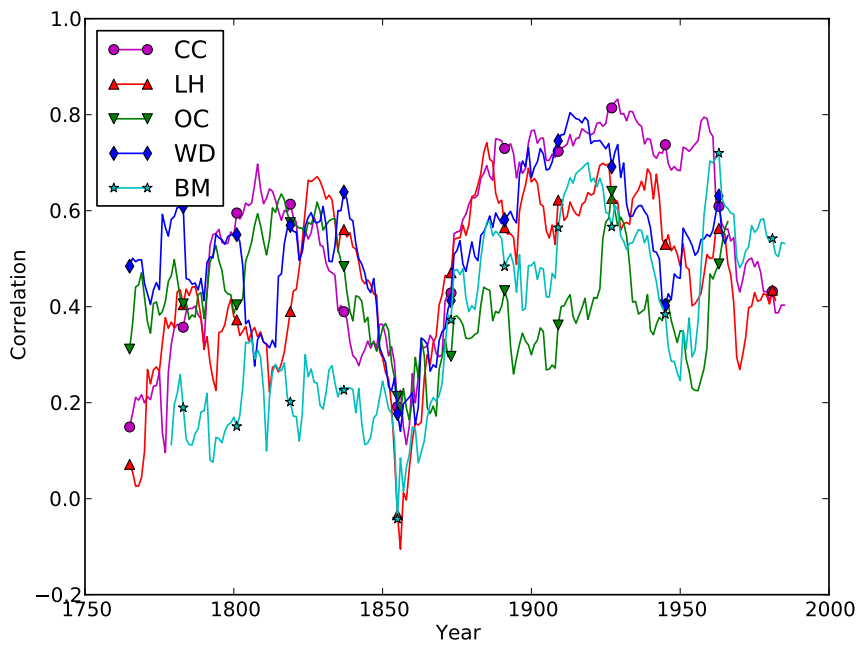


Figure 5.16: A 31 year windowed correlation plot between each of the chronologies and the Cook PDSI reconstruction. Note the interval of abrupt poor correlation during the years 1855-1863.

# Bibliography

- Anchukaitis, K., Evans, M., Kaplan, A., Vaganov, E., Hughes, M., et al. Forward modeling of regional scale tree-ring patterns in the southeastern United States and the recent influence of summer drought. *Geophysical Research Letters*, 33(4):L04705, 2006.
- Beniston, M., Diaz, H., and Bradley, R. Climatic change at high elevation sites: an overview. *Climatic Change*, 36(3):233–251, 1997.
- Board on Global Change, N.R.C. *Solar Influences on Global Change*. The National Academies Press, 1994.  
URL [http://www.nap.edu/openbook.php?record\\_id=4778](http://www.nap.edu/openbook.php?record_id=4778)
- Büntgen, U., Frank, D., Kaczka, R., Verstege, A., Zwijacz-Kozica, T., et al. Growth responses to climate in a multi-species tree-ring network in the Western Carpathian Tatra Mountains, Poland and Slovakia. *Tree Physiology*, 27(5):689–702, 2007.
- Committee on Surface Temperature Reconstructions for the Last 2,000 Years, N.R.C. *Surface Temperature Reconstructions for the Last 2,000 Years*. The National Academies Press, 2006.
- Cook, E. The decomposition of tree-ring series for environmental studies. *Tree-Ring Bulletin*, 47:37–59, 1987.
- Cook, E., Meko, D., Stahle, D., and Cleaveland, M. Drought reconstructions for the continental United States. *Journal of Climate*, 12(4):1145–1162, 1999.
- Cook, E., Meko, D., and Stockton, C. A new assessment of possible solar and lunar forcing of the bidecadal drought rhythm in the western United States. *Journal of Climate*, 10(6):1343–1356, 1997.
- Cook, E. and Peters, K. The smoothing spline: a new approach to standardizing forest interior tree-ring width series for dendroclimatic studies. *Tree-Ring Bulletin*, 41:45–53, 1981.
- Cook, E. and Peters, K. Calculating unbiased tree-ring indices for the study of climatic and environmental change. *The Holocene*, 7(3):361–370, 1997.
- Cook, E., Woodhouse, C., Eakin, C., Meko, D., and Stahle, D. Long-term aridity changes in the western United States. *Science*, 306(5698):1015–1018, 2004.

- Cook, E.R., Briffa, K.R., and Jones, P.D. Spatial regression methods in dendroclimatology: a review and comparison of two techniques. *International Journal of Climatology*, 14(4):379–402, 1994.
- Dickson, R. and Tomlinson, P. Oak growth, development and carbon metabolism in response to water stress. In *Annales des Sciences Forestières*, vol. 53, pp. 181–196. 1996.
- Druckenbrod, D., Mann, M., Stahle, D., Cleaveland, M., Therrell, M., et al. Late-eighteenth-century precipitation reconstructions from James Madison’s Montpelier plantation. *Bulletin of the American Meteorological Society*, 84(1):57–72, 2003.
- Edwards, D. Characteristics of 20th century drought in the United States at multiple time scales. Tech. rep., DTIC Document, 1997.
- Franks, S. Assessing hydrological change: deterministic general circulation models or spurious solar correlation? *Hydrological Processes*, 16(2):559–564, 2002.
- Fritts, H. *Tree rings and climate*. London, New York, San Francisco.: Academic Press, 1976.
- Fritts, H., Guiot, J., Gordon, G., and Schweingruber, F. Methods of calibration, verification, and reconstruction. *Methods of Dendrochronology*, pp. 163–217, 1990.
- Grissino-Mayer, H. Research report evaluating crossdating accuracy: a manual and tutorial for the computer program COFECHA. *Tree-ring research*, 57(2):205–221, 2001.
- Hancock, D. and Yarger, D. Cross-spectral analysis of sunspots and monthly mean temperature and precipitation for the contiguous United States. *Journal of Atmospheric Sciences*, 36:746–746, 1979.
- Holmes, R. Computer-assisted quality control in tree-ring dating and measurement. *Tree-Ring Bulletin*, 43(1):69–78, 1983.
- Jacoby, G. and D’Arrigo, R. Reconstructed northern hemisphere annual temperature since 1671 based on high-latitude tree-ring data from North America. *Climatic Change*, 14(1):39–59, 1989.
- Kattenberg, K., Giorgi, F., Grassl, H., Meehl, G., Mitchell, J., et al. Climate models—projections of future climate. In J. Houghton, L. Meiro Filho, B. Callander, N. Harris, A. Kattenburg, and K. Maskell (eds.), *Climate change 1995: The science of climate change: contribution of working group I to the second assessment report of the Intergovernmental Panel on Climate Change*, pp. 285–357. Cambridge University Press, 1996.
- Lassen, K. and Friis-Christensen, E. Variability of the solar cycle length during the past five centuries and the apparent association with terrestrial climate. *Journal of Atmospheric and Terrestrial Physics*, 57(8):835–845, 1995.

- Lawson, M. and Stockton, C. Desert myth and climatic reality. *Annals of the Association of American Geographers*, 71(4):527–535, 2005.
- LeBlanc, D. Temporal and spatial variation of oak growth-climate relationships along a pollution gradient in the midwestern United States. *Canadian Journal of Forest Research*, 23(5):772–782, 1993.
- Li, Y. *Dendroclimatic Analysis of Climate Oscillations for the Southeastern United States from Tree-ring Network Data*. Ph.D. thesis, University of Tennessee, 2011.
- Mitchell, T.D. and Jones, P.D. An improved method of constructing a database of monthly climate observations and associated high-resolution grids. *International journal of climatology*, 25(6):693–712, 2005.
- Monserud, R. Time-series analyses of tree-ring chronologies. *Forest Science*, 32(2):349–372, 1986.
- Nichols, J. and Huang, Y. Hydroclimate of the northeastern United States is highly sensitive to solar forcing. *Geophysical Research Letters*, 39(4):L04707, 2012.
- North Carolina Natural Heritage Program (NCNHP). An Inventory of the Significant Natural Areas of Ashe County, North Carolina. 1999. Accessed September 2012.  
URL <http://www.ncnhp.org/Images/Ashe10-10-2005.pdf>
- of California, S. Drought conditions in California. Tech. rep., Department of Water Resources, 1990.
- Oliver, C. Forest development in North America following major disturbances. *Forest ecology and management*, 3:153–168, 1980.
- Pachauri, R. and Reisinger, A. Climate Change 2007: Synthesis Report. Contribution of Working Groups I, II and III to the Fourth Assessment Report of the Intergovernmental Panel on Climate Change. *Intergovernmental Panel on Climate Change*, 2007.
- Pan, C., Tajchman, S., and Kochenderfer, J. Dendroclimatological analysis of major forest species of the central Appalachians. *Forest Ecology and Management*, 98(1):77–87, 1997.
- Peters, K., Jacoby, G., and Cook, E. Principal components analysis of tree-ring sites. *Tree-Ring Bulletin*, 41:1–19, 1981.
- Phipps, R. Comments on interpretation of climatic information from tree rings, eastern North America. *Tree-ring bulletin*, 42:11–22, 1982.
- Pielke Jr, R. and Landsea, C. La niña, el niño and atlantic hurricane damages in the United States. *Bulletin of the American Meteorological Society*, 80(10):2027–2033, 1999.

- Reid, G. Solar irradiance variations and the global sea surface temperature record. *Climate Change: Natural forcing factors for climate change timescales 10-1 to 10-5 years*, 2:7, 2002.
- Robertson, P. Factors affecting tree growth on three lowland sites in southern Illinois. *American Midland Naturalist*, pp. 218–236, 1992.
- Rubino, D. and McCarthy, B. Dendroclimatological analysis of white oak (*Quercus alba* L., Fagaceae) from an old-growth forest of southeastern Ohio, USA. *Journal of the Torrey Botanical Society*, pp. 240–250, 2000.
- Ruffner, C. and Abrams, M. Relating land-use history and climate to the dendroecology of a 326-year-old *Quercus prinus* talus slope forest. *Canadian Journal of Forest Research*, 28(3):347–358, 1998.
- Schweingruber, F.H. et al. *Tree rings-basics and applications of dendrochronology*. D. Reidel Publishing Company, 1988.
- Seager, R., Tzanova, A., and Nakamura, J. Drought in the southeastern United States: Causes, variability over the last millennium, and the potential for future hydroclimate change. *Journal of Climate*, 22(19):5021–5045, 2009.
- Sobolowski, S. and Pavelsky, T. Evaluation of present and future North American Regional Climate Change Assessment Program (NARCCAP) regional climate simulations over the southeast United States. *Journal of Geophysical Research*, 117:D01101, 2012.
- Speer, J. *Fundamentals of tree-ring research*. University of Arizona Press, 2010.
- Speer, J., Grissino-Mayer, H., Orvis, K., and Greenberg, C. Climate response of five oak species in the eastern deciduous forest of the southern Appalachian Mountains, USA. *Canadian Journal of Forest Research*, 39(3):507–518, 2009.
- Stahle, D. and Cleaveland, M. Reconstruction and analysis of spring rainfall over the southeastern US for the past 1000 years. *Bulletin of the American Meteorological Society; (United States)*, 73(12), 1992.
- Stahle, D., Cleaveland, M., Blanton, D., Therrell, M., and Gay, D. The lost colony and Jamestown droughts. *Science*, 280(5363):564–567, 1998.
- Stahle, D. and Cleveland, M. Large-scale climatic influences on baldcypress tree growth across the southeastern united states. In P. Jones, R. Bradley, and J. Jouzel (eds.), *Climatic variations and forcing mechanisms of the last 2000 years*, I41, pp. 125 – 140. NATO ASI, 1993.
- Stokes, M. and Smiley, T. *An introduction to tree-ring dating*. University of Arizona Press, 1996.
- Warrick, R. et al. Drought in the great plains: A case study of research on climate and society in the USA. *Climatic constraints and human activities*, 10:93–123, 1980.

- Wells, N., Goddard, S., and Hayes, M.J. A self-calibrating palmer drought severity index. *Journal of Climate*, 17(12):2335–2351, 2004.
- Wold, S., Esbensen, K., and Geladi, P. Principal component analysis. *Chemometrics and intelligent laboratory systems*, 2(1):37–52, 1987.
- Yamaguchi, D.K. A simple method for cross-dating increment cores from living trees. *Canadian Journal of Forest Research*, 21(3):414–416, 1991.
- Zipper, C., Burger, J., Skousen, J., Angel, P., Barton, C., et al. Restoring forests and associated ecosystem services on appalachian coal surface mines. *Environmental management*, 47(5):751–765, 2011.
- Zweifel, R., Zimmermann, L., Zeugin, F., and Newbery, D. Intra-annual radial growth and water relations of trees: implications towards a growth mechanism. *Journal of Experimental Botany*, 57(6):1445–1459, 2006.

## Chapter 6

# Discussion

In the preceding chapters, I considered problems with a central focus on combining data with mathematical and statistical models to further understand forest ecosystem processes. In particular, this thesis focusses on understanding how tree demography is affected by competition, growth, and climate.

In Chapter 2 retrospective data was used to fit two survival probability models for white spruce – one based on recent growth predictors, and another based on predictors describing competition from neighbors. Results showed that although the recent growth informed model performed better in terms of prediction of tree status, the improvement was only marginal, and hence local competition data can be successfully used to predict mortality in the mixedwood boreal. Both models also identified early summer climate moisture index (CMI) as a significant predictor, which suggests that moisture availability during early summer plays a critical role in determining the fates of individuals.

In Chapter 3 a two-species integral projection model (IPM) was used to describe the spruce-aspen mixedwood ecosystem in the Alberta mixedwood boreal. Two model formulations were considered: one which included competitive structure, and one which did not. Both models were fitted with the retrospective data set, and projections were subsequently compared to an independent permanent sample plot (PSP) data set. Results indicated that the model which included competitive structure was better able to model size distributions for the two-species population, and indicate that the IPM shows potential as a useful tool in forest management. Implementation and analysis of the IPM required a robust numerical implementation of the model, which necessitated the use of a numerical quadrature scheme appropriate for multiple slow-growing species.

In Chapter 4 an analysis of the effectiveness of different quadrature schemes for IPMs was presented. Results suggest that the midpoint rule or Gauss-Legendre quadrature with self-adjusting sub-intervals are the most efficient and accurate methods, although ultimately different quadrature schemes and methods should be evaluated for any given kernel for a range of mesh sizes.

Finally, in Chapter 5 tree ring data from closed-canopy oak forests in the Eastern US was shown to be an effective proxy for reconstructing early summer precipitation, and allowed the meteorological record to be extended by 150 years.

In this discussion Chapter, I discuss the key results of this thesis and their implications in a broader sense, identify limitations of the methods used, suggest possible future directions, and comment on the importance of interdisciplinary collaboration.

## 6.1 Retrospective data collection

This thesis confirms other studies which highlight the success of retrospective sampling techniques (Metsaranta and Lieffers, 2009; Kobe and Coates, 1997; Bigler, 2004). Traditional permanent sample plot (PSP) sampling, which involves revisiting and re-measuring tagged trees in a designated piece of forest, is straightforward to implement and carry-out, but is often not practical due to the length of time needed to acquire data. Additionally, the resolution of this data is often not annual, which forces scientists to make assumptions about how to estimate demographic rates and survival status in intervals between measurements. These assumptions make it difficult, if not impossible, to link demographic rates and events to predictor data such as climate. Alternatively, the retrospective sampling approach employed here uses crossdating techniques to estimate year of death of dead individuals, thereby allowing us to reconstruct past tree density as well as individual annual growth increment. In this study, sampling efforts were focused on spruce, although aspen was also sampled (less intensively). Additionally, the sampling design was geared towards obtaining accurate data on spruce mortality events, and the live tree population was therefore sub-sampled. This data was sufficient for fitting the mortality models described in Chapter 1, and the favorable goodness-of-fit results for the IPM models described in Chapter 3 suggest that the retrospective data set had the ability to capture the dynamics observed in the PSP data set to which the IPM projections were compared.

A potential shortcoming that may arise from sub-sampling a tree population is that

live tree ages may not be accurately estimated based on the representative sample, which means that uncertainty in population size increases as we reconstruct further back in time. This issue may be minimized with an accurate determination of the age the youngest tree belonging to the cohort of interest, which can be used to determine the reconstruction period. Another way to overcome this issue is to sample the entire population of interest, although any increase in sample size leads to an increase in sampling effort. Additionally, in the retrospective data set used for analysis in this thesis, competitive neighborhoods were retrospectively estimated based on average ring width values from sampled individuals from small, medium, or large size classes (which were used to shrink neighborhood trees back to the desired year). Reality surely varies from this assumption, and sampling entire neighborhoods or entire transects would eliminate the need to make this assumption. In the case an entire population is sampled, familiarity with species decay is important. For example, it is common for aspen and poplar to develop heart rot (Basham, 1958), which leads to sampling difficulties and forbids ring width measurement in severely rotted wood.

Overall, this method shows significant promise as a management sampling strategy. Further studies comparing traditional PSP data to retrospective data will help identify potential issues and help with the development of a standard protocol for managers.

## 6.2 Management implications

This thesis was in large part driven by the desire of forest managers to better quantify forest mortality in the Alberta mixedwood boreal, and this objective was addressed in Chapter 2. Chapter 2 described the unique retrospective sampling approach used to sample mid-aged spruce across numerous ecosites, and this data was subsequently used to develop spruce mortality models that had the ability to predict tree status (live or dead) accurately for approximately 75% of the population. The collected data fills a significant data gap for Alberta, which has previously prevented the computation of an appropriate mortality estimate and the ability to link mortality events to predictors. The average background spruce mortality estimate that resulted from the retrospective data set was approximately 0.77-0.81%, which was marginally higher than the previous estimate of 0.7% proposed by Feng et al. (2006). The finding that either recent growth or local competition predictors can be used to predict spruce probability of survival is significant, and suggests a strong link between the local neighborhood effect and annual growth. The perfor-

mance of these models will be further assessed after they are incorporated into the Mixedwood Growth Model (MGM), a stand growth model for the boreal forest used by managers to predict growth and yield.

Chapter 3 includes the development and analysis of an IPM used to describe a mixedwood forest dominated by spruce and aspen, a model which has the potential to be a useful tool in forest management. The IPM has the advantage that it describes species demography using a single redistribution kernel fitted to data. Comparison of the developed model projections to a second independent data set showed surprising promise for this model, even without the consideration of climatic, geographical, or edaphic factors. The next step is to compare projections from the IPM to those obtained using MGM, which will help identify model shortcomings and benefits. If proven useful, this model can be better calibrated to include additional predictors, and can then be easily used to make projections of stand distributions based on a user-defined initial condition.

### **6.3 Forest competition**

Plant competition has been recognized as a phenomenon of interest since the 1300s, and is broadly defined to occur when the removal of neighboring plant matter leads to an increase in biomass of the subject species (Grace et al., 1990). Competition can occur through direct or indirect interaction, and typically in forest ecosystems we focus on two types of competition: interference and exploitation competition. Interference competition occurs when neighboring individuals prevent incoming solar radiation from penetrating to a subject tree, while exploitation competition occurs indirectly through a shared resource, such as soil nutrients and water. Quantifying the effects of competition for a specific resource is difficult due to the confounded effects of inherent individual genetics and the surrounding environment. Due to the complicated nature of tree interactions, competition is typically measured using proxy variables which quantify the dependence on surrounding neighbors. In Chapter 2 and 3, I consider some of the more common forest competition indices: basal area of competition, sum of diameters of competitors, and number of competitors; and focus on the two dominant species occurring in the Alberta mixedwood boreal: spruce and aspen. Competition indices were computed for all neighbors as well as by species, and for competitors of any size as well as for only competitors with a diameter larger than the subject tree.

In both Chapters 2 and 3, competition indices based on thicker neighbors were better predictors than those indices which included neighbors of all sizes, suggest-

ing that asymmetric competition dominates in these forests. When we consider neighbor effects, it is intuitive that thicker spruce and aspen neighbors, which in most cases implies taller neighbors, would dominate the effects of interference competition for light. What is less apparent is whether thicker neighbors is also a useful proxy measure for interference competition. As described in Chapter 3, sapwood area is directly related to leaf area, which in turn is related to both light interception and tree water-use. Typically, within a species, greater leaf area implies greater transpiration assuming that the leaves work in parallel. Both sum of diameters as well as basal area haven been linked to sapwood area, although the exact nature of these relationships is not quite clear (Waring et al., 1980; Huang et al., 2013). Regardless, when used as proxies, these competition indices can be thought of as a crude measure of the relative water use of competitors.

Note that both Chapters 2 and 3 rely on distance-independent competition indices. The effectiveness of the inclusion of distance-dependence when measuring competition has been analyzed, and for the mixedwood boreal it been shown that distance independent indices performed almost as well as those dependent on distance (Stadt et al., 2007). However, in Chapter 2, although not explicitly distance-dependent, competition indices were based on local circular neighborhoods centered at the subject tree whereas in Chapter 3, survival and growth models were fitted for use in the IPM, which, as formulated, does not track individuals and therefore does not permit distance dependence. Although competition indices at the stand level were still found to be significant predictors of growth and survival, the survival model based on stand-level predictors does not perform as well as the survival model based on local neighborhood predictors, which highlights the importance of heterogeneity within a stand. In the case where there is substantial heterogeneity in the distribution of trees within a stand, local neighborhoods have the potential to widely vary, and may need to be considered to obtain accurate estimates of experienced competition.

## 6.4 The Importance of Interdisciplinary Collaboration

Interdisciplinary research has been recognized as important in many fields, including ecology, and has become more prominent in recent years. In Green et al. (2005) it was noted that “imaginative approaches at the interface of ecology, statistics, mathematics, informatics, and computational science can improve scientists’ understanding of complex ecological systems and our approach to biological conservation and resource management”. Many problems in ecology require complex

solutions, and combine elements of data analysis, mathematical and statistical modeling, ecological theory, and the understanding of management implications. Chapter 4 and 5 highlight the importance of interdisciplinary collaboration by demonstrating that while the use of more complex mathematical tools is sometimes necessary to obtain a more complete understanding of ecological questions, there are often inherent difficulties within the tools that require a deeper mathematical understanding to overcome. Chapter 4 arose out of problems I encountered when attempting to perform numerical integration using default functions in a software package - two different functions meant to serve the same purpose yielded different results. After further investigation, I realized this problem had been recognized in the literature, but had yet to be formally addressed – likely because it lies at the interface of ecology and mathematics. In Chapter 5, the use of a combination of mathematical and statistical tools allowed me to discover that a precipitation signal can in fact be identified in closed-canopy oak forests, allowing for inference about past climate. Without a deeper understanding of mathematics, the work which appears in these chapters would not have been possible. However, as recognized in the literature, interdisciplinary research comes with challenges (Naiman, 1999). Interdisciplinary projects have been noted to be more time consuming because of the challenges of learning a new field and associated terminology, communication among collaborators, and the challenges of publishing interdisciplinary research in journals. Despite these challenges, I believe that interdisciplinary research has a necessary place in the advancement of science.

## 6.5 Closing Remarks

This thesis deals with problems that lie in the intersection of forest ecology and mathematical and statistical modeling, some of which are clearly related to issues in forest management. One of the underlying principles in this thesis is the importance of “confronting models with data”, as worded by Hilborn and Mangel (Hilborn and Mangel, 1997), and without the data and the stories they tell, this thesis would not have been possible.

In particular, this thesis has made contributions to these fields through: filling the spruce data gap; development of spruce mortality models which improve upon our current understanding and estimates; development of a spruce-aspen IPM; analysis of the validity of the IPM in a novel way; analysis of the effectiveness of integration methods for the IPM; and linking closed-canopy oak growth data to early summer precipitation to extend the meteorological record.

# Bibliography

- Basham, J. Decay of trembling aspen. *Canadian Journal of Botany*, 36(4):491–505, 1958.
- Bigler, C. Assessing the performance of theoretical and empirical tree mortality models using tree-ring series of Norway spruce. *Ecological Modelling*, 174(3):225–239, 2004.
- Feng, Z., Stadt, K.J., and Lieffers, V.J. Linking juvenile white spruce density, dispersion, stocking, and mortality to future yield. *Canadian Journal of Forest Research*, 36:3173–3182, 2006.
- Grace, J., Tilman, D., et al. *Perspectives on plant competition*. Academic Press, Inc., 1990.
- Green, J., Hastings, A., Arzberger, P., Ayala, F., Cottingham, K., et al. Complexity in ecology and conservation: mathematical, statistical, and computational challenges. *BioScience*, 55(6):501–510, 2005.
- Hilborn, R. and Mangel, M. *The Ecological Detective: Confronting Models with Data (MPB-28)*, vol. 28. Princeton University Press, 1997.
- Huang, J.G., Stadt, K.J., Dawson, A., and Comeau, P. Modelling growth-competition relationships in trembling aspen and white spruce mixed boreal forests of western Canada. *Submitted to PLoS One*, 2013.
- Kobe, R.K. and Coates, K.D. Models of sapling mortality as a function of growth to characterize interspecific variation in shade tolerance of eight tree species of northwestern British Columbia. *Canadian Journal of Forest Research*, 236:227–236, 1997.
- Metsaranta, J.M. and Lieffers, V.J. Using dendrochronology to obtain annual data for modelling stand development: a supplement to permanent sample plots. *Forestry*, 82(2):163–173, 2009.
- Naiman, R. A perspective on interdisciplinary science. *Ecosystems*, 2(4):292–295, 1999.
- Stadt, K., Huston, C., Coates, K., Feng, Z., Dale, M., et al. Evaluation of competition and light estimation indices for predicting diameter growth in mature boreal mixed forests. *Annals of Forest Science*, 64(5):477–490, 2007.

Waring, R., Thies, W., and Muscato, D. Stem growth per unit of leaf area: a measure of tree vigor. *Forest Science*, 26(1):112–117, 1980.

# Appendix A

## Numerical considerations for the multi-species IPM

### 1.1 Numerical implementation of the IPM and model projections

The midpoint method was used to numerically approximate the integrals in the two-species IPM model (3.3). The midpoint method was chosen since it is relatively easy to implement and has been shown to perform adequately for single-species IPMs as long as a sufficiently large number of mesh points are used to discretize the domain of interest. For simplicity here we use a common domain  $\Omega = [L, U]$  for both species.

The two-species form of the midpoint method is obtained by discretizing the continuous populations  $n_m(x, t)$  by storing their values at a discrete set of  $N$  uniform mesh points  $x_i \in [L, U]$  for  $i = 1, \dots, N$ . The discretized populations are denoted by  $n_{m,i}^t \approx n_m(x_i, t)$ . Similarly, the projection kernels  $k_m(x, t, n_1, n_2)$  are approximated throughout the domain (to first order) by their value at the nearest mesh point. With these discretizations, the two-species IPM (3.3) becomes

$$n_{m,j}^{t+1} \approx \sum_{i=1}^N k_m(x_i, y_j, n_1, n_2) n_{m,i}^t dx \quad (1.1)$$

for  $m = 1, 2$  and  $j = 1, \dots, N$ , where  $dx = (U - L)/N$ . The summation in 1.1 can be expressed more compactly using matrix notation by defining population vectors

$\mathbf{n}_m^t = [n_{m,1}^t, \dots, n_{m,N}^t]^T$ , after which (3.3) becomes

$$\mathbf{n}_1^{t+1} = P_1^t \mathbf{n}_1^t \quad \text{and} \quad \mathbf{n}_2^{t+1} = P_2^t \mathbf{n}_2^t \quad (1.2)$$

where  $P_m^t$  are  $N \times N$  *projection matrices*, obtained by sampling the projection kernels. The entries of the projection matrices (for the midpoint rule) are given by

$$(P_m^t)_{i,j} = k_m(x_i, x_j, \mathbf{n}_1^t, \mathbf{n}_2^t) dx. \quad (1.3)$$

Note that the projection matrices must be recomputed every year since the projection kernels depend on both populations through competitive interaction terms.

The steps required to perform one projection of the two-species IPM (3.3), given the discrete populations  $\mathbf{n}_1^t$  and  $\mathbf{n}_2$ , are summarized by:

1. For each  $i = 1, \dots, N$ : compute (and cache) the discrete interaction terms

$$N_1^*(x_i; \mathbf{n}_1) = \sum_{j=i}^N n_{1,j}^t, \quad A_2^*(x_i; \mathbf{n}_2) = \frac{\pi}{4} \sum_{j=i}^N x_j^2 n_{2,j}^t, \quad S_1^*(x_i; \mathbf{n}_2) = \sum_{j=i}^N x_j n_{1,j}^t. \quad (1.4)$$

2. For each  $m = 1, 2$ : compute the projection matrix  $P_m^t$  by:
  - (a) For each  $i = 1, \dots, N$  and  $j = 1, \dots, N$ : compute the probability  $(P_m^t)_{i,j}$  of transitioning from  $x_i$  to  $x_j$  according to the species specific growth and survival models and the interaction terms computed above.

3. Perform the matrix multiplications in (1.2) to obtain the next population distributions  $\mathbf{n}_m^{t+1}$ .

## 1.2 Assessing domain eviction

To ensure that trees are not evicted from the computational domain erroneously a simple numerical experiment was performed. All survival probabilities  $s_m$  were set to unity and initial populations from the PSP data set were evolved through time for several years. Since the survival probabilities were unity we expect: (i) that the initial projection (from measurements to discrete populations) should preserve the total number of trees in each sample plot, and (ii) that after evolving the discrete populations through several years the total number of trees in each sample plot should remain constant. The maximum relative tree loss during the first projection

was found to be 0.125%, and the maximum relative tree loss during subsequent projections was found to be 0.05%. From these loss rates we conclude that trees are not being erroneously evicted from the computational domain and that the numerical scheme chosen is performing adequately for our purposes.